ASSESSING THE EFFECT OF FRICTION ON COMPRESSION SPLIT HOPKINSON PRESSURE BAR TESTS

by

R. S. HARTLEY

A Dissertation submitted in Part Fulfilment of the
Requirements for the Degree MSc (Engineering)

Department of Mechanical Engineering
University of Cape Town
September 2004

DECLARATION

I, Ross Stephen Hartley, declare that this dissertation contains my own work, except where reference and acknowledgment is made to contributions by others. I declare that this material has not been submitted for any purpose or examination to any other Department or University.

Signed this . . . . .13TH. . . . . day of . . . .OCTOBER . . .2004. . . .

Signed by candidate

. . . .

ABSTRACT

An enhanced understanding of material behaviour during rapid loading allows designers to improve the safety and efficiency of industrial processes and commercial products. These improvements are due, in part, to the use of increasingly powerful and sophisticated numerical simulation codes, which in turn, depend on accurate high strain rate material data. A Split Hopkinson Pressure Bar (SHPB) facility had previously been developed at the University of Cape Town to allow high strain rate testing of materials in compression. However, uncertainties regarding aspects of the test method that can affect the accuracy of the results, such as interface friction and specimen inertia, still required further clarification.

This report details a thorough experimental and numerical investigation into the effect of friction on SHPB test data. The objectives are to assess the magnitude of the effect of friction under various conditions and to suggest strategies for reducing friction error in SHPB tests to an acceptable level.

The ring compression test was used to obtain experimental friction factors. The effect of surface finish, lubricant, and strain rate on the friction experienced by mild steel, copper and aluminium samples was investigated. Numerical simulation was used to assess an energy-based analytical solution by Avitzur [1], and in particular to establish the effect of neglecting barrelling. Avitzur's analytical solution [1] was then used to interpret the experimental results. The tested specimen microstructure was examined and used to estimate the stress distribution in the specimen during deformation. Uneven deformation and fold-over diminished at higher strain rates.

Optimal surface finish and lubricant conditions were found for which experimentally measured coulomb friction coefficients lay between $\mu = 0.04$ and 0.08, with copper samples exhibiting marginally higher friction. By Avitzur's analytical solution [1] the error in SHPB tests under these recommended conditions was estimated to lie between 1% and 2%. The results show that roughened compression and specimen surfaces, lubricated with a suitable grease containing molybdenum disulphide, are useful in effectively reducing the error in SHPB tests due to friction effects.

ACKNOWLEDGEMENTS

I would like to extend my most sincere appreciation to the following people. Without their advice and contributions successful completion of this project would not have been possible.

Professor G.N. Nurick for supervising the work. His willing advice and guidance was much appreciated.

Mr. T. J. Cloete for his advice, assistance and enthusiasm throughout this project. His insight and knowledge of the subject were invaluable and he provided help and encouragement at all times.

Associate Professor R. Knutsen for his advice with the material testing, preparation and analysis.

Mrs P. Parkross for her patient assistance in demonstrating and supervising the use of the equipment in the Materials Centre.

Mr J. Meyer for assistance with the electronics.

The workshop staff of the Department for their assistance and for the production of the specimens.

The administrative staff of the Department and Faculty.

The National Research Foundation, the Armaments Corporation of South Africa (ARMSCOR) and the University of Cape Town Postgraduate Funding Office for the financial assistance.

CONTENTS

LIST OF FIGURES

NOTATION

A	cross-sectional area
c	fundamental wave speed
d	diameter
E	elastic (Young's) modulus
E_{xy}	elasticity tensor
F	force
h	specimen thickness
l_o	initial specimen length
l_s	instantaneous specimen length
m	constant friction factor
P_{ave}	average surface (contact) pressure
R_i	inner radius
R_n	neutral radius
R_o	outer radius
t	time
U	anvil (compression) speed
u	displacement
v	particle velocity
v_1	velocity of the specimen/incident bar interface
v_2	velocity of the specimen/transmitter bar interface
W_f	work to overcome friction
W_T	total work done
x	position along the bar of interest
ε	natural (logarithmic) strain (in accordance with the literature compressive strain is taken as positive throughout this work)
$\dot{\varepsilon}$	strain rate
μ	coulomb friction coefficient
ρ	mass density
σ	stress
σ_f	flow stress

σ_y	static yield stress
τ	shear stress

Subscripts

b	bar
i	incident stress pulse
o	initial
r	reflected stress pulse
s	instantaneous
t	transmitted stress pulse
1	incident bar
2	transmitter bar

1 INTRODUCTION

This report sets out the results of an investigation into the adverse effects of friction on high strain rate material characterisation tests conducted in compression using a Split Hopkinson Pressure Bar. Such an apparatus is currently in use at the University of Cape Town. This project forms part of an ongoing research effort in the field of structural impact by the Blast Impact and Survivability Research Unit (BISRU) within the Department of Mechanical Engineering at the University of Cape Town.

One of the goals of modern industry is to enhance the safety and efficiency of products and manufacturing processes. The metal-forming industry, for example, is continuously seeking better production techniques, and is achieving this objective through improved understanding and application of the physics governing metal behaviour. Mathematical descriptions of the complex thermo-mechanical interactions involved can be practically solved using numerical techniques. Advances in the field of computational mechanics continue to provide designers and engineers with the software required for product and process design and analysis [2]. Representative material behaviour models are fundamental to the accurate simulation of real systems. Thorough validation and verification of the numerical techniques used is also essential. These prerequisites to successful numerical analysis demand methods of experimentation that can provide accurate material test data and are precise enough to allow validation of numerical results [2].

Macroscopic tests of material samples are conducted to obtain data for models that attempt to describe material behaviour. Standard screw-driven or servo-hydraulic testing machines are generally used [3]. The force history is measured using remote load cells, under the assumption that the load cell is in equilibrium with the material sample. As the strain-rate is increased the material response time reduces to the order of the wave transit time in the load cell. Typical high strain rate tests are of such short duration that the stress waves reflecting within the cell begin to foul the readings and mask the specimen response. This places an upper strain rate limit of approximately $200s^{-1}$ on these conventional techniques.

The Hopkinson Bar approach overcomes this problem by creating what is essentially a very long load cell, designed to contain a complete stress wave. This allows measurement of the entire stress wave generated during the specimen loading, with no interaction between the initial wave and subsequent reflections. The true stress-strain history of the sample can then be obtained by the application of one-dimensional stress wave propagation theory. This technique has enabled material testing at strain rates between 10^2 and $10^4 s^{-1}$ [4]. Practical applications of such high strain rate data are found in, for example, (i) the high-speed metal forming, wire-drawing, shot-peening and shock welding industries; (ii) defence industries, in assessing armour and explosives interactions; (iii) the aerospace industry, from improving commercial airline safety to advancing satellite and space station technologies; (iv) structural design, for earthquake protection and (iv) occupied vehicle crashworthiness studies for road and rail transportation [3, 5].

Testing of materials at high rates of strain is necessary because their mechanical properties may differ significantly from those measured under quasi-static conditions. As the rate of strain is increased many engineering materials display a significant increase in the material flow stress from the quasi-static value [3]. This strain rate effect is incorporated into well-established material models such as the Johnson-Cook model [6], as used in finite-element computer codes [7]. Material behaviour models require accurate material parameters from valid material tests under all represented conditions. Gorham *et al* [8] suggest that for results to be consistent across different experimental configurations the absolute error in the calibration and resolution of results from high strain rate tests should be less than 1%. The Split Hopkinson Pressure Bar provides a method that is capable of providing material parameters with the required accuracy. However, errors due to friction effects need to be accounted for or effectively eliminated, as discussed in this work.

A major assumption made when calculating stress-strain curves from raw material test data is that the stress in the specimen is uniform [9]. In general, a compression test specimen is prone to the development of a non-uniform stress state due to the frictional constraint imposed on the specimen at the specimen-anvil interface. This results in the measured stress, which is assumed to represent the uniaxial flow stress of the material, being greater than the true flow stress. This investigation seeks to assess the error introduced due to friction for practical Split Hopkinson Pressure Bar test conditions, and to study the effect of variables such as lubricant and surface preparation.

The report begins with an overview of the Split Hopkinson Pressure bar technique and some of the limitations on this technique, particularly those due to friction. The friction problem is further clarified with a review of the relevant literature and the conclusions drawn from previous work, including an introduction to the experimental technique used in this work. The test method that was adopted for measuring friction is then discussed, along with the published analytical analysis that was used to obtain theoretical friction factors. This is followed by the results of a numerical investigation into this test method. Next the experimental details and results are presented and discussed. A study of the specimen microstructure, undertaken to identify the specimen deformation behaviour, is described. Finally the results of the various investigations are discussed, conclusions are drawn and recommendations made.

2 THE SPLIT HOPKINSON PRESSURE BAR

2.1 Introduction

The Split Hopkinson Pressure Bar is used to measure material properties at high strain rates. This chapter outlines the Split Hopkinson Pressure Bar technique, describing the history, the layout of the apparatus, the testing procedure and the theory and method used to analyse the results. Some of the uncertainties and errors inherent in the technique are introduced, such as those due to the effects of friction. The friction problem is expanded upon in *Chapter 3*.

2.2 History of the Hopkinson Pressure Bar Concept

In 1914 Bertram Hopkinson developed a method for measuring the pressures associated with dynamic events through a study of the propagation of stress pulses in a long metallic bar [3, 5]. Due to this pioneering work the application of stress wave theory in this fashion became known as the Hopkinson Pressure Bar technique [3]. Later Kolsky (1949) developed the Split Hopkinson Pressure Bar (SHPB) (also known as the Kolsky Bar) when he used two Hopkinson bars, arranged in series, to study the high strain rate response of material samples [3]. The technique was initially used for compression testing [9] and has since become the standard apparatus for conducting compression tests at strain rates between 10^2 and $10^4 s^{-1}$ [3,4,10]. Further work by several contributors has introduced modifications that allow testing in tension and torsion, across a range of temperatures and for a variety of material types [3,9]. Ongoing contributions and modifications have broadened the range of application of the Hopkinson Pressure Bar concept [3]. For a more detailed account the reader is referred to references [3,9,11].

2.3 Layout of a Typical Split Hopkinson Pressure Bar Apparatus

A schematic diagram of a Split Hopkinson Pressure Bar testing rig appears as *Figure 2.1*. A photograph of the equipment at the University of Cape Town is included in *Chapter 5*.

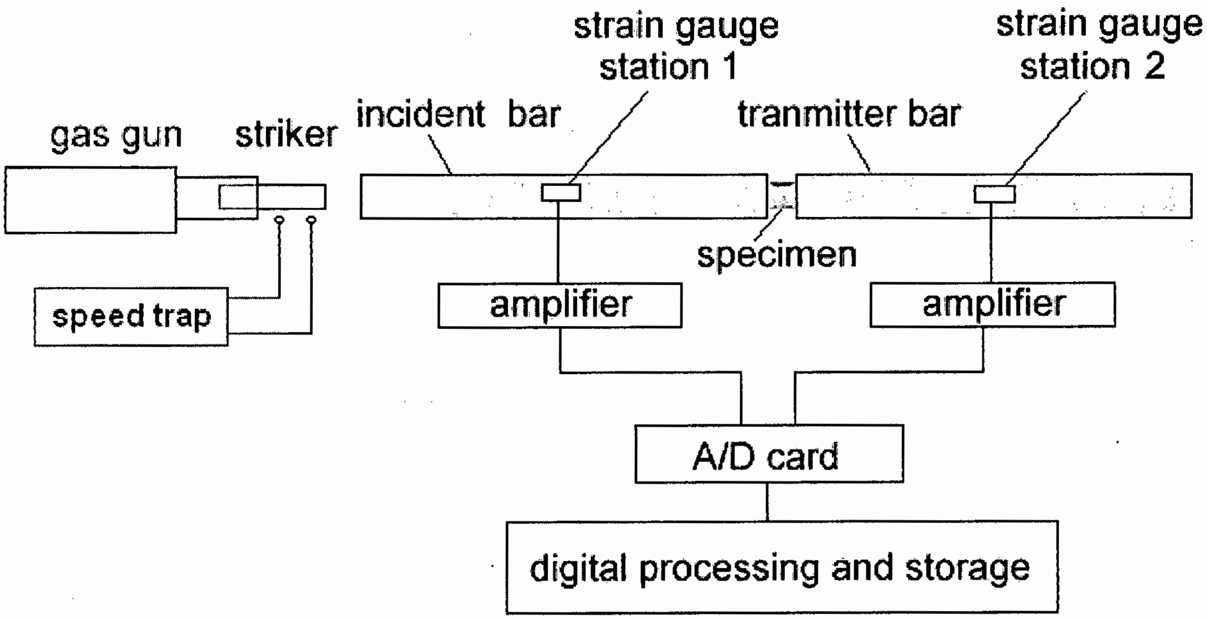

Figure 2.1 Schematic diagram of a Split Hopkinson Pressure Bar apparatus.

The apparatus typically consists of:

- **A gas-gun** capable of firing a cylindrical striker at up to 25m/s.
- **Two long, straight, round, metallic bars**. The use of high strength steel enables greater strain rates to be achieved, as the bars must remain within the elastic range at all times.
- **A stiff support structure** or mounting for the bars and the gas-gun.
- **Adjustable bar-supports**, to enable optimal alignment and support of the gas-gun barrel and the two bars, and often incorporating running-fit PTFE bushes that allow free movement in the axial direction.

- **An alignment system,** physical or optical, that ensures accurate alignment of both bars and the gas-gun barrel.

- **Two longitudinally mounted strain gauges** pasted on opposite sides of each bar to cancel bending effects, and connected using a Wheatstone bridge configuration. Dummy gauges are incorporated to cancel temperature effects.

- A **speed-trap** to obtain the velocity of the striker bar at impact. This velocity is required for calibration of the system.

- **Amplifiers** with a range of up to at least 1MHz.

- **Recording** equipment with a sampling rate of at least 10MHz.

2.4 Compression Testing using a Split Hopkinson Pressure Bar

This section contains an overview of the basic concepts and procedures applied when using a Hopkinson Pressure Bar apparatus for testing material samples in compression. The experimental approach followed in the current work is presented in more detail in *Section 5.4*. The necessary theory is briefly summarised in *Section 2.5*, with a more detailed account appearing in *Appendix A*.

A regular cylindrical compression test specimen is positioned axially between the bars and in contact with their end faces. A striker bar of the same material as the pressure bars and of a smaller or equal diameter is loaded into the barrel of the gas gun and fired at the free end of the incident bar. During impact a stress pulse is set up in the incident bar. This incident pulse travels along the incident bar and is measured at the first strain gauge station. Once this incident pulse reaches the bar/specimen interface it is partially reflected and partially transmitted through the specimen and into the transmitter bar. The reflected portion, known as the reflected pulse, is measured at the first strain gauge station as it travels back along the incident bar. The portion that is transmitted, known as the transmitted pulse, is measured at the second strain gauge station. A voltage-time signal is obtained by suitable amplification of the signal received from the strain gauge stations [5]. The recorded voltage-time signals are then used to obtain the velocity histories of the specimen-bar interfaces, from which the true stress-strain curve of the specimen is determined, along the lines of the method described in *Section 2.5.* A typical Split Hopkinson Pressure Bar voltage-time signal appears in *Figure 2.2* with the associated strain rate and true stress-strain curves appearing in *Figure 2.3.*

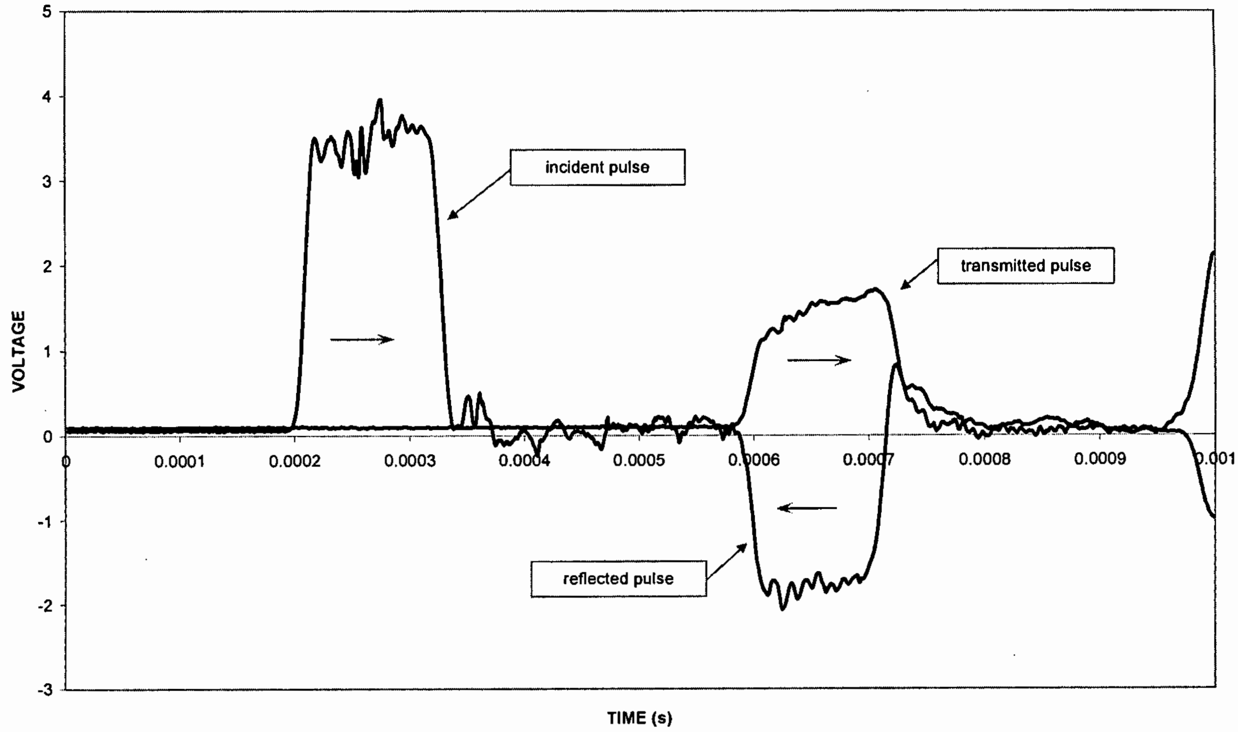

Figure 2.2 A voltage-time plot showing the typical signal obtained from a Split Hopkinson Pressure Bar compression test.

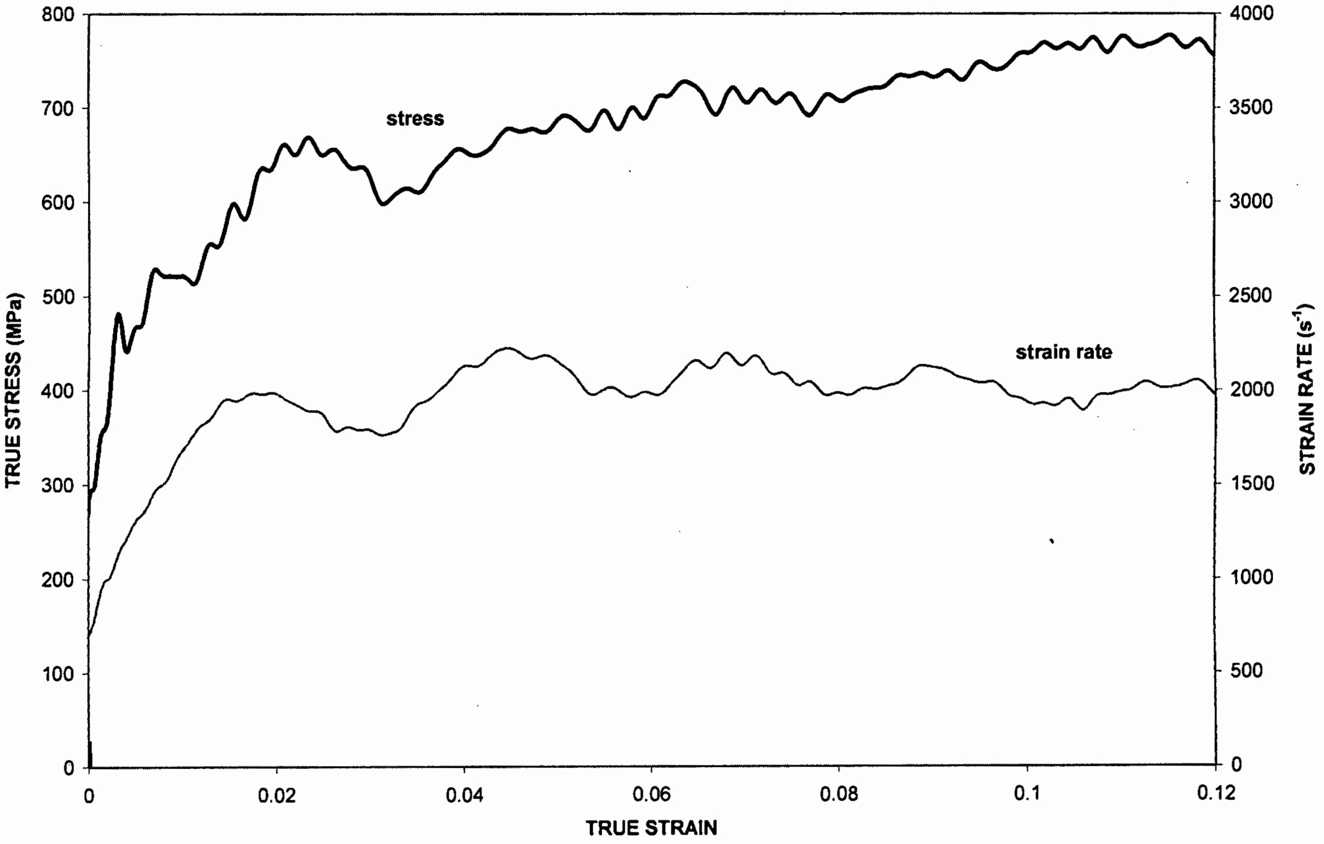

Figure 2.3 Graph showing the true stress-strain curve and the strain rate, as obtained from the voltage-time curve in *Figure 2.2*, for the compression of a strain-hardened copper specimen using a Split Hopkinson Pressure Bar.

The striker bar length and impact velocity affect the total strain and strain rate achieved in the specimen. A higher striker velocity results in a higher strain rate but a practical limit is reached since the stress induced cannot exceed the yield strength of the pressure bar material [3]. Selecting a higher strength material for the bar allows a higher strain rate to be achieved in the specimen. A greater striker bar length will result in a greater total strain. However both the incident and reflected pulses are measured at the first strain gauge station. Therefore, in order to avoid interference, the incident pulse must be shorter than the incident bar. The incident stress pulse set up initially will be twice the length of the striker bar (see *Appendix A*) and the striker bar is therefore chosen to be less than half the length of the incident bar.

2.5 A Summary of Split Hopkinson Pressure Bar Theory

The theory behind the Split Hopkinson Pressure Bar concept is presented in *Appendix A*. This section contains a brief summary, highlighting the aspects applied and approach adopted in the current work.

The Split Hopkinson Pressure Bar can be used to obtain the stress-strain curve of material samples at approximately constant strain rates in the $10^2 - 10^4 s^{-1}$ range. The method is based on the theory of one-dimensional stress wave propagation in long cylindrical rods. Although this theory is only approximate it is well understood, simple to apply and provides good results [9]. The important aspects of the theory [3] as applied in this work are briefly described in this section, with further details appearing in *Appendix A*.

One-dimensional elastic stress wave propagation theory is described by the well-known wave equation:

$$\frac{\partial^2 u}{\partial x^2} = \frac{1}{c^2}\frac{\partial^2 u}{\partial t^2} \tag{2-1}$$

where u is displacement, t the time and c, the wave speed in the bar material, is a constant given by:

$$c = \sqrt{\frac{E}{\rho}}$$

The general solution to the wave equation is:

$$u = f(x - ct) + g(x + ct) = u_i + u_r \tag{2-2}$$

where u_i and u_r are the displacements of the particles in the incident bar due to the incident and reflected waves respectively and f and g are functions that describe the incident and reflected wave shapes.

Differentiating *Equation* (2-2) with respect to x gives the strain in the incident bar, ε_1

$$\varepsilon_1 = f' + g' = \varepsilon_i + \varepsilon_r$$

For the transmitter bar *Equation* (2-2) takes the form:

$$u = h(x - ct) = u_t \tag{2-3}$$

where h describes the transmitted wave shape and u_t the particle displacement in the transmitter bar. The strain in the transmitter bar, ε_2, is then:

$$\varepsilon_2 = h' = \varepsilon_t$$

Differentiating *Equations* (2-2) and (2-3) with respect to time provides the velocities at the bar end faces, v_1 and v_2, illustrated below.

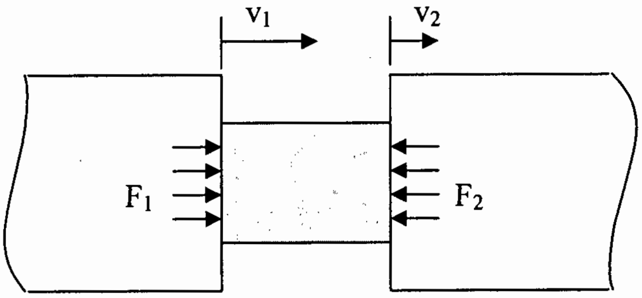

Figure 2.4 Schematic diagram of the specimen and bar end faces.

Thus

$$v_1 = c(-f' + g') = c(-\varepsilon_i + \varepsilon_r) \tag{2-4}$$

and

$$v_2 = c(-h') = -c\varepsilon_t \tag{2-5}$$

The ends of the bar are assumed to remain in contact with the specimen and v_1 and v_2 can therefore be used to determine the strain rate in the specimen:

$$\dot{\varepsilon} = \frac{v_1 - v_2}{l_s}$$

or

$$\dot{\varepsilon} = \frac{c}{l_s}(-\varepsilon_i + \varepsilon_r + \varepsilon_t) \tag{2-6}$$

where l_s is the instantaneous specimen length and can be found by:

$$l_s(t) = l_o - \int_{t=o}^{t} v_1 - v_2 dt$$

In order to be able calculate the stress in the specimen it is assumed that:

1. The specimen is in force equilibrium.
2. The specimen is deforming uniformly.

Thus $$F_1 = F_2$$

The forces acting on the specimen can be determined from the material properties of the bars, since, by definition

$$F_1 = AE(\varepsilon_i + \varepsilon_r)$$
$$F_2 = AE(\varepsilon_t)$$

And thus

$$\varepsilon_i + \varepsilon_r = \varepsilon_t$$

Substituting this relation into *Equation* (2-6) allows the strain rate to be determined using only the reflected strain.

$$\dot{\varepsilon} = \frac{2c\varepsilon_r}{l_s} \tag{2-7}$$

The true strain in the sample is determined by integration of *Equation* (2-7). By definition, $\sigma = F_2/A$, and the true stress in the sample is therefore:

$$\sigma(t) = \frac{AE\varepsilon_t}{A_s} \tag{2-8}$$

where the instantaneous area, A_s, can be calculated by assuming plastic incompressibility in the specimen, i.e. $A_o l_o = A_s l_s$. *Equations* (2-7) and (2-8) were used to obtain the strain rate and the stress in the specimen for the high strain rate experimental work conducted, as presented in *Chapters 5* and *6*. Split Hopkinson Pressure Bar theory is presented in greater detail in *Appendix A* and for further information the reader is referred to references [3,4,5,9].

2.6 Limitations of the Split Hopkinson Pressure Bar Technique

It is essential in any material test that steps are taken to minimise the effects of apparatus-specific conditions on the measured specimen response, and hence on the inferred material characteristics. The major assumptions underlying the measurement of material data using the Split Hopkinson Pressure Bar method are [11]

- Uniform stress and strain in the specimen
- One-dimensional stress in the specimen

Any deviation from this assumed stress state results in spurious effects in the resulting stress-strain curve such that it no longer accurately represents the material behaviour.

The diameter of the specimen relative to the bars is chosen so that the forces induced at the interfaces will cause the specimen to undergo plastic deformation. Elastic wave theory is therefore not applicable in the analysis of specimen behaviour. For the purposes of data analysis it is assumed that the stress state in the specimen is uniform and uniaxial and that the specimen is deforming uniformly. However several stress wave reflections must occur within the specimen before these assumptions are valid. A finite period is required for stress waves to travel back and forth through the specimen thickness and this is known as the 'ring-up' or specimen rise time [3]. The above analysis can only be correct after this initial 'ring-up' time has elapsed and the specimen has reached force equilibrium. Ensuring that the specimen is short relative to the main body of the stress pulse allows several reflections to take place during the early stages of the test. The measured data is then useful at lower strains as the 'ring-up' time forms a smaller portion of the test duration. Another useful technique to make useful data available at earlier strains is to increase the rise-time of the incident pulse by pulse-shaping [3], as described in *Section 5.4*.

However, even after this 'ring-up' period, force equilibrium and a one-dimensional, uniform stress state cannot be guaranteed [2,10]. Friction and inertia can both result in non-uniform stress states in typical Split Hopkinson Pressure Bar compression test specimens [8,11]. Reducing the specimen thickness reduces the effect of the specimen 'ring-up' time but increases the effects of friction and radial inertia. A thinner specimen has a greater relative area in contact with the compression anvils and hence a greater proportion of material affected by friction [11]. The specimen aspect ratio therefore plays an important role in determining the validity of test results and several different configurations have been used by various authors [3,11]. Some compromise is required to minimise 'ring-up' time, while simultaneously limiting the adverse effects of friction and inertia.

Inertia of the deforming specimen may cause a non-uniform stress distribution. Radial inertia causes a radial restraint, resulting in a hydrostatic or hoop stress in the specimen. Analytical studies of inertia have been conducted. Gorham [12] used an energy balance approach to analyse the axial compression of a cylindrical specimen. He suggested that the inertial error may exceed 1% in many popular test configurations. However he noted that the assumption he made of uniform deformation of the specimen is not valid if inertia becomes significant. He therefore recommended that his analytical approach is not used to correct experimental data but rather to design tests for which the effects of inertia can be determined to be theoretically negligible [8,12]. This can be achieved by reducing the specimen size and by altering the specimen aspect ratio.

The effects of friction are largely dependant on the surface condition of the bars and specimen and the lubricant used. The mechanism of friction is highly complex and not fully understood [13]. Hence, at present no method exists for predicting the theoretical friction for given test conditions, necessitating an experimental approach. The results of some published investigations are reviewed in *Chapter 3*. Some useful data has been produced and theoretical methods do exist for inferring the error due to friction for experimentally measured conditions. However, to the author's knowledge no universal standard currently exists for inferring the error in Hopkinson Bar test results from measured friction parameters. The ASM Handbook [4] mentions friction and the fact that this may introduce some error but provides no method for estimating the potential extent of this error. Lubrication is recommended but caution is required as even a very thin (25μm) lubricant layer may influence the timing of the recorded stress pulses, affecting the results [4].

In order to improve the quality of high strain rate data, a thorough investigation into the effects of friction in Split Hopkinson Pressure Bar tests is required. The aim of the current work is to address some of the issues raised in this section. Numerical and experimental approaches were pursued, in line with investigations that appear in the literature. A review of published investigations appears in the next chapter.

3 FRICTION IN SPLIT HOPKINSON PRESSURE BAR TESTS

3.1 Introduction

Friction, as mentioned in the previous chapter, can result in errors in Hopkinson Bar test results. This chapter begins with a review of some of the published investigations that have been conducted in trying to assess the effects of friction. The ring compression test, used in the current work to measure friction, is introduced. Next an analytical analysis of this test by Avitzur [1] is discussed. Published work in which this solution has been used to interpret experimental results is then reviewed. The conclusions and recommendations arising from a previous experimental investigation are then discussed. The chapter concludes with a summary of the results obtained in these investigations and applied in the current work.

3.2 Friction Investigations Applicable to Hopkinson Bar Tests

Stresses obtained from Hopkinson Bar tests are assumed to represent the true uniaxial flow stress of the material. When testing in compression friction between the specimen and the compression surface acts as a radial constraint. This produces a hydrostatic stress that is superimposed over the assumed deviatoric stress state, resulting in a non-uniform, tri-axial stress state in the specimen. This violates the necessary assumption of uniform, one-dimensional stress and results in a stress-strain curve that does not reflect the true material flow stress [3,9,10,14].

Friction is suspected to be the cause of the greatest error in Hopkinson Bar tests [8,10]. Mousawi *et al* [9] and Bertholf & Karnes [11] have shown that the measured stress may exceed the one-dimensional flow stress and that this error can be mistaken for a strain rate dependant material response. They conclude that efforts to reduce friction are essential. The following sections contain an overview of published investigations conducted in an attempt to characterise and account for the effects of friction in Hopkinson Bar tests.

3.2.1 Analytical Studies

Gorham *et al* [8] quote the result of an analytical analysis by Siebel which gives the pressure required to compress a cylindrical specimen that is subject to frictional restraint as:

$$P_{ave} = \left(1 + \frac{\mu d}{3h}\right)\sigma_y \qquad (3\text{-}1)$$

where P_{ave} is the average pressure, σ_y is the material flow stress, μ is the coulomb coefficient of friction and d and h are the diameter and height of the specimen. This result provides an estimate of the apparent strength increase due to friction, provided the theoretical friction coefficient, μ, can be obtained for given test conditions. The aspect ratio of the deforming specimen with time is also required in the form of the d/h ratio as this has a significant effect on the pressure required to effect deformation. As the specimen height is reduced and the outer diameter increases a larger relative area comes into contact with the anvils and the total work required in overcoming friction increases.

In reference to the early experimental work of Davies & Hunter [15], Gorham *et al* [8] demonstrated that the approximate values obtained for μ of between 0.02 and 0.06 would result in an error in the experimentally measured material flow stress of between 1.3% and 4%, for the specimens used. Gorham *et al* [8] cautioned that for a typical Hopkinson bar test scenario the coulomb friction coefficient is not constant in either space or time and hence that this analysis is only suitable for obtaining an estimate of the error. They recommended that a comprehensive test series be conducted to establish values of μ for a variety of Hopkinson bar test conditions, in an attempt to obtain a more precise and accurate estimate of the effect of friction. They also suggested that published Hopkinson Bar results include specific details of the specimen surface preparation and the method of lubrication, and if possible an estimate of the frictional restraint or the error in the results due to friction.

3.2.2 Numerical Studies

Bertholf & Karnes [11] used a Lagrangian finite element code to conduct a two-dimensional analysis of the Hopkinson Bar system to investigate the effect of friction and to assess the accuracy of various published analytical results of the effects of friction and inertia. By comparison with published experimental results they determined that for a relatively thin specimen with a height:diameter ratio of 0.3 a coulomb coefficient of friction, μ, of 0.02 could introduce a 2% error in the measured stress and with $\mu = 0.1$ the error may well be over 8%. They also found that friction introduced non-uniformities in the axial stress of around 10%, as well as a 10% deviation from a uni-axial stress state. They concluded however that proper lubrication should limit friction errors to acceptable limits.

Meng & Li [16] expanded on this work by testing various friction coefficient and aspect ratio combinations. The simulations conducted were modelled on the work of Bertholf & Karnes [11] and showed good correlation.

3.3 Characterising Friction

Characterising friction for given conditions is difficult because of the combined effects of the following variables [13, 17]:

1. Surface properties that differ from those of the bulk material due to corrosion and entrained contaminants.
2. Lubricant conditions and the unknown lubricant state under stress.
3. Surface roughness that changes with deformation.

Due to the complexity of the phenomenon and the influence of the above variables the friction problem is not readily amenable to analytical analysis. Many investigators have therefore adopted an experimental approach. Traditionally friction testing involves using some form of sliding rig to measure the shear forces between contacting surfaces in relative motion. The loads are below the yield limit of the material and so there is no plastic deformation and the stresses in the material remain relatively low. It may be argued that this arrangement differs fundamentally from the conditions of Split Hopkinson Bar testing, to the extent that the results are not applicable.

3.4 The Ring Compression Test

Characterising friction for the specific case of Split Hopkinson bar compression testing requires an experimental technique that adequately represents the large plastic deformation that takes place. The ring compression test involves large loads and significant deformation. Male & Depierre [14] report on the development of this test by Kunogi and on the refinement of the method by Male & Cockroft. Walley *et al* [10], Gorham *et al* [8] and Male & Depierre [14] recommend this test as a means of investigating friction during forming operations.

The test involves compressing a flat ring or annulus between parallel faces or anvils. This causes the inner and outer diameters to change, in accordance with the principle of mass conservation. For frictionless conditions a ring would be expected to behave as if it were a part of a solid disc, with the inner and outer diameters expanding in proportion to their distance from the centre. However, when friction is present this radial expansion is constrained. The resulting inner and outer diameters are found to be less than would be the case if friction were zero. *Figures 3.1* and *3.2* illustrate this behaviour as observed in typical aluminium ring compression test specimens.

(a) *(b)*

Figure 3.1 Photographs of typical ring compression test specimens (a) before and (b) after compression for low friction conditions, as can be achieved by using grease and a lightly roughened surface finish (note the enlarged internal diameter).

(a) *(b)*

Figure 3.2 Photographs of typical ring compression test specimens (a) before and (b) after compression for high friction conditions, as would result when testing specimens without lubrication (note the reduced internal diameter).

The internal diameter provides a sensitive measure of friction conditions as it shows a distinct change in behaviour, expanding initially but later shrinking if the friction is high enough. Avitzur [1] assumes, in his analytical analysis of this method, that the change in the geometry depends only on the friction conditions and not on the forming force required. If this assumption is reasonable it presents a major advantage of the ring compression test in that the deformed geometry alone provides a measure of the frictional restraint and no direct measurement of force is required. Thus the need for accurate values of the flow stress of materials under varying conditions is negated, eliminating a major source of uncertainty.

Factors that will influence the results of this test are the initial ratio of the internal and external diameters and the thickness of the annulus used. Specimen geometries are generally referred to by giving the ratio of external diameter:internal diameter:thickness. A specimen geometry ratio of 6:3:2 is described by Male & Depierre [14] as a ‘standard’ geometry. They investigated the effects of varying this ratio, as discussed in *Section 3.6*, and concluded that the 6:3:2 geometry was the best overall geometry for friction measurement.

Analytical analyses of the ring compression test have been performed. An estimate of theoretical friction factors can be obtained by comparing experimental results with these analyses [10,14]. The solution used in this work to extract theoretical friction factors is described in *Section 3.5*.

3.5 An Analytical Solution of the Ring Compression Test by Avitzur

Avitzur presented an analytical solution in 1964 [1] and this has been widely used as a basis for comparison with experimental results [8,14]. An energy approach was used to find an optimum upper bound solution. The observable changes in the inner and outer diameters of a ring suggest that at any instant there exists a specific diameter upon which no radial movement occurs. This position is termed the neutral radius and was assumed to occur at a position such that the work done to deform the specimen to a given strain was minimised.

This work of deformation is made up of two components, the work done to deform the specimen plastically and the work to overcome friction between the specimen and the anvil. The work required for plastic deformation, as a result of Mises assumptions, is a function of the flow stress of the material and the interface surface area. This component will therefore increase linearly with cross-sectional area, and due to conservation of mass, with time. As the outer radius and inner radius change with time, the surface material is forced to slide while in contact with the anvils, giving rise to frictional work. Avitzur's approach [1] was to solve for the neutral radius assuming that these two components, with respect to time, sum to a minimum.

Figure 3.3 shows the predicted dimension changes for a ring initially of a 6:3:2 geometry ratio, and subject to an 'm' friction factor of 0.08. The ratio of forming pressure to material yield stress is plotted on the secondary axis.

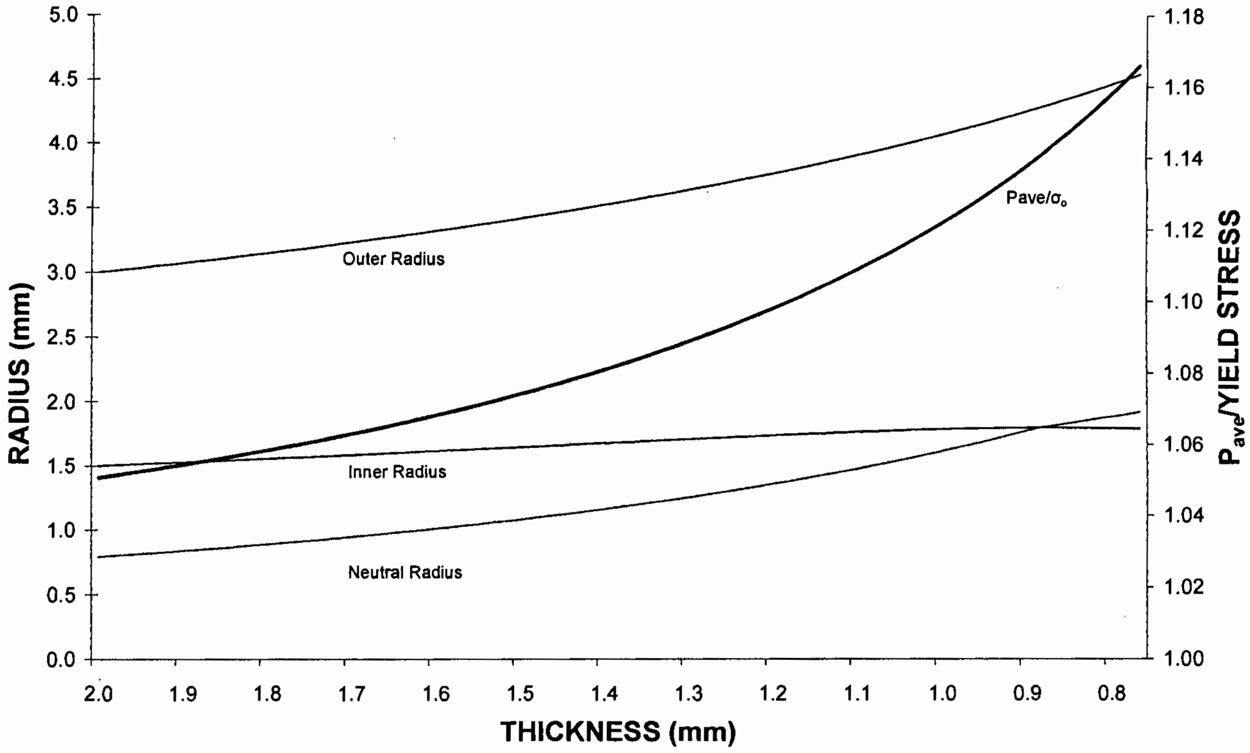

Figure 3.3 Graph showing the typical dimension changes and increase in forming pressure due to friction for ring compression test specimens with m = 0.08, as calculated using the results of Avitzur's analysis [1].

Avitzur [1] assumed that the material behaves according to the Levy-Mises' stress-strain rate laws, implying no strain-hardening, no elastic deformation and hence no volume change. Strain hardening may become substantial for metals and hence the theory becomes less accurate at higher strains, as noted by Male & Depierre [14]. Avitzur [1] also neglected out-of-plane strain and assumed that the frictional stress was transmitted uniformly through the specimen. These assumptions led to a velocity field that effectively precluded barrelling of the specimen. This approximation is less accurate at higher strains as barrelling or 'bulging' becomes significant.

In order to find a closed form solution Avitzur [1] had to use the constant shear stress assumption, which fixes the frictional stress at a constant fraction of the yield stress, expressed as:

$$\tau = m\frac{\sigma_y}{\sqrt{3}} \tag{3-2}$$

This is also known as the constant friction factor or 'm' factor friction model. Male & Depierre [14] point out that, provided this approximation is valid, strain hardening may be conveniently neglected because the frictional stress, τ, remains a constant fraction of the increasing yield strength of the material. Thus the analysis may be performed over small increments of strain where for each increment the constant 'm' factor would imply that the yield stress and frictional stress show a proportional increase.

Avitzur's solution [1] can be used to infer effective theoretical friction factors from ring compression test results [8,11,14], by a comparison of the measured change in internal diameter with the analytical prediction. Avitzur [1] calculated the extent to which the work required to overcome friction causes the required forming pressure to exceed the value predicted based purely on the yield strength of the material. This ratio (average pressure/yield stress) can be obtained for a ring specimen and for the special case of a solid cylinder, as is typically used for Hopkinson Bar test specimens. Thus the error in Hopkinson Bar tests for various friction conditions can be inferred. For the special case of a solid cylinder Avitzur's solution [1] predicts

$$P_{ave} = (1+\frac{m}{3\sqrt{3}}\frac{d}{h})\sigma_y \tag{3-3}$$

The result of *Equation* (3-3) is plotted in *Figure 3.4* in terms of the expected error in SHPB tests for given 'm' friction factors for a typical SHPB cylindrical specimen with a height:diameter ratio of 1.

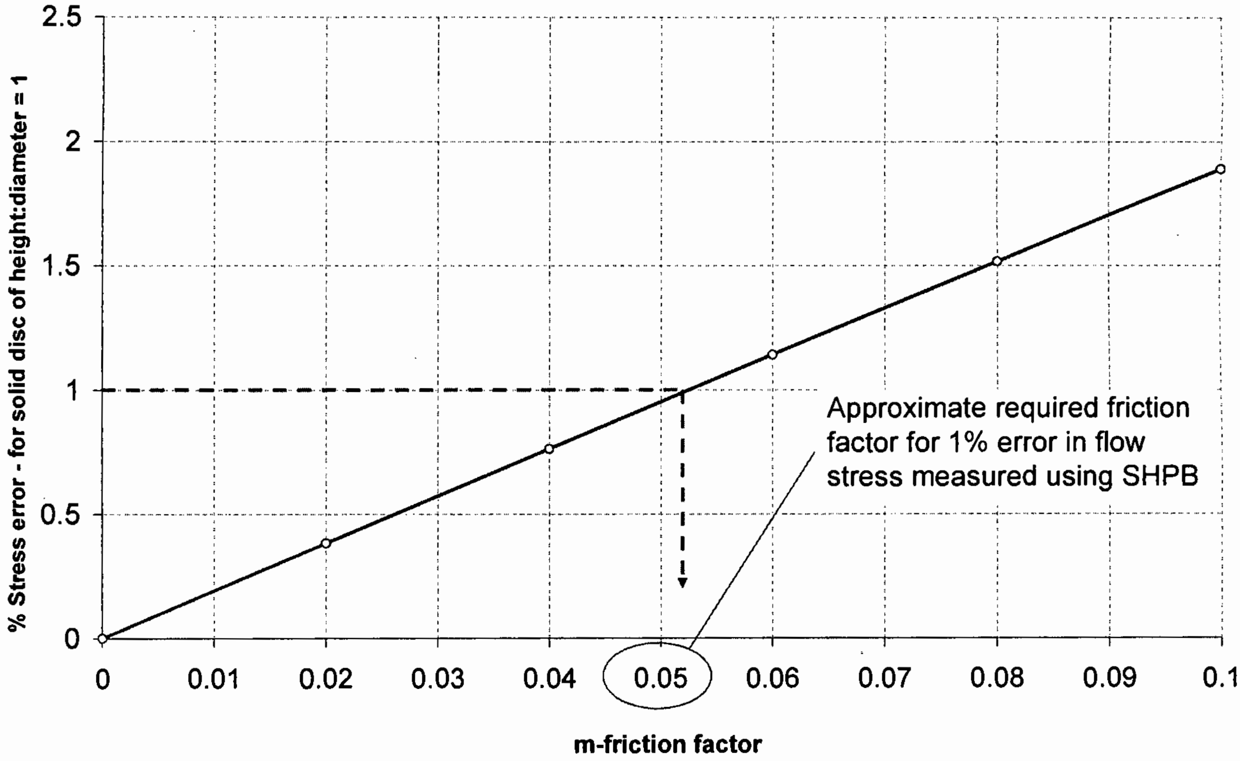

Figure 3.4 Graph showing the predicted percentage by which the actual forming pressure for a cylinder exceeds that for assumed uniform uniaxial stress, as for SHPB tests, for different friction factors, according to Avitzur's theory [1].

The curves of internal diameter change for a given strain as generated for the ring specimen geometry tested (6:3:2) are shown in *Figure 3.5*. The x-axis indicates percent logarithmic compressive strain and the y-axis indicates the percent increase in internal diameter. The different curves indicate different assumed values for the constant 'm' friction factor, as indicated and discussed below.

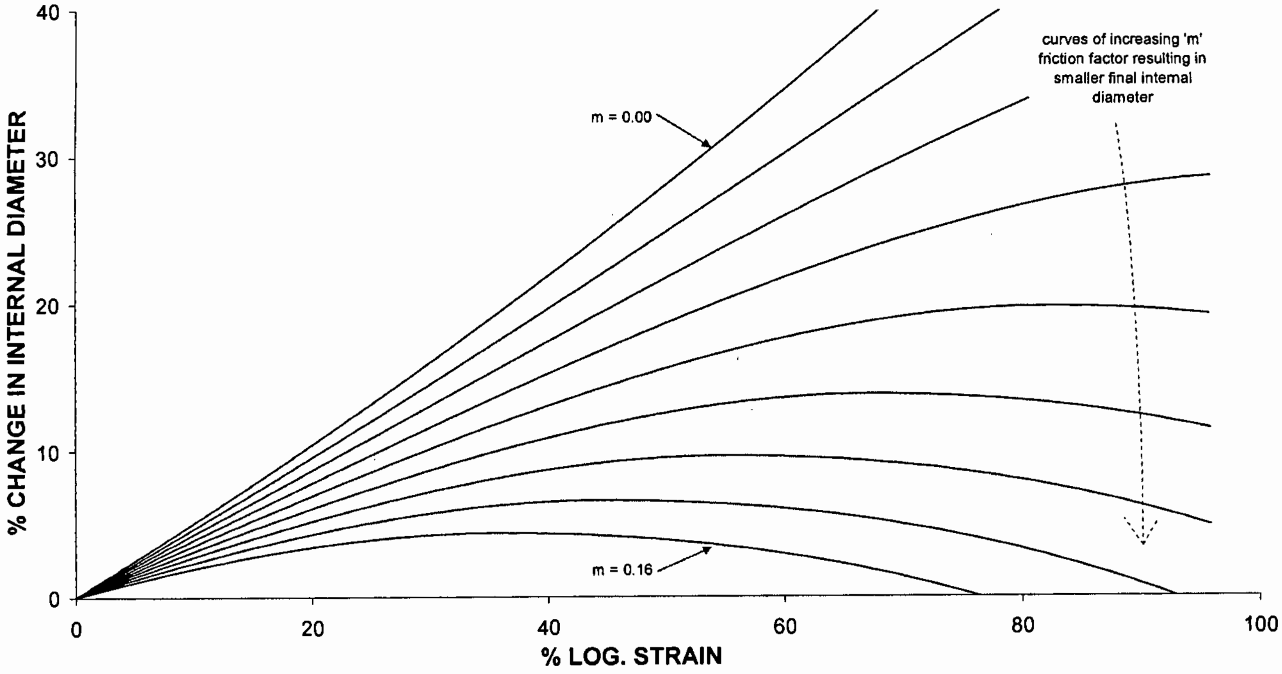

Figure 3.5 Typical theoretical curves as generated according to Avitzur's solution [1] for a 6:3:2 specimen geometry and m factors from 0.00 to 0.16.

The widely used coulomb coefficient of friction, μ, can be derived, for small values of m and μ, from the 'm' factor by expressing the shear stress in terms of these two constants:

$$\tau = \mu P_{ave}$$

and

$$\tau = m\frac{\sigma_y}{\sqrt{3}}$$

thus

$$\mu = \frac{m}{\sqrt{3}}\frac{\sigma_y}{P_{ave}} \qquad (3\text{-}4)$$

where P_{ave}/σ_y, the ratio of the average surface pressure to the yield stress of the material, is a product of Avitzur's solution [1].

This ratio was thus required to convert the 'm' factors that were used to generate geometry changes using Avitzur's solution [1] to the equivalent coulomb coefficients. Equivalent coulomb coefficients were needed for comparison with the numerical investigation discussed in *Chapter 4* and other published analyses based on coulomb friction. The above result also demonstrates the correlation between *Equation (3-1)* and *Equation (3-3)* for small values of m and μ. From the definition above only one of the two different theoretical coefficients can remain constant during a given deformation process and so an average value was generally used where comparisons between 'm' factors and coulomb coefficients were made. Where necessary a discontinuous, step-wise approximation was used. *Table 3.1* gives equivalent m-factors and coulomb coefficients. The exact values, as specified to generate analytical and numerical solutions are included for the 'm' friction factors and the coulomb coefficients used, with the approximate equivalent values providing a quick reference between the two coefficients.

m	μ
0.00	0.000
0.04	0.023
0.08	0.046
0.12	0.069
0.16	0.092
0.20	0.120

μ	m
0.00	0.000
0.02	0.035
0.04	0.069
0.06	0.103
0.08	0.138
0.10	0.173

Table 3.1 Approximate m-factor and coulomb coefficient conversion table for the values typically assigned analytically and modelled numerically in this work.

A summary of the approach followed by Avitzur [1] and the relevant solutions appear in *Appendix B*, along with the method followed and calculations for generation of curves from the analytical solution.

3.6 Studies Conducted using the Ring Compression Test

In an attempt to establish the validity of various analytical and numerical solutions used to calibrate the ring compression test, Male & Depierre [14] experimented at the two extremes of friction, maximum or sticking friction, and as close to zero friction as possible, at strain rates around $25s^{-1}$. Sticking friction was assumed when no tiny scratches were observed on the anvils, indicating that no relative motion had taken place. Conditions for sticking friction were achieved at very specific temperatures for specific materials, with tiny scratches observed under all other conditions. Minimum friction was approached by compressing wax rings, heated to just below the melting point, between anvils heated to just above the melting point. The melted wax layer was assumed to provide almost zero frictional restraint.

A comparison of these results with Avitzur's analytical curves [1] is shown in *Figures 3.6, 3.7* and *3.8*. As can be seen a practical minimum friction factor between m = 0.02 and m = 0.14 was achieved during the compression of wax rings. For the experiments under conditions of sticking friction 'm' values in excess of unity were recorded.

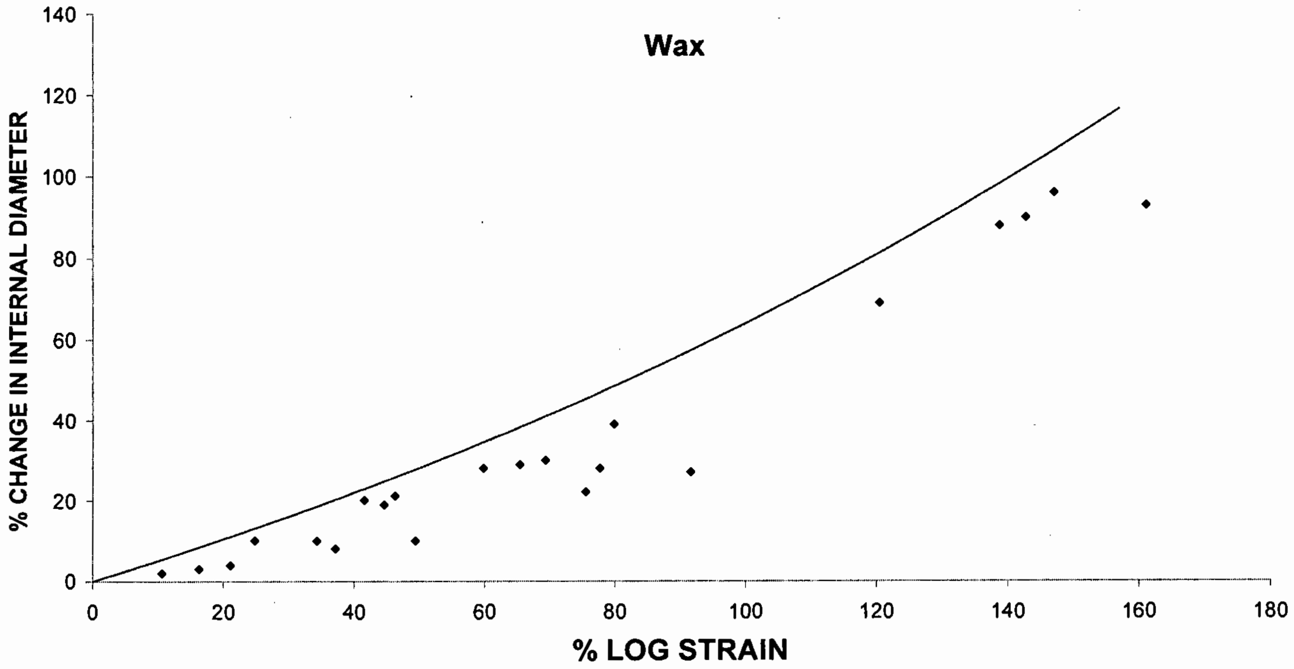

Figure 3.6 Graph showing practical minimum friction test result of Male & Depierre [14] as obtained using wax rings, plotted with the theoretical zero friction (m = 0) line according Avitzur's solution [1].

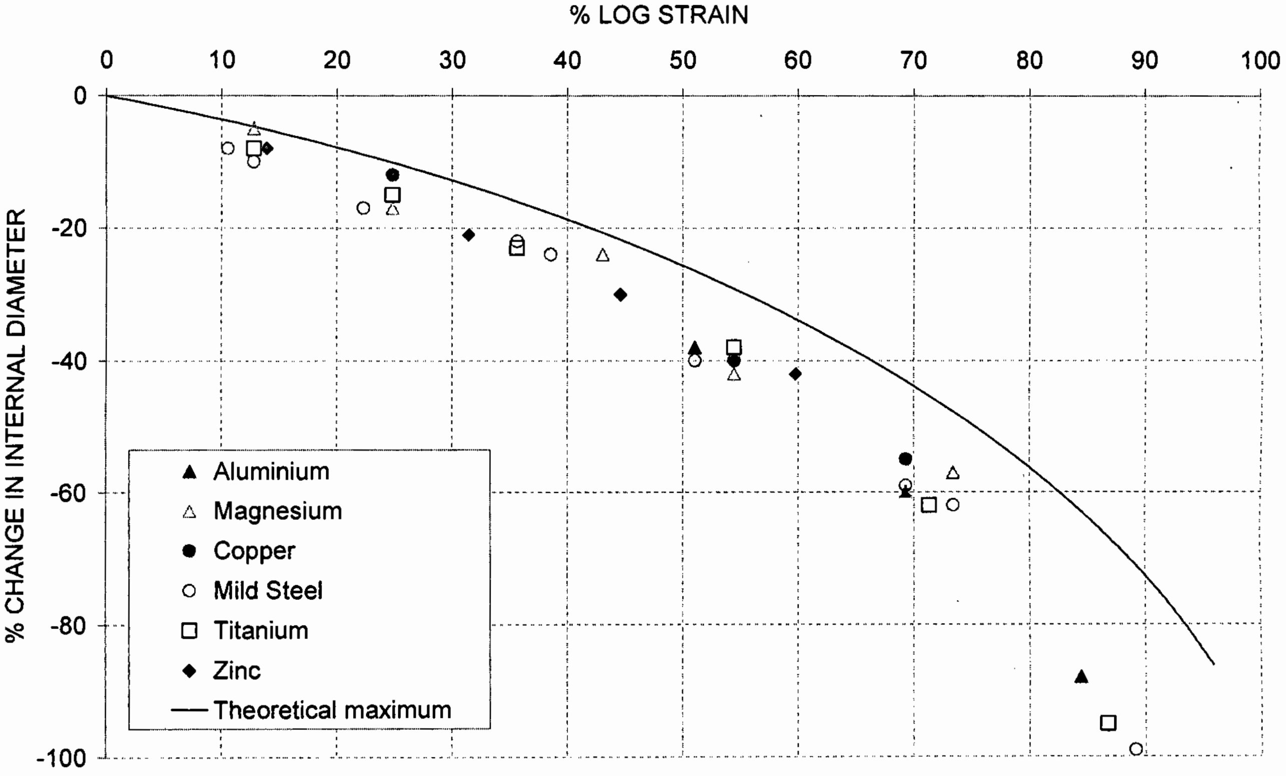

Figure 3.7 Graph showing results of maximum (sticking) friction experiments [14], against theoretical maximum friction [1].

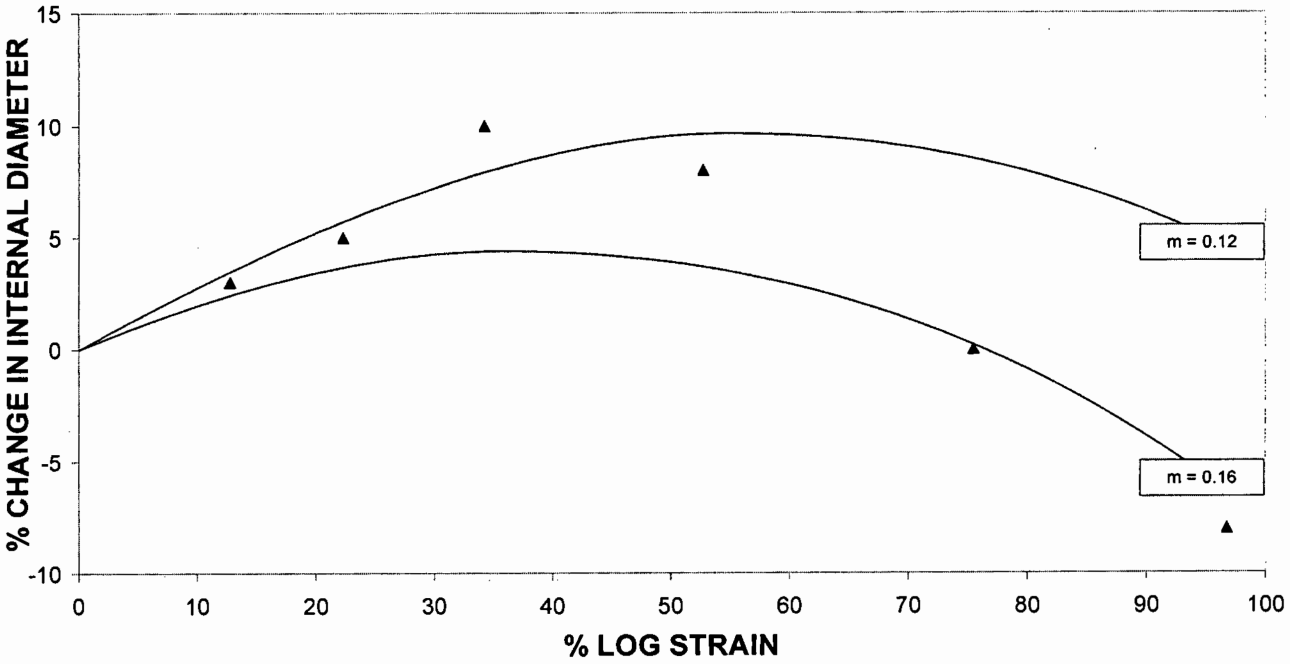

Figure 3.8 Graph showing typical result from tests by Male & Depierre [14] on aluminium using paraffin oil as a lubricant, against theoretical curves as indicated [1].

Under high friction conditions excessive distortion of the specimen is likely to occur, with attendant strain hardening and fold-over of the specimen edges, as described by Schey [18]. Fold-over describes the collapse and rotation of the sides of the ring onto the compression anvils so that they become part of the frictional surface, as noted by Walley *et al* [10]. The topic is addressed more fully in *Chapter 7*. Such behaviour contrasts sharply with the assumptions of Avitzur's analysis [1] and could explain the recorded 'm' values in excess of unity. The authors therefore caution against over-optimistic interpretation of test results and acknowledge the counsel of Schey, who noted in reviewing the work [10] that the friction theories used are highly idealised and that the actual behaviour involves a complex, unknown combination of sliding and sticking friction. Nevertheless the general applicability of Avitzur's analysis [1] under low friction conditions was demonstrated by the overall correlation between the analytical solution and the experimental results. They concluded that the results of Avitzur's analysis [1] are reasonably accurate to approximately 50% strain, and display better correlation for lower friction conditions and thinner specimens.

Various material, lubricant and ring geometry combinations were also tested with the 'm' friction factor ranging between 0.08 and 0.10 for a 6:3:2 geometry specimen and 0.06 and 0.14 for a 6:3:1 specimen. They experimented with specimens of varying height and internal diameter, under maximum friction conditions. Good agreement in predicted 'm' factors was found when changing the internal diameter through 6:4:2, 6:3.2:2, 6:2.4:2 and 6:1.6:2 geometries and they concluded that the theory was consistent and independent of internal diameter.

When reducing the specimen height through the 6:3:2, 6:3:1 and 6:3:0.5 geometries the thinner specimens showed better correlation with the theory. This was attributed to the theoretical assumption that the frictional restraint is transmitted uniformly through the specimen height, which infers that there should be no barrelling.

As a first estimate Avitzur's results [1] predict that m-factors of between 0.08 and 0.14 translate to a theoretical friction error in Hopkinson Bar tests of between 1.6% and 2.8% initially and increasing with increasing strain to over 2% and 3.5% respectively. Although these errors are reasonably small conditions need to be established that provide consistently low friction and ideally enable the friction error to be kept consistently below 1%.

By comparison with some of their previous experimental work that was correlated against a coulomb friction model Male & Depierre [14] reported the following approximate empirical relationship between m and μ for ring specimen tested to 50% strain:

$$m \approx 2\sqrt{3}\mu$$

This relationship is a factor of two greater than that suggested by a comparison of *Equation 3-1* and *Equation 3-3* for a solid cylinder and would suggest that the friction effect was significant in these tests.

Gorham *et al* [8] recommended the ring compression test as a useful method for investigating friction in Split Hopkinson Bar tests and suggested that it may be possible to obtain parameters and predictions of sufficient accuracy to allow SHPB data to be corrected. Conditions such as lubricant and surface roughness play a large role in the friction experienced and thus different experimental parameters need to be tested to determine the effect of friction. Using aluminium specimens of a 4:2:1 geometry on very smooth anvils they obtained the results in *Table 3.2*.

Surface Lubricant	3µm diamond-polished	600-grade SiC	Bead-blasted
Rocol A.S.P.	0.03 - 0.07	0.02 - 0.08	0.05 - 0.09
Rocol J166	0.04 - 0.06	0.02 - 0.04	0.05 - 0.07
Graphoidal Developments BG15	0.01 - 0.07	0.03 - 0.05	0.05 - 0.09

Table 3.2 Estimated 'm' friction factors for high strain rate ring compression tests by Gorham *et al* [8] for a variety of finishes and lubricants.

From these results it seems that an m factor of about 0.05 can be practically achieved if care is taken in specimen lubrication and preparation. Gray [3] confirmed this estimate of $m \approx 0.05$ as a practical limit for friction under Hopkinson Bar conditions and also recommended the ring compression test for measuring friction experimentally. He suggested the following practices in attempting to reduce friction and hence the error in Hopkinson Bar tests [3]:

1. The use of a suitable molybdenum disulphide grease. Thin films of lubricant are required to avoid influencing transmission of the stress pulse.
2. Limiting the strain in any one test to less than 20%. The same sample may be loaded repeatedly to obtain greater strains.
3. Re-machining of a specimen to remove barrelling between successive tests
4. Avoiding high interface velocities between the specimen and bar to prevent lubricant breakdown. This can be achieved by using very small specimens

Walley *et al* [10] presented a unique approach to the investigation of friction by expanding on the ring compression test using high-speed photography and numerical modelling. Numerical modelling of contact problems remains very difficult because constitutive models have not yet been developed to fully describe interfacial friction, due to the complex nature of the phenomenon. An assumption inherent in all theoretical analyses and hence incorporated into results derived from experimental work is that friction remains constant. This is probably violated by lubricant breakdown, lubricant ejection or jetting, a change in the surface roughness due to deformation, and fold-over. These effects have not been adequately investigated. Walley *et al* [10] assumed a constant coefficient of friction or Coulomb model, with μ between 0.1 and 0.2. A coefficient of $\mu = 0.1$ (equivalent to $m \approx 0.2$) gave the best correlation with their experimental results, indicating that friction may well be high, even when using a suitable lubricant, such as MoS_2 or graphite-based lubricants.

3.7 Conclusions drawn from a Previous Investigation using the Ring Compression Test at Low Strain Rates

A previous investigation in the form of a final year research project [19] had been undertaken to establish a test methodology for investigating friction. The ring compression test, as described above, was used. This test is dependant upon a number of factors in the preparation and testing process, the influence of which need to be assessed before an accurate and reliable test methodology can be established. Some of these factor are:

- The method used for bulk specimen preparation, which influences:
    - The consistency of the surface finish
    - The accuracy and repeatability of dimensions and regularity
- The protection of specimens from corrosion between preparation and testing
- The amount and type of lubrication
- The hardness of the compression anvils

Specimens were machined in large batches, demanding careful quality control. Abrasion or grinding was used to generate the desired surface and specimens were carefully examined during this process. To make potential Split Hopkinson Pressure Bar testing as practical as possible the range of investigated surface finishes was limited to readily available SiC grinding papers and standard polishing equipment. 600-grit, 1200-grit papers and a 3µm diamond polishing pad were used to provide various combinations of specimen and compression anvil roughnesses.

Quasi-static compression of as-received mild steel and commercially-pure copper and aluminium ring specimens was performed. The effects of lubrication, specimen geometry and surface roughness were assessed. The general test methodology and specimen preparation process were established through experimentation. The test details are similar to those described in *Chapter 5* as a similar approach was used in the current work.

The pertinent information and results are summarised in *Appendix C*. The outcomes that relate to (a) the development of an accurate and practical test methodology for high strain rate tests and (b) suggested potential for advances in the search for conditions that minimise friction are particularly relevant. The main results and applications are discussed in *Sections 3.7.1 – 3.7.4* and a summary of the general conclusions and recommendations that were applied or further investigated in the current work appears in *Section 3.7.5*.

3.7.1 Maximum Strain and Strain Increments

Specimens tested to greater than 50% strain displayed wrinkling of the compression surface and large barrelling. The assumptions made in the analytical solution [1] used to infer theoretical friction factors become less accurate with increasing strain. It was thus recommended that testing be focussed on strains below 40%. Repeatedly loading a single specimen in small increments allows a better approximation of and agreement with the theory because more data points are obtained and friction conditions can be kept more consistent. Hence more reliable and accurate theoretical friction parameters can be extracted.

Strains obtained in a single Split Hopkinson Pressure Bar test seldom exceed 30% [3] and therefore in the current investigation strains were generally kept below 30%, with testing performed in small strain increments, as described in *Chapter 5*.

3.7.2 Surface Roughness Orientation and Preparation

Surface roughness orientation had a significant effect on the uniformity of specimen deformation. Abrasion on standard rotating abrasion pads tends to introduce linear surface scratches. Under compression this caused the initially round specimens to deform into an irregular or ‘oval’ shape and this had a highly detrimental effect on the measuring technique used. An investigation was undertaken using aluminium specimens abraded on a rough 320-grit SiC paper with care taken to introduce abrasion scratches aligned in the same direction on both faces. This caused severe uneven deformation with almost all the radial expansion occurring against the direction of grinding, as can be seen in *Appendix C.1*.

Care was therefore taken to ensure that specimens were ground in an isotropic fashion.

3.7.3 Friction on Polished Surfaces

Highly polished surfaces can contribute to high, unpredictable and inconsistent friction levels (see *Appendix C.3*). This is a well-known phenomenon. Beyond a certain point reducing surface roughness actually increases friction. Sticking friction eventually occurs, as discussed by Bowden [13]. This observation is echoed in the internal combustion field, in which new cylinder bores are lightly cross-hatched or roughened to provide a finish that helps to trap lubricant and reduce friction [20].

Polishing of specimens and anvils was therefore not pursued in the current investigation. 600-grit and 1200-grit SiC-paper finishes were further investigated, as they resulted in lower friction conditions and more consistent results.

3.7.4 Surface Appearance

The surface of every specimen was closely examined after testing and in most cases a zone or region that appeared smoother than the rest of the surface was evident around the outer rim. This seemed to reflect what was described by *Gorham et al* [8] as a lubricant 'breakdown' zone and by Walley *et al* [10] as a region of 'fold-over'. This prompted the recommendation that a study be conducted of the microstructure of tested ring compression specimens.

Such a study was conducted in the current work and the details and results appear in *Chapter 7*.

3.7.5 Conclusions and Recommendations arising from Previous Work

1. The ring compression test is sensitive to interface friction and can be practically applied as a method for investigating friction during compression. As such it may be further utilised to establish and potentially limit the effect of friction on Split Hopkinson Pressure Bar data.
2. The sensitivity of the ring compression test to variations in lubricant condition, surface finish and method of preparation is good but demands that care be taken in controlling extraneous variables.
3. The method is dependant on the accuracy with which very small geometries can be measured. The method devised (see *Section 5.5.3*) was found to be adequate for the level of accuracy required.
4. The inherent scatter and unpredictability of the results would suggest that tests need to be repeated several times for any reliability to be achieved.
5. Small increments of strain are required to accurately follow the geometry changes of the specimen and to be able to infer useful theoretical friction parameters. Tests should be conducted over small increments of strain, between about 5 and 10 percent, to yield accurate and reliable data. To maintain approximately constant friction conditions re-greasing between steps may be required.
6. Exceeding 60% logarithmic strain results in poor specimen surface quality and non-uniform deformation or barrelling. This value should be applied as an upper limit to specimen strain.
7. Testing of surfaces roughened using a 600-grit or 1200-grit SiC grinding paper is recommended as this seems to provide low friction and simplifies the preparation process over polishing.
8. Non-uniformity in the surface finish can cause uneven deformation of the specimen, resulting in unacceptable inaccuracies in the measurement technique devised. Care should always be taken to ensure a uniform surface finish, free from any linearity or specific orientation in the surface scratches.
9. Lubrication plays a vital role in reducing interface friction. Lubrication has a very large effect and an appropriate lubricant should always be used to limit the effects of friction.

10. Lubricant is squeezed out from under the specimen and the surface roughness changes with deformation, indicating that friction conditions are probably not constant during deformation.
11. Different materials display similar friction parameters for otherwise identical specimen preparation and test conditions.
12. An investigation into the microstructure of the specimens should be conducted, in order to identify any characteristics or trends specific to the testing method, and to explain observed surface features.

3.8 Summary of the Results of Investigations into Friction Effects

This section contains a summary of the results discussed in this chapter.

It has been shown [9,11] that due to friction the stress measured using a typical compression Split Hopkinson Bar apparatus may exceed the one-dimensional flow stress. A first estimate of this error for a given theoretical friction factor is expressed by Avitzur [1] and Gorham *et al* [8] as:

$$\frac{P_{ave}}{\sigma_y} = \left(1 + \frac{\mu d}{3h}\right)$$

Gorham *et al* [8] demonstrate that experimentally measured values for μ of between 0.02 and 0.06 could result in an error in the experimentally measured material flow stress of between 1.3% and 4%. Bertholf & Karnes [11] estimated from published experimental results that for a relatively thin specimen (d/h = 3.33) a coulomb coefficient of 0.02 would introduce an error greater than 2% in the measured stress and with $\mu = 0.1$ the error may well be over 8%. They also found that friction introduced non-uniformities in the specimen stress and a 10% deviation from a uni-axial stress state.

Male & Depierre [14] demonstrated the general applicability of Avitzur's analysis [1] from the overall correlation between the theoretically derived curves and the experimental results. They concluded that the ring compression test is the best available technique for the investigation of friction during metal forming, although they cautioned against over-optimistic interpretation of the results. They achieved a practical minimum friction factor, using heated wax specimens, of between m = 0.02 and m = 0.14 and for experiments under conditions of sticking friction 'm' values in excess of unity were recorded. Various other material, lubricant and ring geometry combinations were tested with the 'm' friction factor ranging between 0.06 and 0.14. As a first estimate Avitzur's results [1] predict that these 'm' factors translate to a theoretical friction error in Hopkinson Bar tests of between 1.6% and 2.8% initially and increasing with increasing strain to over 2% and 3.5% respectively.

Gorham *et al* [8] performed high strain rate compression tests and from their results (see *Table 3.2*) it seems that an 'm' factor of approximately 0.05 can be practically achieved if care is taken in specimen lubrication and preparation. They recommended that a comprehensive test program be conducted to establish friction factors for a variety of Hopkinson bar test conditions, in an attempt to obtain a more realistic and accurate estimate of the degree and effect of friction. Gray [3] also suggested a possible lower limit of $m \approx 0.05$ and recommended the ring compression test for experimental friction measurement, suggesting strategies for friction investigation and reduction. Walley *et al* [10] achieved numerical and experimental correlation using a coulomb coefficient of 0.1 (equivalent to $m \approx 0.2$), indicating that friction may well be high, even when using a suitable MoS_2 or graphite-based lubricant. Follansbee [4] and Gray [3] cautioned that the thickness of the layer of lubricant between the specimen and the bar must be carefully controlled since a layer as thin as 25μm may have a significant effect on the timing of the stress pulses recorded.

The ring compression test has thus been analysed and applied to the measurement of friction during Hopkinson Bar tests under a variety of conditions. Coulomb friction coefficients of $\mu = 0.02$ to 0.12 ($m \approx 0.04 - 0.26$) have been recorded. For these values Avitzur's analysis [1] predicts a P_{ave}/yield stress ratio, which gives an indication of the potential for error in Split Hopkinson Pressure Bar tests, of between 1.007 and 1.05, and hence an error of between 0.7 and 5%, for specimens that initially have a d/h ratio = 1. Thus it seems plausible that conditions may be found for which the error in Hopkinson Bar tests can be limited to less than 1%.

Issues reported during these tests, and which are investigated in the current work include:

- After testing, the appearance on the specimen surface of a distinct smooth or discoloured region near the outer diameter [8].
- Barrelling of the specimen, which is contrary to theoretical assumptions made and suggests a non-uniform stress state [3].
- The effect of the thickness of a lubricant layer on the timing of the measured Hopkinson Bar data [3,4].

4 NUMERICAL INVESTIGATION

4.1 Introduction

Various simplifying assumptions are required to enable analytical solution of complex mathematical descriptions of physical systems. Numerical analysis can provide approximate solutions using fewer simplifying assumptions. Thus, provided a representative theoretical description exists, a numerical solution may provide a better approximation of the actual behaviour of the system than an analytical solution.

This chapter contains the details and results of a numerical investigation into the ring compression test, using ABAQUS version 6.4-3. The simulations performed were designed to help establish the reliability of Avitzur's [1] analytical solution in predicting the final specimen geometry for given friction conditions.

Avitzur's analytical analysis [1] was made tractable through the application of various assumptions. The effect of neglecting barrelling was investigated numerically, as described in *Sections 4.4.4* and *4.4.5*. Discrimination between the effects of such influencing factors was made possible numerically by the control available over the model constraints and conditions, and by the number of similar scenarios that can be rapidly solved and evaluated. The change in the internal diameter and the average surface pressure obtained from the simulations were compared to Avitzur's solution [1] in order to verify the model. A visual examination of the deformation and behaviour of the modelling elements also provided clues to the possible internal behaviour of the specimen.

4.2 Numerical Modelling Assumptions

The numerical model was designed to match the specimen geometry and behaviour, while incorporating simplifying assumptions that approximate as closely as possible those used in Avitzur's analytical solution [1]. This allowed the numerical results to be verified against Avitzur's solution. By relaxing these simplifying approximations the effects of barrelling could be assessed.

The major assumptions of Avitzur's analysis [1] are:

1. A perfectly plastic material through the use of Mises' strain rate laws.
2. That the frictional restraint is transmitted uniformly through the specimen thickness, which implies no barrelling.
3. That relating the shear stress due to friction to the material yield stress by a constant, m, through the constant shear assumption, is reasonable.
4. No strain-rate sensitivity or inertia effects.

The numerical model incorporated similar assumptions. An elastic-perfectly plastic material model was assumed with strength and stiffness values obtained for copper from quasi-static tensile tests (see *Appendix F)*. Thus the numerical and analytical predictions are similar in that they both neglect strain hardening. Although the material parameters for copper were used in the simulations the results are generally applicable to any isotropic, perfectly plastic material, as the absolute magnitude of the internal stresses does not affect the final geometry.

The coulomb friction model was used. This model differs from the friction model used by Avitzur, as discussed in *Section 3.5*. This difference needs to be accounted for when comparing the analytical and numerical results. The factor P_{ave}/σ_Y (where P_{ave} is the average surface pressure and σ_Y is the material flow stress) was determined using Avitzur's solution [1] and this allowed the equivalent constant friction or 'm' factor to be calculated for the coulomb coefficients modelled. For a given coulomb coefficient (μ) the equivalent 'm' factor varies over a small range across the amount of strain modelled. The range is relatively small with $\mu \approx 2m$ as illustrated in the following examples.

For $\mu = 0.06$ the 'm' factor ranges from 0.112 at 0% strain to 0.122 at 69% strain.
For $\mu = 0.08$ the 'm' factor ranges from 0.151 at 0% strain to 0.170 at 69% strain.

These upper and lower limits of 'm' were both plotted when comparing the numerical and analytical geometry predictions. Where it was desired to compare the numerical and analytical solutions more exactly a step-wise approximation was used. As an example, when comparing the numerical solution for $\mu = 0.08$ to the analytical solution the curve for m = 0.15 may be used in the 0% to 25% strain range, m = 0.16 for 25% to 50% strain and m = 0.17 for 50% to 75% strain. More intervals could be used to provide a more accurate 'fit' but two or three intervals were considered sufficient to provide qualitative evidence of the correlation. For examples of this approach see *Figures 4.8* and *4.9*.

Avitzur [1] made the assumption that the frictional restraint is transmitted uniformly through the specimen, and hence no barrelling occurs. From the final geometry of the test specimens, this assumption would appear to introduce the largest deviation from the actual specimen behaviour. Thus the numerical model could be usefully applied to estimate the effect of barrelling when using Avitzur's solution to interpret experimental geometry changes and infer theoretical friction factors.

4.3 Numerical Model Details

4.3.1 Material Model

An Elastic-Perfectly Plastic material was assumed (Lévy Mises assumptions were used in Avitzur's analytical approach). This implies that if a uniform, uniaxial stress state does exist in the specimen then the contact pressure should be a constant. The material parameters used appear in *Table 4.1*.

Yield Strength	273 MPa	(as obtained by tensile testing)
Elastic Modulus	110 GPa	[21]
Poisson's ratio	0.33	[21]
Density	8870 kg/m^3	(measured)

Table 4.1 The material properties of commercially pure copper (as-received) that were used in the numerical model.

4.3.2 Element Details

The element used for the simulations was an axi-symmetric, 8-node, quadratic quadrilateral and was evaluated using reduced integration. Various simulations were performed to refine the mesh and establish the optimal modelling element.

4.3.3 Boundary Conditions

An axi-symmetric, two-dimensional model was used, with a 6:3:2 geometry specimen compressed between analytical rigid[1], axi-symmetric, planar surfaces. A penalty friction model was applied [20], with the coulomb coefficient of friction, μ, specified in five increments between 0.00 and 0.10. The compression lasted sixty seconds to a logarithmic strain of 69.3% (an engineering strain of 50%), after which the load was removed and the specimen allowed to return to a zero stress state. Higher strains were found to cause increasing numerical problems, such as excessive element distortion. The analytical assumptions listed in *Section 4.2* also become more approximate with increasing strain. Thus results were only useful below about 50% logarithmic strain, which was sufficient given the amount of deformation obtained experimentally.

4.4 Simulations and Results

Various simulations were performed to investigate different aspects of the model and the analytical solution. Convergence and verification of the model, the effect of the rate of deformation, and the effect of barrelling were studied. The details and results of the various simulations are presented in this section. The main input files used with ABAQUS/Standard version 6.4-3 are included in *Appendix E.*

---

[1] 'analytical rigid' is a modelling term used to describe a surface for which only rigid body motions are considered and hence deformations, stress and strain calculations are not required. This description can be applied to parts with a much greater stiffness than the rest of the model, significantly reducing simulation run-times [20].

4.4.1 Model and Convergence Verification

Before simulations could be performed suitable constants were required and convergence of the model had to be confirmed. Various modelling elements and mesh densities were considered. The effect of mesh refinement on the final specimen geometry, the surface pressure and the element behaviour in the highly strained corner regions were examined. Numerical singularities and warnings were also monitored. The mesh selected is illustrated in *Figure 4.1.* The deformed mesh is shown in *Figure 4.2* at 60% logarithmic strain, for a coulomb friction coefficient of 0.08.

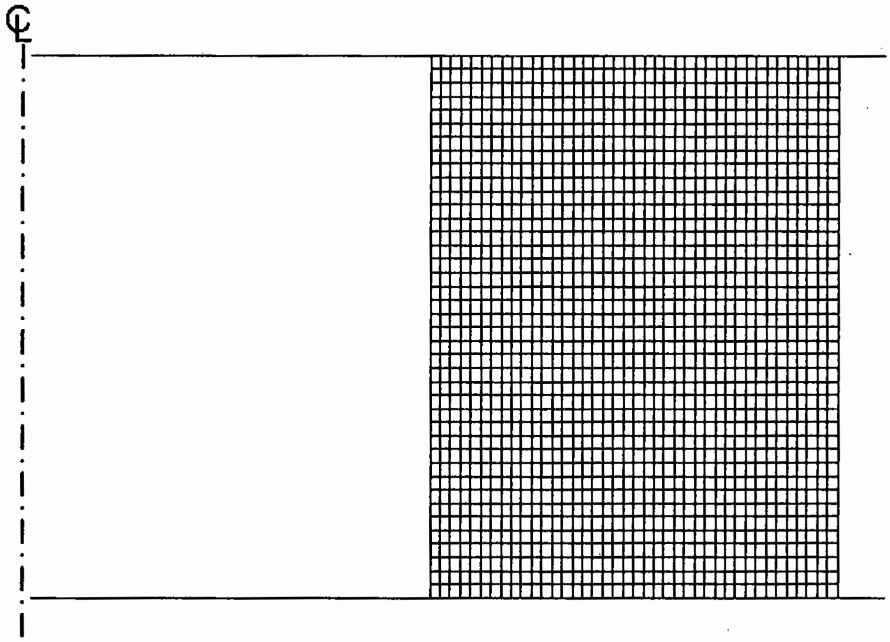

Figure 4.1 Mesh consisting of 1600 quadrilateral elements as used for the axi-symmetric simulation of the ring compression test.

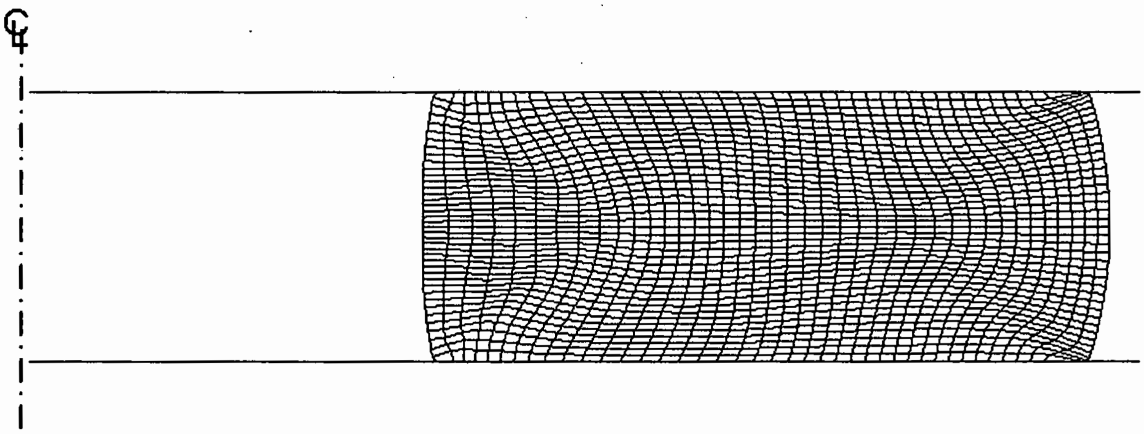

Figure 4.2 Element mesh at 60% logarithmic strain for $\mu = 0.08$. Note the distortion of elements in an X-shaped pattern and the barrelling visible.

As the mesh was refined through 600, 1200, 1600 and 2400 linear and quadratic elements the dimension changes were compared at the four corners and at the inside and outside diameters on the mid-line of the specimen. The change in internal diameter with strain was not significantly affected by changes in the mesh density or the element used. *Figure 4.3* confirms that the internal diameter change had converged.

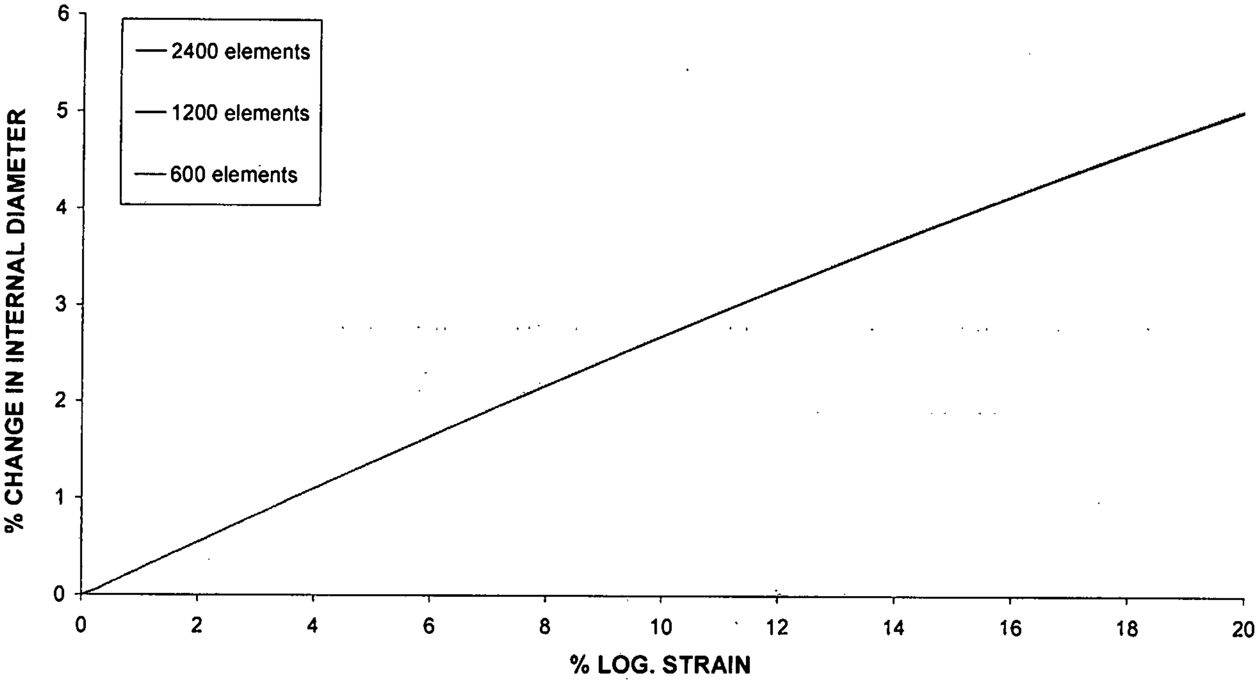

Figure 4.3 Graph showing convergence of the internal diameter change across 600, 1200 and 2400 element meshes.

4.4.2 Element Behaviour

Although the overall deformed geometry and forming pressure were not affected, the different elements displayed marked differences in behaviour in the highly strained corner regions of the mesh. This is illustrated in *Figures 4.4, 4.5* and *4.6* for linear, quadratic and reduced-integration quadratic elements respectively. Reduced-integration quadratic element refers to a quadratic element formulation evaluated using a single point, reduced integration scheme.

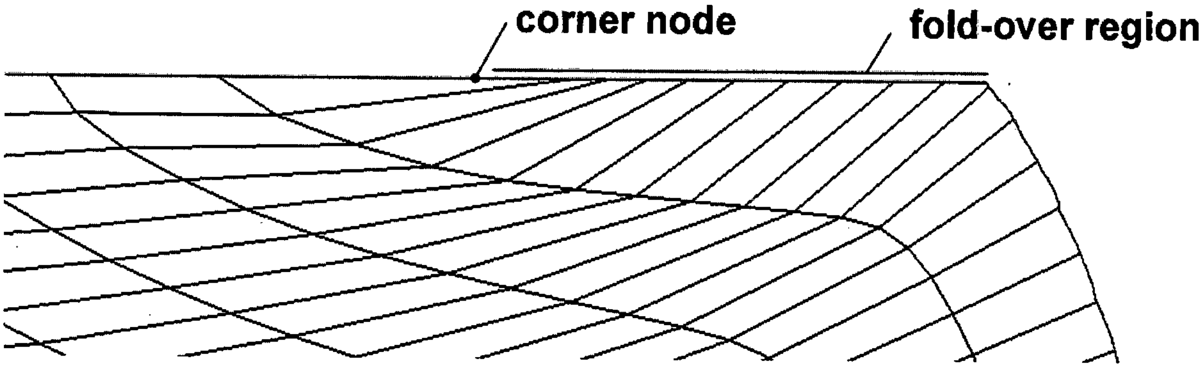

Figure 4.4 Deformation of linear quadrilateral elements in the highly strained corner region of the model, displaying fold-over.

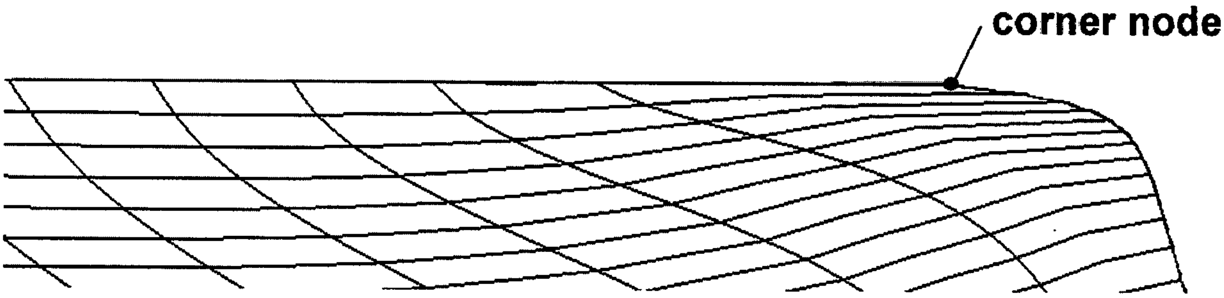

Figure 4.5 Deformation of quadratic quadrilateral elements in the highly strained corner region of the model. No fold-over occurred.

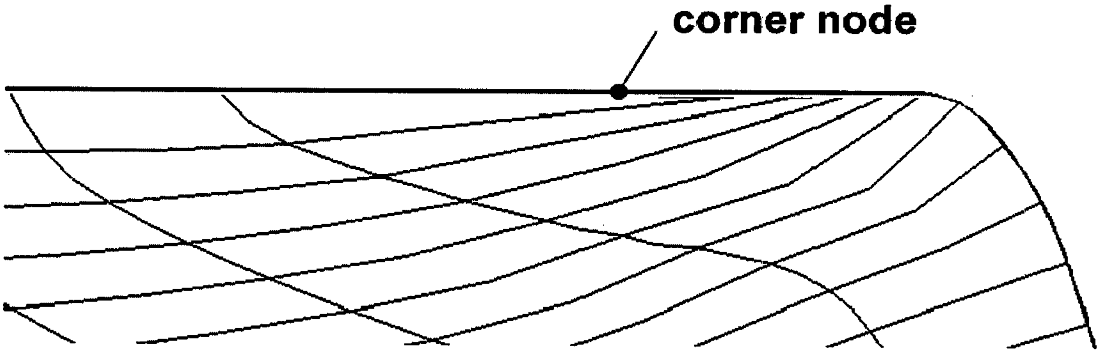

Figure 4.6 Deformation of quadratic quadrilateral elements in the highly strained corner region of the model when reduced integration was used. Some fold-over is evident.

The linear elements displayed fold-over after 50% logarithmic strain. This is evident in *Figure 4.4* where ten of the forty elements initially on the side of the specimen have come into contact with the compression surface or anvil. The quadratic elements displayed some resistance to fold-over. Although the elements experienced large deformation, becoming very elongated, at no stage did the nodes on the side of the specimen come into contact with the compression surface. When the same quadratic elements were evaluated using reduced integration fold-over did occur, although not as significantly as was observed for the linear elements. Increased friction resulted in earlier and greater fold-over although never before approximately 50% logarithmic strain. This behaviour prompted the microstructural investigation conducted, the details of which are presented in *Chapter 7*. Fold-over was also observed experimentally but greater strain was required numerically to achieve the same degree of fold-over (see *Chapter 7*). It is clear from a comparison of the numerical results with observed experimental results that this specific aspect of the specimen behaviour was not simulated accurately and a more comprehensive model would be required for more detailed investigation and simulation.

Since the average surface pressure and internal geometry change were not significantly affected by the element used, the criteria for selecting a suitable element became model stability and efficient simulation run-times. A higher order element was preferred but the quadratic element tested seemed to resist fold-over, even for very high friction values, and thus the behaviour of this element appeared unrealistic. Using reduced integration did allow some fold-over and helped to reduce run-times with the only caution against this approach being the possible appearance of non-physical singular or 'hourglass' modes" [7]. However this element is recommended for two-dimensional axi-symmetric meshes and according to the ABAQUS manual:

> *The reduced-integration second-order serendipity interpolation elements in two dimensions—the 8-node quadrilaterals—have one such mode, but it is benign because it cannot propagate in a mesh with more than one element."*
>
> *ABAQUS CAE User manual version 6.4 [22]*

Thus the 8-node quadratic quadrilateral element evaluated using reduced integration was used for the majority of the simulations. This element is referred to as *CAX8R* in ABAQUS version 6.4-3. Forty nodes were used per side and since the initial section is rectangular the elements were forced to deform through square, helping to limit excessive element distortion in the radial direction.

4.4.3 Strain Rate Effects

Although the material model used had no specifically incorporated strain rate sensitivity, at higher strain rates inertia could affect the specimen behaviour or stress distribution [8]. To establish whether the numerical results would apply to experimental results at all strain rates, as is assumed in the case of Avitzur's solution [1], identical simulations were run at a higher strain rate. The simulations were initially run with the anvil velocity set at 1mm/min, as used in the quasi-static compression tests, to provide a strain-rate of less than $10^{-2}s^{-1}$ (approximately $0.0084s^{-1}$). The simulations were then re-run with an anvil velocity of 2m/s, to provide a strain rate in the order of $10^{3}s^{-1}$. The results were compared to try to ascertain whether any inertia effects had been realised in the numerical model. There was no significant difference in the results at the two strain rates and thus it was concluded that inertia affects were negligible.

The analytical solution reported by Gorham [12] confirms this result. Gorham used his analytical solution to show that the error introduced due to inertia in a 13mm diameter specimen compressed at a strain rate of $\pm 1000s^{-1}$ is less than 1.2%. The error due to inertia was shown by Gorham [12] to decrease with specimen diameter and therefore for a 6mm specimen diameter the error would be significantly lower than this. In addition Gorham's analysis [12] was based on typical solid cylindrical Hopkinson Bar specimens. Ring specimens should be less affected by inertia because material can flow radially inwards as well as outwards, reducing the peak velocity and acceleration and hence the inertia effect.

4.4.4 Analytical and Numerical Correlation

In order to simplify the analytical solution of the ring compression test Avitzur [1] assumed a uniform velocity field in the axial direction, effectively preventing barrelling and fold-over. **This was the only significant difference between the assumptions made numerically and those made analytically.** Therefore in order to establish the validity of the numerical solution simulations were performed in which barrelling was removed geometrically at increments during the analysis. Coulomb friction coefficients of 0.06 and 0.08 were used. The model described in *Section 4.3* was run for three seconds for a given initial geometry. The final internal diameter was averaged to remove the small barrel that had developed. This average internal diameter was then used to obtain a new external diameter by applying conservation of mass, neglecting elastic deformations. The specimen geometry was redrawn, with the initial volume, the change in height and the new internal and external diameter, effectively removing any barrelling that had occurred during the previous step.

The results were compared to Avitzur's analytical solution [1] and to the results obtained when running the simulation without interruption or alteration to 69.3% logarithmic strain. Comparison with these results, for which the code was allowed to generate the deformed geometry as the governing equations dictated, provided an estimate of the extent to which neglecting barrelling affects the results.

The results of this investigation are plotted against the results for which barrelling is incorporated (solid lines) and the relevant analytical curves (broad lines) in *Figure 4.7*. The numerical results without barrelling show very good agreement with the analytical results, within the range of equivalent 'm' factors (included for μ = 0.06 and μ = 0.08). The discontinuities in the equivalent analytical 'm' factors were chosen from a comparison of m and μ across the strains considered (see *Appendix E.3*). As very similar geometry changes were predicted numerically and analytically, under similar assumptions, the numerical model was shown to accurately represent the specimen behaviour.

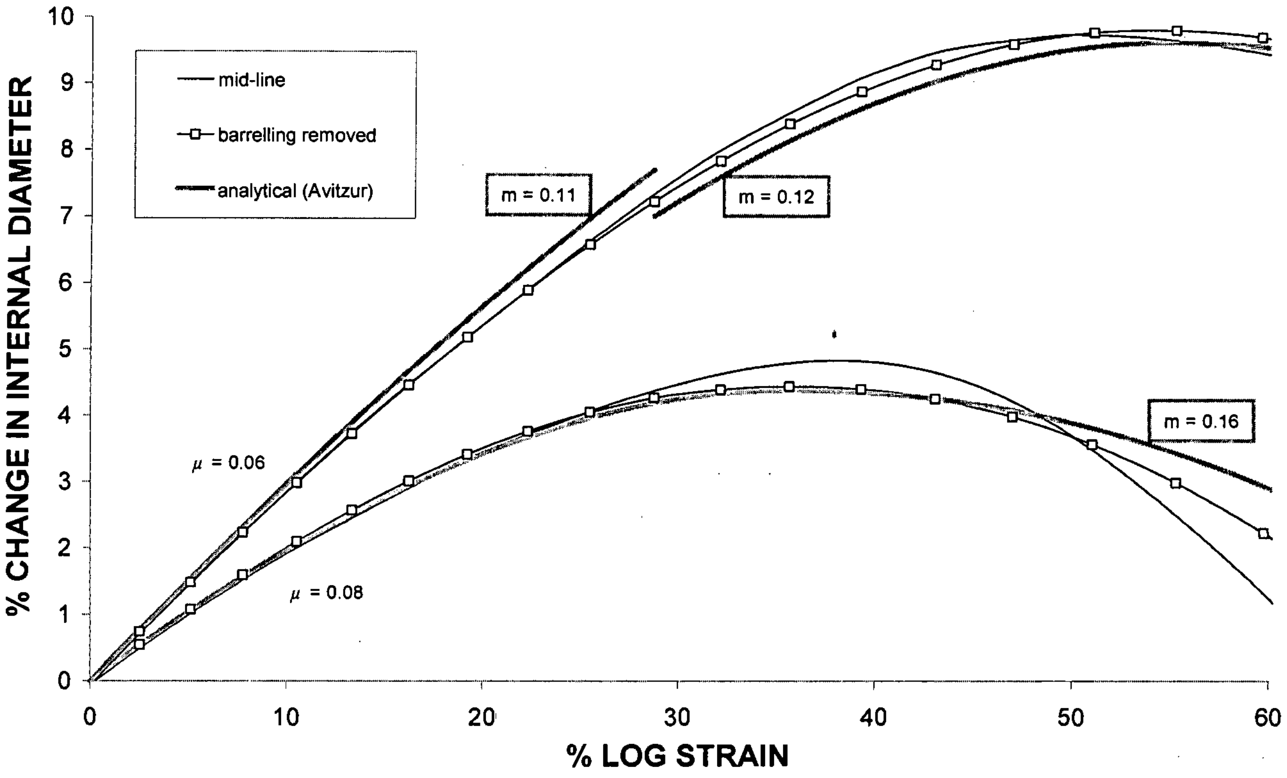

Figure 4.7 Graph showing the results of simulations with barrelling removed geometrically. Solid lines indicate the internal diameter change on the specimen mid-line including barrelling, while the square markers give the result when barrelling is removed. The analytical curves for the nearest equivalent 'm' factors are included.

4.4.5 The Effect of Barrelling

Having established the validity of the numerical results the effect of barrelling could be assessed. Coulomb coefficients of μ = 0.00, 0.02, 0.04, 0.06, 0.08 and 0.10 were modelled, which represent constant friction factors of approximately m = 0.00, 0.036, 0.075, 0.11, 0.16 and 0.20. *Figure 4.8* and *Figure 4.9* show the results of the investigation into the predicted dimension changes of the deforming rings. The internal diameter change (measured at the specimen surface and mid-line) and the contact pressure at the surface were extracted and compared to Avitzur's results [1]. The thick grey lines represent Avitzur's analytical solution. The solid lines show the internal diameter change on the mid-line of the specimen and the dashed lines the changes at the surface of the specimen, as illustrated in *Figure 4.10.*

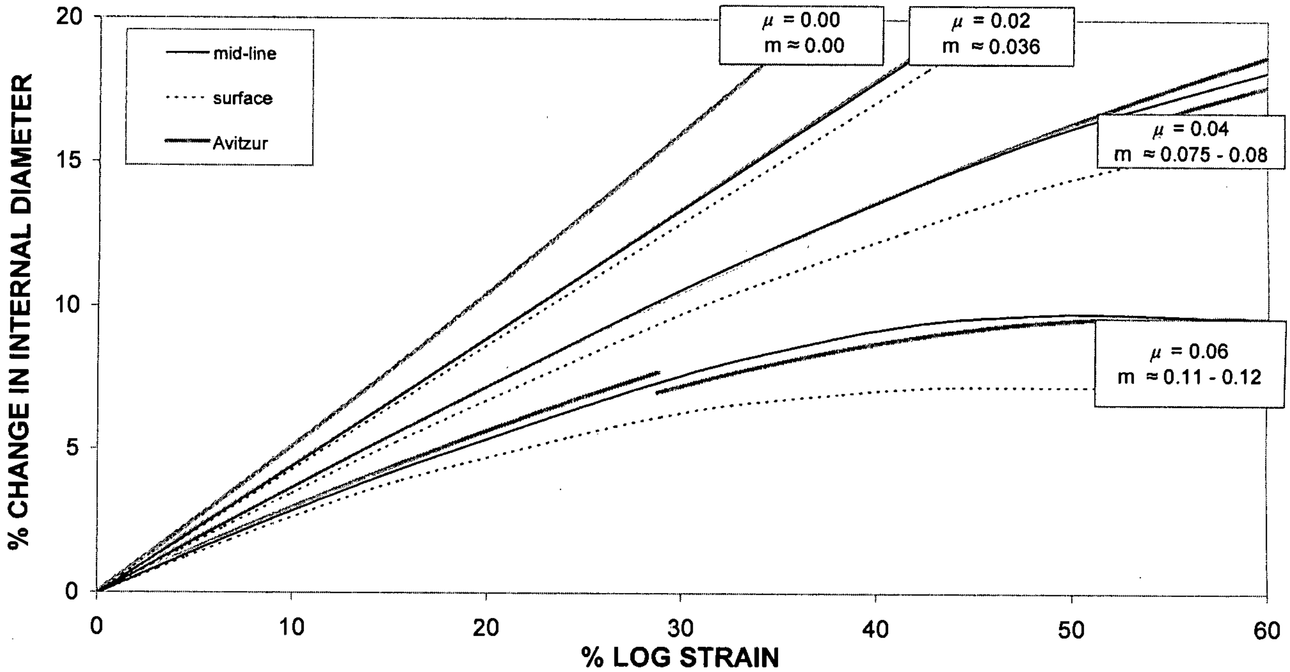

Figure 4.8 Graph of numerical results, for $\mu = 0$ to $\mu = 0.06$, showing % change in internal diameter measured at specimen surface and mid-line, with theoretical curves of the equivalent m factors, as indicated, from Avitzur's theory.

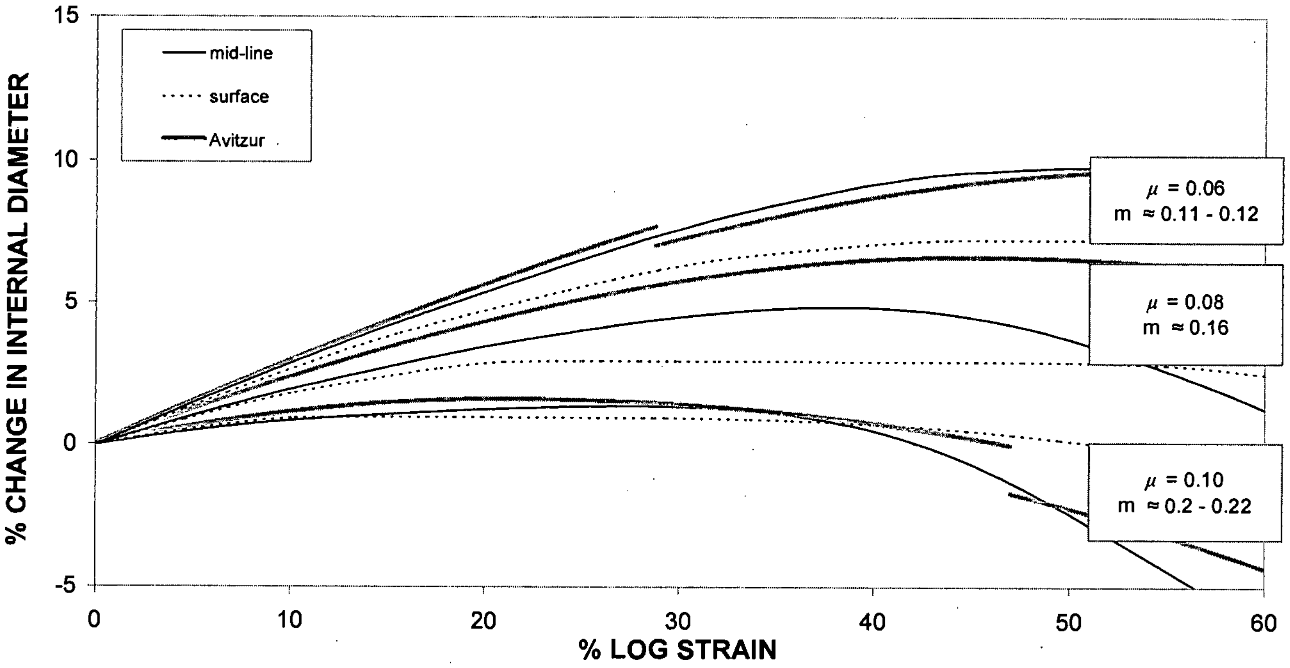

Figure 4.9 Graph of numerical results, for $\mu = 0.06$ to $\mu = 0.12$, showing % change in internal diameter, measured at specimen surface and mid-line, with theoretical curves of the equivalent m factors, as indicated, from Avitzur's theory.

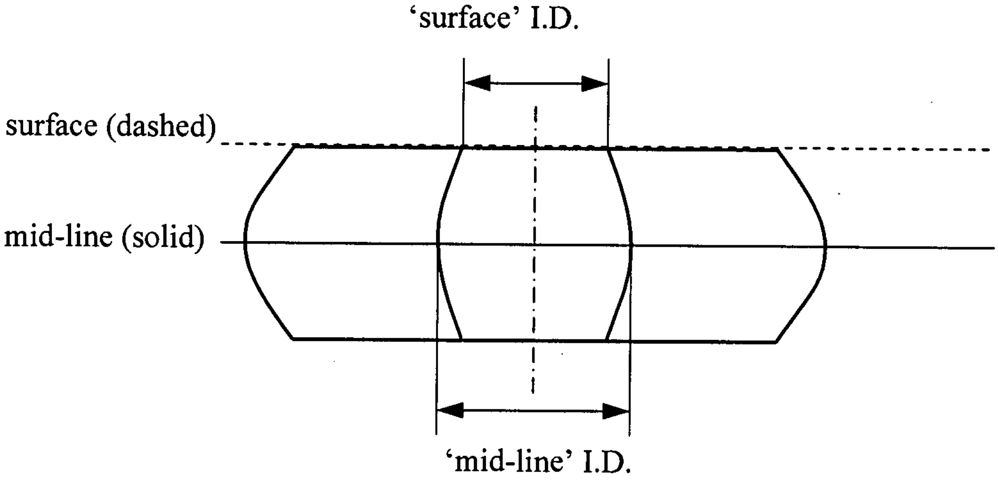

Figure 4.10 Schematic diagram showing the cross-section of a barrelled specimen, illustrating the effect of the position at which the internal diameter is measured.

As can be seen in *Figure 4.10* barrelling causes a discrepancy between diameter measurements taken at the specimen surface and those taken at the mid-line. Due to a greater frictional restraint the surface movement always lags the bulk material movement. The neutral radius, discussed in *Section 3.5*, is the instantaneous position at which no radial movement occurs. As the specimen is deformed and the aspect ratio decreases the neutral radius moves outwards. At some point the neutral radius lies at the same position as the internal radius. After this point the internal radius begins to reduce. The surface material then remains stationary while the barrel on the internal diameter changes from convex outwards to convex inwards. This explains the plateau observed in *Figures 4.8* and *4.9*.

Barrelling was neglected in the analytical solution but was evident in the specimens tested. The numerical solution may therefore provide a more accurate prediction of the experimental results as some barrelling was observed numerically. The numerical solution generally indicated a smaller increase in internal diameter than the analytical solution, for equivalent friction factors. Better agreement between the analytical and numerical results is observed when the internal diameter is measured at the specimen mid-line rather than at the specimen surface. This discrepancy increases with an increase in μ until $\mu \approx 0.08$, with agreement improving thereafter. When $\mu \approx 0.08$ the neutral radius lies close to the internal radius and the change in the specimen response becomes erratic as the internal radius stops expanding and begins to contract.

It would appear that Avitzur's solution [1] slightly overestimates the internal diameter change for given friction conditions, especially at high strain and for high friction conditions, as suggested by Male & Depierre [14]. This is significant as the friction factors quoted in this investigation were inferred using Avitzur's analytical solution [1] with measurements of the internal diameter taken at the specimen surface (as described in *Chapter 5*), and thus the factors obtained probably over-estimate the actual friction conditions. This means that the error due to friction for the given conditions will probably be lower than what is inferred using these values. The predicted errors in flow stress can therefore be considered as an upper limit or 'worst-case scenario' of the actual conditions and therefore include some inherent safety margin.

4.4.6 Average Surface Pressure

The average pressure at the specimen surface was obtained numerically and compared to the analytical prediction, as shown in *Figure 4.11*.

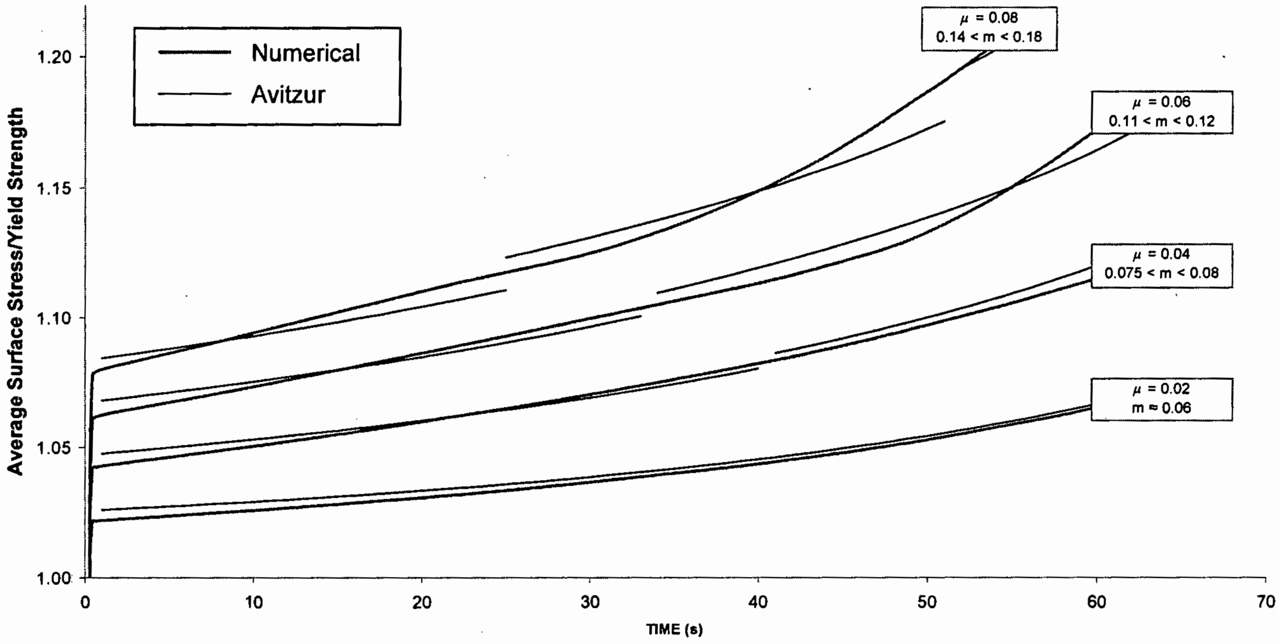

Figure 4.11 Graph showing the average surface stress factor predicted numerically (thick lines) for various coulomb coefficients, against closest equivalent constant friction 'm' factors indicated.

This pressure is expressed as a factor of the quasi-static yield stress, σ_y. For zero friction no constraint is predicted and the factor is therefore unity. As frictional constraint and hence the hydrostatic specimen stress and the required surface pressure increases this factor rises and gives an indication of the potential error in Split Hopkinson Pressure Bar tests. The theoretical curves for two different 'm' factors from Avitzur's analysis [1] are plotted in a step-wise fashion to represent the range of 'm' factors that correspond to the constant coulomb coefficients used in the numerical model.

Figure 4.12 shows the typical pressure distribution at the specimen anvil interface for a strain of 60% (shown for $\mu = 0.06$). A darker colour indicates greater pressure. The hydrostatic stress induced by the frictional restraint is greatest within the ring material. Due to the free boundary the shear stress must be zero on the inner and outer diameters and the pressure therefore reduces from a maximum somewhere within the ring material to the material flow stress at the edges. This pattern is observed in *Figure 4.12.*

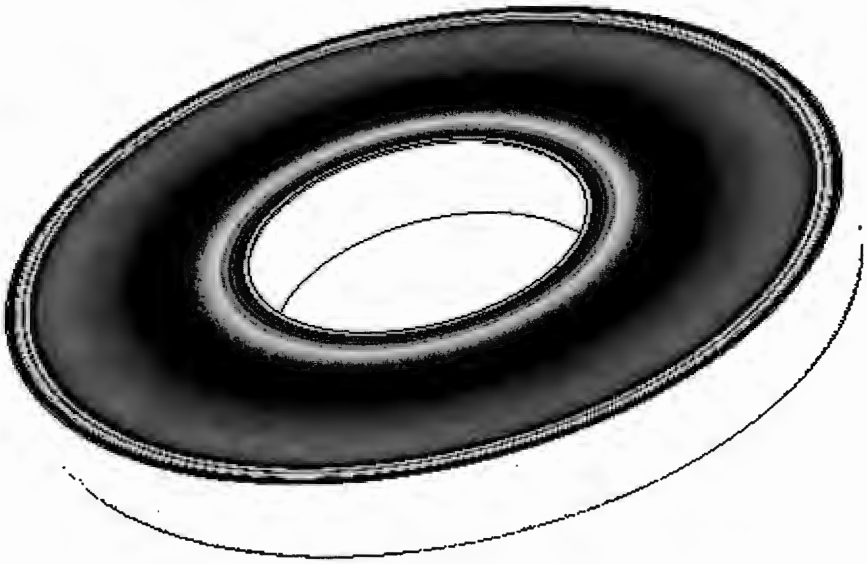

Figure 4.12 Extruded representation of ring compression specimen from numerical simulation showing surface pressure distribution at 60% strain with $\mu = 0.06$. The bands on the outer edges arise due to numerical discontinuities and fold-over.

4.5 Conclusions

The numerical model was shown to correlate very well with Avitzur's analytical solution, provided similar assumptions and approximations were applied. Barrelling, and in particular the position on the axis of the specimen at which the internal diameter is measured was shown to affect the predicted geometry changes. Measuring the internal diameter at the surface of the specimen and using Avitzur's analytical solution to infer theoretical 'm' friction factors may well result in friction factors that over-estimate the actual friction level achieved. This implies that the values inferred from the experiments performed in this work may be regarded as upper limits on the friction factors representing the given conditions. The friction factors obtained and the error inferred due to friction can therefore be considered conservative or 'safe' estimates when designing Split Hopkinson Bar tests.

5 EXPERIMENTAL DETAILS

5.1 Introduction

This chapter contains the details and general parameters for both the quasi-static and the high strain rate tests performed. Details of the equipment used and procedures for calibration of the Split Hopkinson Pressure Bars are included. The method used for measuring the final specimen geometry is also described.

The ring compression test introduced in *Chapter 3* was the basis for the experimental work conducted. A testing configuration similar to that found in the published work of Male & Depierre [14] and Gorham *et al* [8] was used as a starting point, facilitating comparison of the experimental results. Results from a previous investigation [19] (as discussed in *Section 3.7*) were useful in the development of an accurate and reliable test methodology. The test methodology was enhanced as specific details were refined through experimentation. A suitable specimen geometry and scale, as well as practical and accurate methods of specimen preparation and measurement were required, in order to provide a suitable benchmark for the investigation of the effects of lubrication and surface finish. An appropriate strain interval was also required, as well as a means for repeatedly attaining the desired strains. A program of quasi-static testing was conducted initially, followed by a series of high strain rate tests performed using the Split Hopkinson Pressure Bar apparatus.

5.2 Overview

- The ring compression test, as described by Male and Depierre [14] and recommended in previous work [19], was used to measure friction.
- The energy analysis by Avitzur [1] was used to interpret the results and infer theoretical friction factors.
- Testing was performed on regular annular specimens six (6) mm in diameter, with an inner diameter of three (3) mm and two (2) mm thick. According to convention this is referred to as a 6:3:2 geometry specimen.

- Copper, aluminium and mild steel specimens were tested, all in the as-received state. Specimens were machined from rods 10 mm in diameter.
- Quasi-static tests were performed at a nominal strain rate of $0.0084s^{-1}$
- High strain rate tests were performed using a Split Hopkinson Pressure Bar at a strain rate in the order of $10^3 s^{-1}$, typically between 1000 and $2000s^{-1}$.
- All tests were conducted at room temperature (20°*C*).
- Due to the inherent scatter and sensitivity of the ring compression test, all tests were repeated three times to establish repeatability and improve the confidence in the final results, as recommended in previous work [19].
- Testing was performed dry and using MoS_2-containing grease as a lubricant. Specification details appear in *Appendix H.*
- The specimens tested quasi-statically were compressed between hardened, 1% carbon steel (silver steel)[1] anvils. The Hopkinson Bars used for the high strain rate tests were also of hardened silver steel.
- The surface finish on both the specimen and the compression surfaces was achieved by grinding with 600-grit or 1200-grit SiC grinding paper.
- Force-deflection data and specimen geometry were recorded for the quasi-static tests.
- Hopkinson bar data, in the form of voltage-time histories, and specimen dimensions were recorded during the high strain rate tests.

5.3 Details of the Quasi-Static Tests

Building on the recommendations of previous work [19] (discussed in *Section 3.7*) required a refinement of the test technique and the identification of optimum test conditions for the high strain rate tests. An optimum surface roughness for the specimen and bars was required so that the two Hopkinson Bars available could be prepared to the correct surface finish. A program of quasi-static compression testing was conducted to (a) confirm the results of previous work [19], (b) refine the methods of specimen preparation, and (c) identify the surface roughness that provided the minimum frictional restraint. This roughness was used to prepare the Hopkinson Bars

---

[1] 1% carbon tool steel (approximate composition: 1%C, 0.3%Si, 0.4% Cr, 0.35% Mn) [23] is commonly referred to as 'silver steel'. This term will be used for the remainder of this report.

and this enabled the number of bars required to be limited to just two. This approach also allowed a reduction in the number of tests required on the Split Hopkinson Pressure Bar apparatus. Aside from strain rate the quasi-static test conditions and the high strain rate test conditions were kept as similar as possible. The analytical analysis by Avitzur [1], as used to obtain theoretical friction factors from the ring compression test results, is strain rate independent and therefore generally applicable.

A major distinction between the two test programs is the potential for the development of squeeze film lubrication, which could not occur under quasi-static conditions. Should this develop it may significantly reduce the effective interfacial friction. The quasi-static tests were expected to be generally more repeatable and consistent because large interface velocities and phenomena such as jetting or lubricant film breakdown would not occur.

5.3.1 Quasi-Static Test Program

The quasi-static testing was focussed primarily on mild steel specimens. The results from previous work indicated that mild steel specimens showed the best repeatability and were easiest to prepare. Mild steel specimens, presumably due to their greater structural strength, also kept their regular shape better under deformation and hence were more easily and more accurately measured. Following the recommendations discussed in *Section 3.7.3* specimens were prepared with 600-grit or 1200-grit paper and tested on anvils that were similarly roughened. The compression was interrupted at regular intervals and the specimen measured, yielding one data point. The specimens were re-greased between each strain increment. In addition six copper specimens, finished using 1200-grit, were tested on the three different anvil surfaces: 600-grit, 1200-grit and 3μm diamond-polished to establish whether the anvil roughness played a significant role in the friction conditions.

5.3.2 Quasi-Static Test Apparatus

Quasi-static testing was performed on a Zwick Universal Testing Machine, equipped with a 200kN load cell. Time, cross head displacement and force data was routed to a computer and recorded in a .DIF file (Data Interchange

Format). The assembled specimen, anvils and compression rig are shown in *Figure 5.1*.

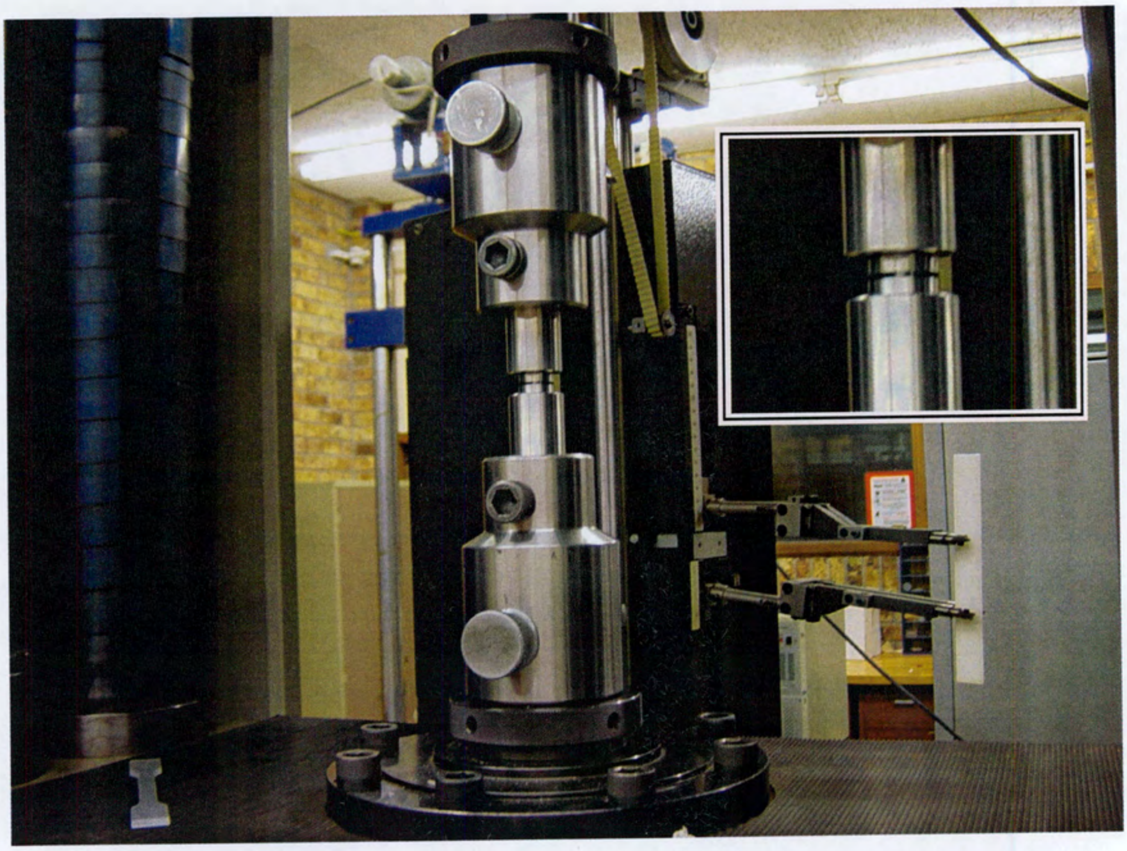

Figure 5.1 Photograph of the assembled quasi-static test rig showing specimen and compression anvils (anvils visible in enlarged portion).

The cross head was moved at 1mm/min (giving a nominal stain rate of $0.0084s^{-1}$) and stopped at predetermined displacements. Specially prepared anvils were used so that a suitable hardness and the specified surface finish could be used consistently for the quasi-static and the high strain rate tests. The anvils comprised solid discs of silver steel 20mm in diameter and 5mm thick (see *Appendix I*). To simplify the specification of the surface finish the anvils, despite their superior hardness, were finished using the same method as was used for the specimens, resulting in a smoother surface for a specified paper grade and surface specification.

It was discovered after the first mild steel trial tests that the silver steel anvils were being indented by the mild-steel specimens. The following method was used to increase the hardness of the silver steel anvils.

5.3.2.1 Silver Steel Anvil Hardening Procedure

1. Heat treatment in a furnace at 850°C for 15 minutes.
2. Oil quenching.
3. Tempering for 1 hour at 300°C.
4. Cooling in air at room temperature.

Further testing of the mild steel specimens to 80% logarithmic strain did not cause any discernible damage to the anvils, which were thus considered sufficiently hard for further testing.

5.3.3 Quasi-Static Test Procedure

The Zwick UTM was controlled via computer from a file containing stored test parameters. Once the load cell on the Zwick UTM had been allowed to warm up for thirty minutes the assembled rig was installed and the reading zeroed. The specimens were greased and placed between the appropriate anvils. Machine compliance and specimen elasticity account for a portion of the cross-head displacement and thus the required displacement value for a desired plastic strain in the specimen had to be obtained by trial and error. Between tests specimens were cleaned and measured, providing one experimental data point, and the condition of the specimen and anvils was noted. The specimen was then re-greased and strained further. After each test the mass error (see *Section 5.5.3*), deformation, and change in internal diameter were calculated, for each increment of strain.

5.4 Details of High Strain Rate Tests

5.4.1 High Strain Rate Test Program

High strain rate tests at strain rates in the order of $10^3 s^{-1}$ (typically between 1000s and $2000s^{-1}$, depending on the material) were performed using a Split Hopkinson Pressure Bar apparatus. The theory behind the method is introduced in *Section 2.2* and discussed in *Appendix A*. Different test scenarios were planned based on questions raised during a review of the literature and during the quasi-static testing. The test procedure differed very slightly for the different testing scenarios. The five different tests performed were:

1. Eight incremental compressions (using limit collars) of an individual specimen, with light greasing.
2. One compression (using various limit-collars) of eight similar specimens, to successively increasing strains, with light greasing.
3. Eight incremental compressions (using limit-collars) of an individual specimen with a large amount of grease.
4. Three large successive compressions of an individual specimen with light greasing.
5. Four incremental compressions (using limit-collars) of an individual specimen with no lubricant.

5.4.2 High Strain Rate Test Apparatus

5.4.2.1 Bars and Gas Gun

The bars used were of silver steel and were both 2m long and 20mm in diameter. The ends were faced-off to a suitable finish and then roughened by hand using 600-grit SiC paper. This roughness was maintained for all the tests, as the quasi-static tests had provided evidence that rougher anvils helped to reduce friction. Two fully adjustable supports were used for each bar, mounted on a single I-beam along with the gas gun. PTFE bushes of a 20mm nominal bore provided a running fit while maintaining the axial alignment of the bar. The striker used was also of silver steel, 300mm long and 12mm in diameter, with a mass of 286g. Pulse shaping, as recommended by Marais [5] and Gray [3], was used to increase the rise time of the input pulse to the order of the 'ring-up' time in the specimen. This was achieved by covering the impacted end of the bar with a layer of paper tape. This also helped to reduce the very high frequency components in the stress pulse, reducing dispersion. Dispersion occurs because different frequencies within the stress pulse travel at slightly different speeds. A detailed discussion is not pertinent here and for more information the reader is referred to Gray [3]. The end of the striker bar was rounded slightly to provide a more central impact with the bar, improving the uniformity of the stress wave and hence the quality of the recorded signal. The Split Hopkinson Pressure Bar apparatus used is shown in *Figure 5.2*.

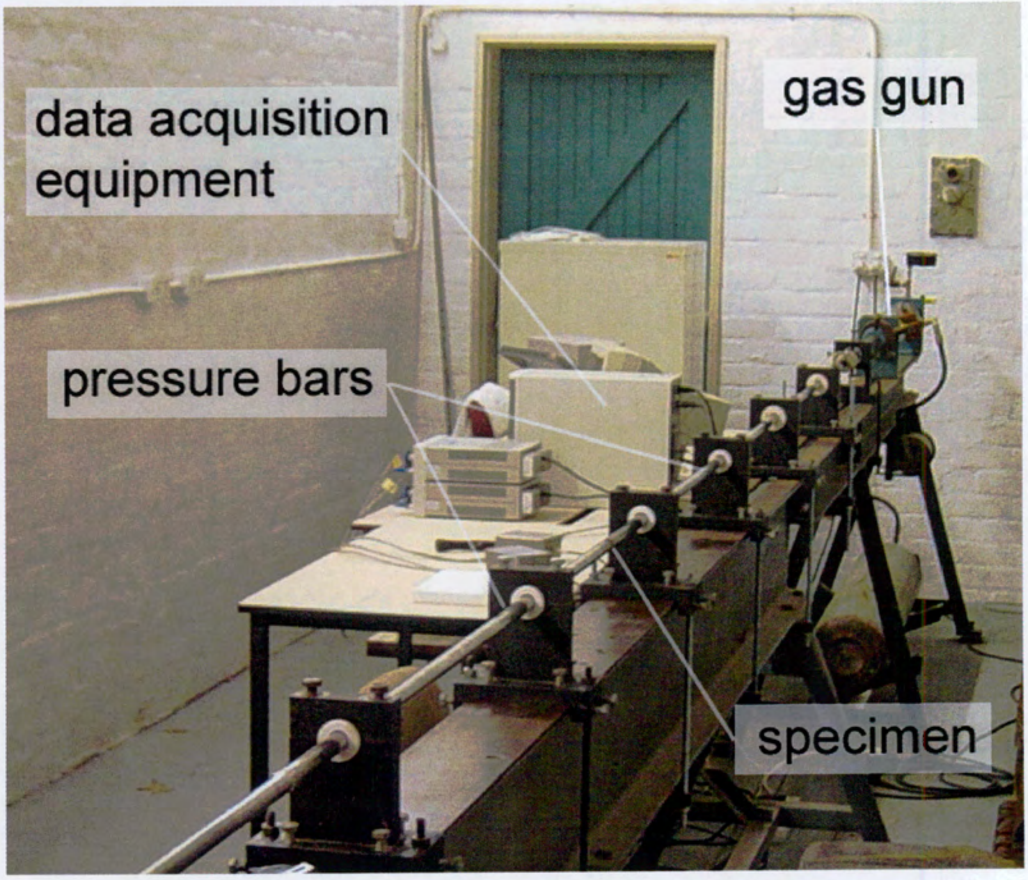

Figure 5.2 Photograph of the Split Hopkinson Pressure Bar Apparatus used for the ring compression tests performed at high strain rates.

Alignment was adjusted until the bars moved freely in the support bushes and the interfaces of the bars remained aligned over a displacement of about

300mm (the free axial travel of the bars). Alignment was checked and adjusted periodically.

5.4.2.2 Strain Gauges and Electronics

Foil strain gauges (KYOWA type KFG-2-120-C1-11) were bonded to the bars with the recommended cyano-acrylate cement (CC-33A). The measurement system comprised two independent channels, one per bar. Four strain gauges were arranged in a Wheatstone bridge configuration, two mounted diametrically opposite on each bar to cancel bending effects, and two mounted nearby in the amplifier case for temperature compensation. The amplifiers used were custom built, making use of two Burr-Brown INA110 fast settling instrumentation amplifiers, set to gains of 100 and 10 to provide an overall gain of 1000V/V, as developed by Marais [5]. The *ADLINK PC-9218 High Speed Data Acquisition Card* used to convert the measured voltage signals had a range of ±5V and recording frequency of 10MHz [5].

5.4.2.3 Strain-limiting Collars

Quasi-static testing had revealed that limited specimen geometry changes over small increments of strain were needed to be able to reliably infer theoretical friction factors. Limiting the final strain of specimens tested using the Split Hopkinson Pressure Bar was achieved by placing a steel collar around the specimen, as illustrated in *Figure 5.3* and shown as applied in *Figure 5.4*.

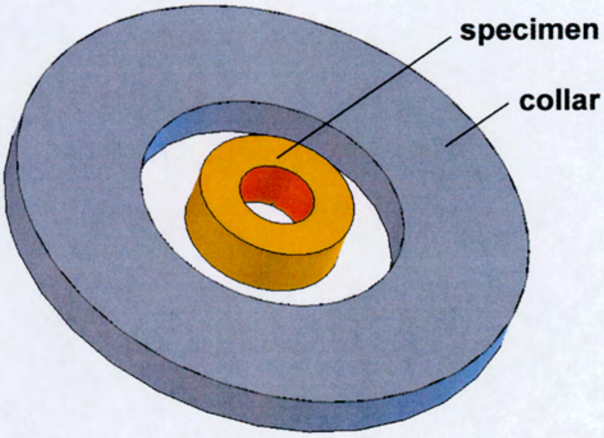

Figure 5.3 Diagram showing ring compression test specimen with limit-collar in position.

During testing the specimen was compressed by the bar until it matched the thickness of the limit-collar being used, after which time the stress pulse travelled through the collar and into the output bar and the stress in the specimen dropped to zero. The collars were of hardened maraging steel, with a 20mm external diameter (to match the bars) and a 10mm internal diameter to house the specimen. Eight different thicknesses in uniform increments between 1.95 and 1.60mm were used, with a tolerance of 0.02mm. Accuracy was achieved by careful abrasion on fine grade SiC paper by hand before the hardening process. Hardening was performed in a salt bath at $500^{\circ}C$ for three (3) hours. The various collars were used successively to achieve small incremental strains of the same specimen, or of eight initially identical specimens.

5.4.3 High Strain Rate Test Procedure

The amplifiers were zeroed (according to the method utilised by Marais [5]) and the data acquisition system and speed trap were checked with a calibration test before each testing run. The striker velocity at impact is determined by a combination of gas gun pressure and the depth to which the striker is loaded into the barrel. A pressure of 400 kPa and striker depth of 150mm provided a suitable velocity of around 12m/s.

The specimen was checked and mounted between the bars with the appropriate grease. The thickness of the grease layer can affect the timing of the stress waves [4] and this effect was investigated in one of the test scenarios (see *Section 5.4.1*). For half the tests grease was applied liberally and for the other half very moderately. The thickness of the layer was qualitatively controlled by the pressure applied when the bars and specimen were brought together by hand. The final thickness could therefore not be measured or accurately estimated. The appropriate collar was placed around the specimen, as shown in *Figure 5.4*.

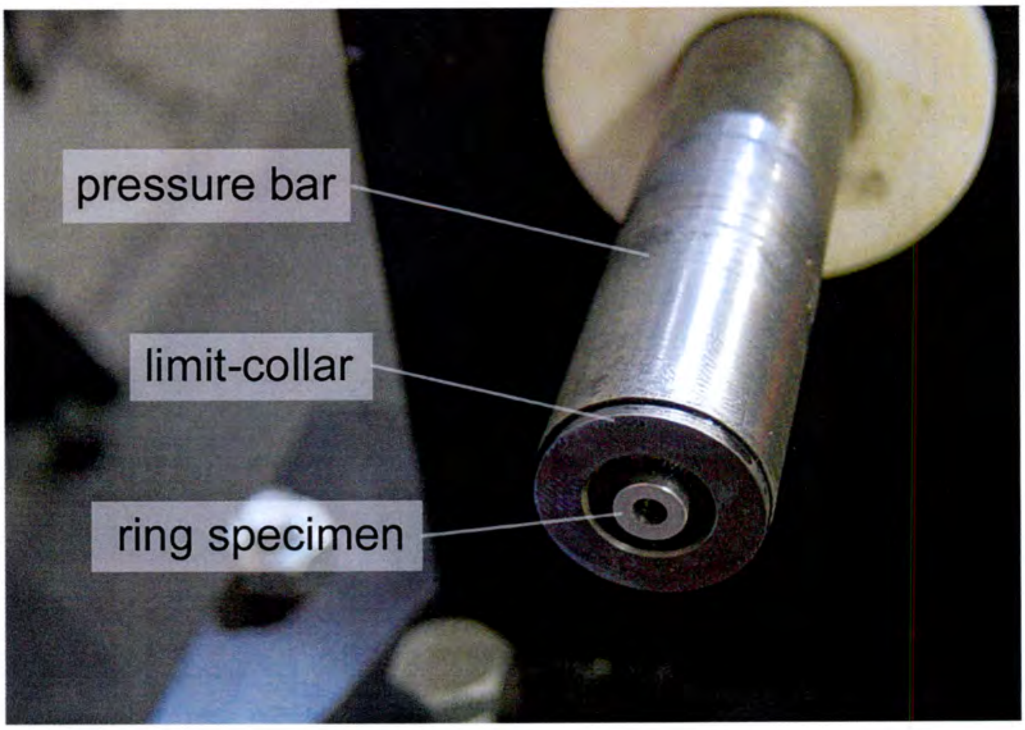

Figure 5.4 Photograph showing a ring compression specimen on the end of a pressure bar with strain-limiting collar in position.

The data-logging program was initialised and the gas gun fired. After each test the speed trap time was obtained from the oscilloscope and saved with the voltage-time data. Ten thousand data points were recorded per channel, giving a test duration of 1ms. The specimen was carefully measured (using the procedure described in *Section 5.5.7*) before the next specimen was tested.

5.4.4 Split Hopkinson Pressure Bar Calibration

Calibration of a Hopkinson Pressure Bar apparatus involves determining the constant calibration factor which relates the strain in the bar to the output voltage signal measured via the strain gauge bridge, and confirming the accuracy of this measurement. The gauge factor and electrical characteristics of the strain gauges and the amplifier gain and phase shift, as supplied by the respective component manufacturers, can be readily used to obtain a theoretical calibration factor. This however cannot confirm the quality of strain gauge placement, or reveal errors or non-linearity in amplification or recording equipment. Two indirect dynamic calibration methods were used to confirm the accuracy of the system and to check the calibration factor obtained theoretically.

1. Calibration through application of one-dimensional wave theory.

One-dimensional wave theory can be used to predict the magnitude of the stress wave generated for a given striker mass and velocity, for known bar material properties. Dispersion, as discussed by Gray [3], is neglected in the theory and this affects the stress wave and hence the measured voltage to some degree.

2. Calibration through application of the conservation of momentum principle.

Conservation of momentum prescribes that the momentum change in the striker equals the total impulse transferred to the bar. The time integral of the voltage signal over the pulse is directly proportional to this impulse. Integration of the signal automatically accounts for dispersion because it incorporates the entire energy in the pulse and not simply the amplitude. Although the impact velocity of the striker could be measured, the required rebound velocity has to be determined using one-dimensional wave theory. The theory behind these two approaches is pursued more fully in *Appendix D.*

The calibration procedure involved using a striker of known mass and cross-sectional area. The velocity was measured at the speed trap. The first calibration test, termed 'bars-apart', involves striking only the incident bar. The bars were then tested in contact, termed 'bars-together'. A thin layer of grease was placed between the bars, as this was found to improve the transfer of the pulse. The recorded voltage-time curves and striker velocity were used according to the theory in *Appendix D* to check the theoretical calibration factor. These three calibration factors were compared and the error used as an indication of the calibration of the system. If the error was less than five percent the system was assumed to be adequately calibrated and functioning correctly. The theoretical calibration factor was used for stress-strain calculations. A sample of the calibration results is included in *Appendix D.*

5.5 General Test Parameters

5.5.1 Materials Tested

Commercially-pure copper, commercially-pure aluminium and mild steel were used as they are readily available and are often used during material testing, allowing ready comparison with published results. The composition of commercially-pure copper is relatively consistent, and although the degree of work-hardening will affect the stresses measured, it will be assumed for this work that this will not significantly affect the prevailing friction conditions. Thus all materials were tested as-received and standard tensile tests were performed to obtain accurate material properties.

5.5.2 Specimen Geometry and Scale

The issue of a suitable specimen geometry was investigated by Male & Depierre [14], as discussed in *Section 3.6.* They referred to the 6:3:2 geometry as a standard geometry and used it extensively, suggesting that it had been adopted as an 'unofficial standard'. Thinner specimens reportedly did display slightly less barrelling but were not used because of the difficulties involved in accurate specimen preparation. It was inferred that measurements were generally made at the midline, where the effects of barrelling are the most pronounced. It is worth noting that when internal diameter measurements were made at the specimen surface the effect of barrelling seemed to diminish, especially at increasing strain.

Male & Depierre [14] recommended the 6:3:2 geometry on general sensitivity and the practicality of production and experimentation, although the correlation with theoretical solutions was not as good as with the thinner specimens. To facilitate accurate specimen production this geometry was adopted throughout this investigation. Limited tests had previously been conducted using a 6:3:4 specimen geometry [19] but it was found that this did not offer any advantage in specimen production and no significant differences in behaviour or barrelling were observed.

Male & Depierre [14] typically used specimens of 25.4 – 50.8mm (1 – 2 in.) outer diameter, which provides a significant surface area and would result in large interface velocities at the specimen edges at high strain rates. This is to be avoided, as noted by Gray [3] and hence in this investigation specimens of a 6mm outer diameter were used. Smaller specimens are possible but this size allowed reasonably practical production, preparation and measurement on a large scale. This is also of the same order of magnitude as typical Hopkinson bar test samples, and thus is most appropriate in avoiding any uncertainties associated with scaling effects.

5.5.3 Specimen Dimension Measurement

Accurate specimen dimensions before and after testing are crucial to the accuracy of the ring compression test. Gorham [8] suggests that since the dynamic properties of engineering materials can exceed 25% of the static values, for results to be consistent across different testing apparatus and research centres, error in Hopkinson Bar results should be less than 1%. This value was adopted for all measurements made in this work.

Following specimen preparation each specimen was visually inspected and weighed on a Sartorius electronic lab-balance. Specimens were measured and the internal diameter was calculated according to the method described in *Section 5.5.3.1*. The mass was then determined assuming a regular annulus and using the density obtained from specially prepared cylinders. Density calculations appear in *Appendix G*. Correlation to within 1% was readily achieved.

Invariably errors greater than 1% could be attributed to irregularities in the specimen, for example, a burr was often found adjacent to one of the specimen faces, giving an exaggerated outer diameter. The specimen was either rejected or cleaned, re-weighed, and re-measured and accuracy always returned to around 1%. This ensured that all specimen dimensions were accurate before testing. Errors of the order of 0.02mm would be significant in the final calculations of the change in internal diameter. For example, an error in the measured height of 0.02mm (1% of specimen height) would result in just over 1% error in the internal diameter change. This would typically mean that a theoretical friction factor of 0.03 may be erroneously determined to be approximately 0.07, representing a significant error for the values typically obtained in this investigation.

This technique thus provided a valuable quality control and error trap, especially given the number of specimens prepared. Following testing barrelling occasionally resulted in a discrepancy greater than 1% but all specimens fell within 5% error. All tested specimens also indicated a larger calculated mass than actual mass. This could be attributed to the barrel on the external diameter.

5.5.3.1 Specimen Measurement Technique

The method devised for accurately measuring the internal diameter of the specimens involved placing a ball bearing of known diameter on the specimen so that it protruded slightly into the hole, as depicted in Figure 5.5.

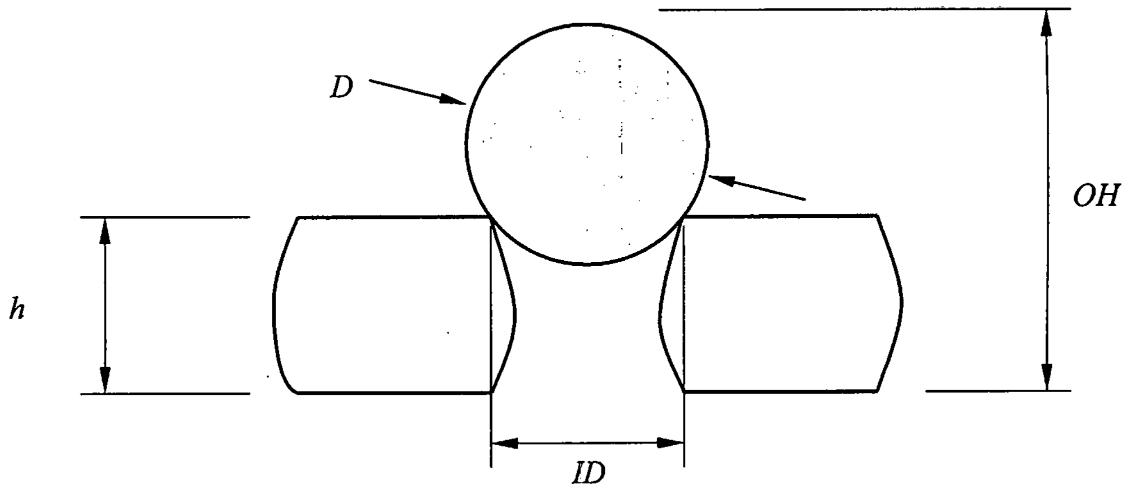

Figure 5.5 Diagram of cross section of deformed specimen with ball bearing in place showing measurement technique.

From the dimensions shown, all of which could be easily and accurately (±0.01mm) obtained using a standard micrometer, the internal diameter can be simply calculated as

$$\mathrm{ID} = 2\sqrt{\frac{D^2}{4} - (OH - h - \frac{D}{2})^2}$$

This technique allows measurement of the internal diameter at the specimen surface, eliminating the large barrelling effect observable on the specimen mid-line. It is important that the inner hole remains round during deformation as this technique will only provide the minimum diameter of an oval-shaped hole. The application of this method is illustrated in *Figure 5.6*.

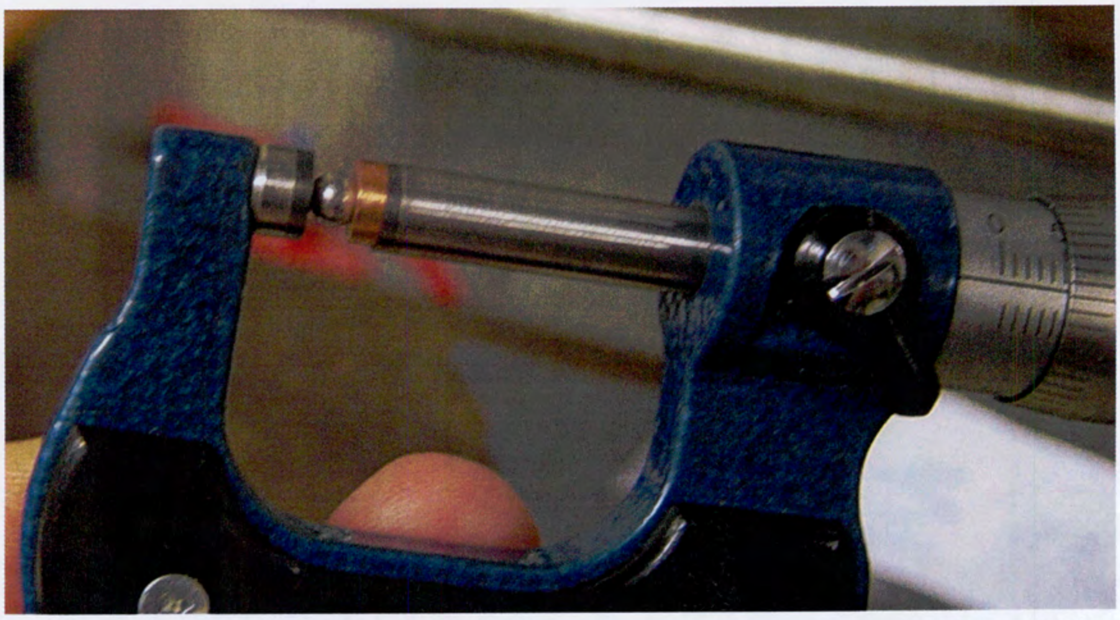

Figure 5.6 Photograph showing the measurement of the internal diameter of a specimen using a standard outside micrometer and a ball bearing, according to the method devised and outlined in *Section 5.5.3*.

5.5.4 Specimen Preparation

Highly regular specimens are required for consistent testing and this presented some manufacturing challenges. Rods were drilled out and then machined to the required outer diameter. The individual specimens were parted off from this tube but this process introduced sizeable burr and irregularities in the specimens. Deformation was particularly severe with aluminium. All specimens had to therefore be carefully cleaned and shaped before preparation. Sharp corners are assumed in the theory and measurement process and were maintained so as not to reduce the effective area in contact with the anvil. Although rounded corners may potentially reduce friction phenomena such as fold-over, this variable could not be adequately controlled and does not match anticipated Hopkinson Bar test specimens, which this investigation attempts to represent as closely as possible.

5.5.5 Surface Finish

Surface roughness is known to be one of the main factors determining friction and as such was an important test variable in this investigation. The different finishes tested were chosen to facilitate eventual bulk Hopkinson bar specimen preparation. For this reason the different roughnesses are specified by the grade of the SiC paper used to finally abrade the surface. The 600-grit and 1200-grit paper grades used are readily available and the surface roughness produced is of a reasonable scale given the specimen size. Specimens were mounted in batches of six on a flat holder using double sided tape, as illustrated in *Figure 5.7*.

Figure 5.7 Photograph showing specimens mounted on the specimen holder, as used for grinding.

This setup was prepared on rotating grinding papers, with cooling water. Preparing six specimens together helped to ensure that the faces of the specimen were ground perpendicular to the sides and that the faces remained parallel to within measurable tolerances. Specimens were carefully ground down to 2mm, one side at a time, and finished on fresh papers to ensure a consistent roughness for a given paper grade. The quasi-static compression anvils were finished on the grinding pads with cooling water in the same manner as the specimens but the Hopkinson bars proved too long for powered abrasion and were simply faced off on a lathe and then carefully and lightly roughened by hand.

5.5.5.1 The importance of a uniform surface finish

Scratches induced during specimen preparation were clearly visible to the naked eye. As discovered in previous work [19] grinding on rotating pads introduced a definite orientation onto the final specimen surface. This resulted in severe uneven, 'oval' deformation during testing and caused the measurement technique devised to be inaccurate (see *Section 5.5.3*). Care was therefore taken to ensure a random pattern, with no specific orientation on the final, roughened faces of the specimen, compression anvils and bar end-faces, as can be seen in *Figure 5.8*.

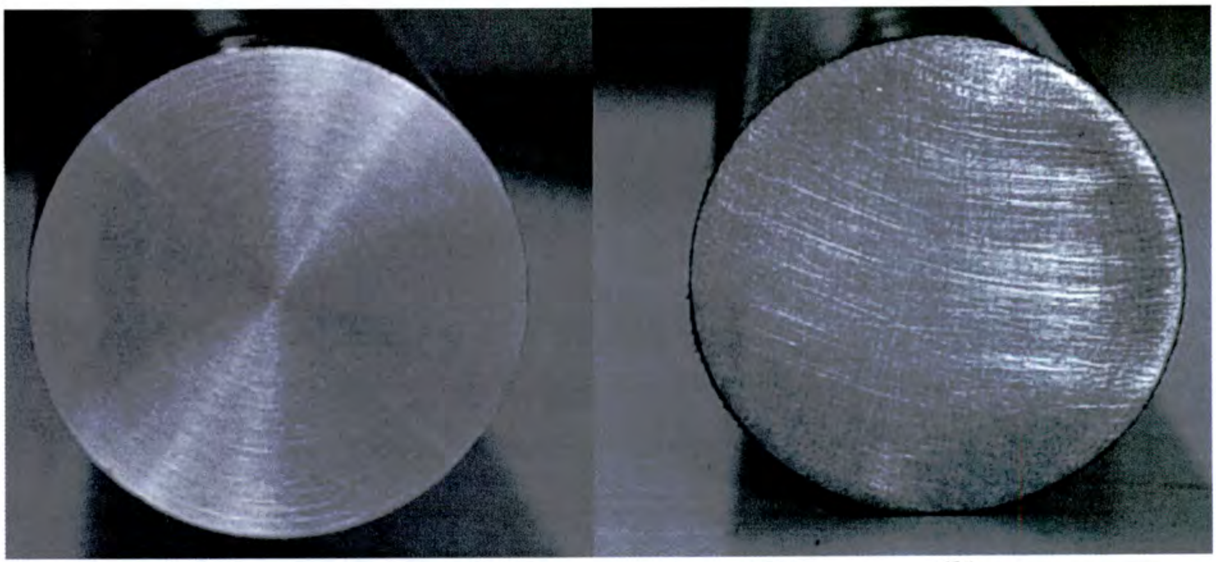

(a) *(b)*

Figure 5.8 Photographs showing the end-face of a typical Hopkinson Bar as-machined (*a*) and the end of a bar that was roughened using a 600-grit SiC grinding paper (*b*), as used for the high strain rate ring compression tests.

5.5.6 Lubrication

As mentioned previously it is generally accepted that lubrication is essential in Hopkinson bar tests to limit the significant effects of friction [3,9,11]. Limited specimens were tested with no lubricant to establish the maximum error that may be experienced, and to provide a benchmark against which different lubricants could be assessed and comparisons made with published test results. Greases containing molybdenum-disulphide were used for the lubricated tests as recommended by Follansbee [4] and Gray [3] and used for high strain rate tests by Gorham *et al* [8]. These greases are relatively inexpensive and readily available, which simplifies potential similar testing and allows use of the investigated scenarios for future, large scale Hopkinson Bar test programs. The grease specifications are included as *Appendix H.*

Because the viscosity of grease increases significantly under pressure it has been suggested that at high strain rates a hydrodynamic squeeze film may develop [8]. There is sufficient time for the grease to be almost completely squeezed out during quasi-static compression, but under high strain rate tests this may not be possible. Lubricant efficiency may thus be markedly improved at higher strain rates. Gorham *et al* [8], having performed ring compression tests at high strain rates, also suggests that there may be a region of lubricant breakdown near the specimen periphery, where relative velocities are greatest. They suggest that an area of increased roughness may help to trap grease more efficiently and reduce the overall friction restraint. Diamond-polished specimens had previously been shown significant and inconsistent frictional restraint (see *Appendix C.3*).

As mentioned in *Chapter 2* the thickness of the lubricant layer may have an effect on the timing of the stress pulses measured using the Split Hopkinson Pressure Bar apparatus. Follansbee [4] states that there may be a significant delay in the stress waves even for a very thin lubricant film. This was investigated by repeating tests with light and heavy greasing, as described in *Section 5.4.3.*

5.5.7 Strain Rate

5.5.7.1 Quasi-static Tests

Quasi-static tests were controlled through cross-head displacement with 1mm/min providing the desired nominal strain rate of less than $10^{-2}s^{-1}$

5.5.7.2 High Strain Rate Tests

The strain rate on a Hopkinson Bar apparatus can be indirectly controlled through striker length and velocity. The strain rate achieved for these tests was typically between $1000s^{-1}$ and $2000s^{-1}$.

6 EXPERIMENTAL RESULTS

6.1 Introduction

This chapter contains the results of the quasi-static tests and the high stain rate tests performed using the ring compression test method. The observations made during the investigation into the effect of lubricant thickness, and in particular on the potential timing discrepancy in Split Hopkinson Bar results, are also presented.

6.2 Quasi-Static Test Results

The quasi-static test program facilitated the development of an accurate and reliable test methodology. The specimen preparation, grinding, lubrication and measurement processes were established and the trends and observations of previous work, as discussed in *Section 2.8*, were confirmed. The repeatability of the results, agreement with the analytical solution, and accuracy of measurement were all good.

The experimental results and 2nd order polynomial best fits for the mild steel specimens appear as *Figures 6.1* and *6.2*. The best fit curves are compared with the theoretical curves from Avitzur's analysis [1] in *Figure 6.3*. *Table 6.1* gives the approximate 'm' friction factors obtained for the given test conditions.

Specimen Surface Finish	**Anvil Surface Finish**	**Lubricant**	**m**
600-grit	600-grit	MoS_2 grease	0.14
1200-grit	**600-grit**	**MoS_2 grease**	**0.07**
600-grit	1200-grit	MoS_2 grease	0.16
1200-grit	1200-grit	MoS_2 grease	0.14

Table 6.1 Theoretical friction factors obtained by comparison with Avitzur's analytical solution [1], for the various quasi-static tests on mild steel.

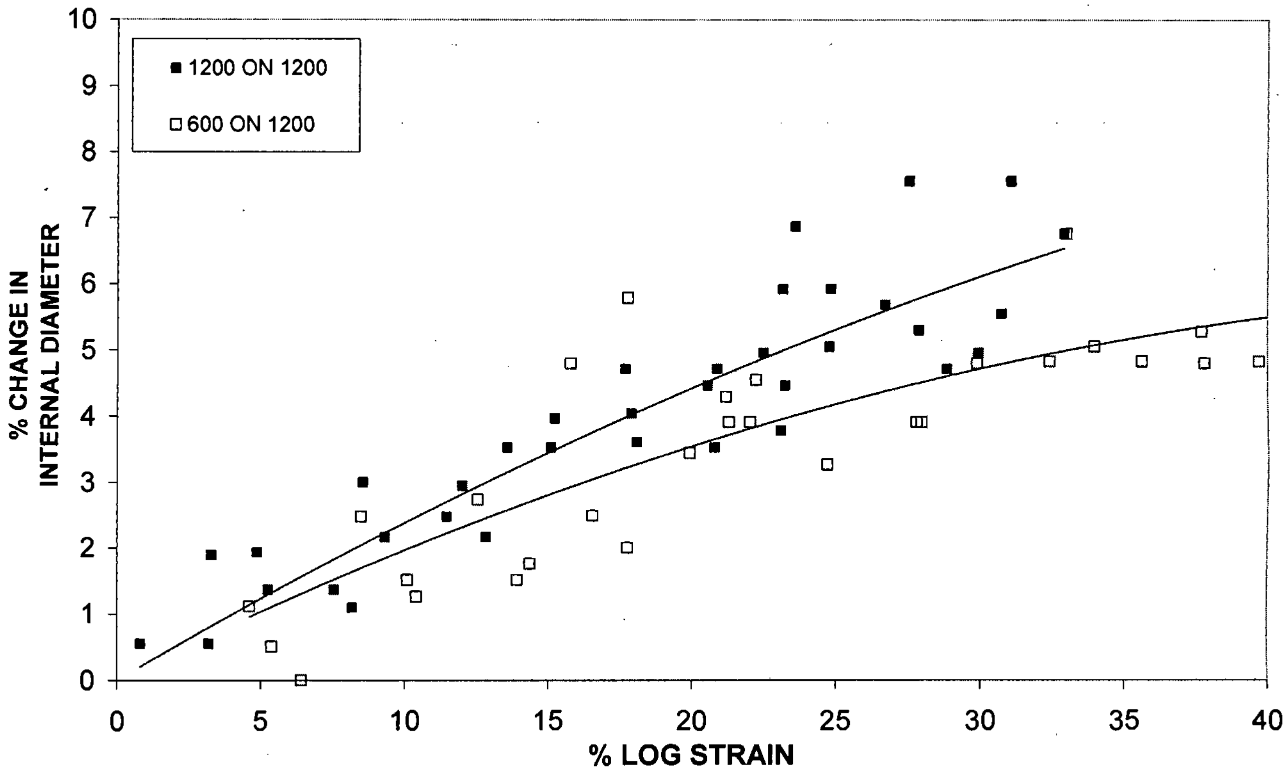

Figure 6.1 Graph of quasi-static ring compression test results for mild steel specimens tested on 1200-grit anvils, with least squares 2nd order polynomial fit.

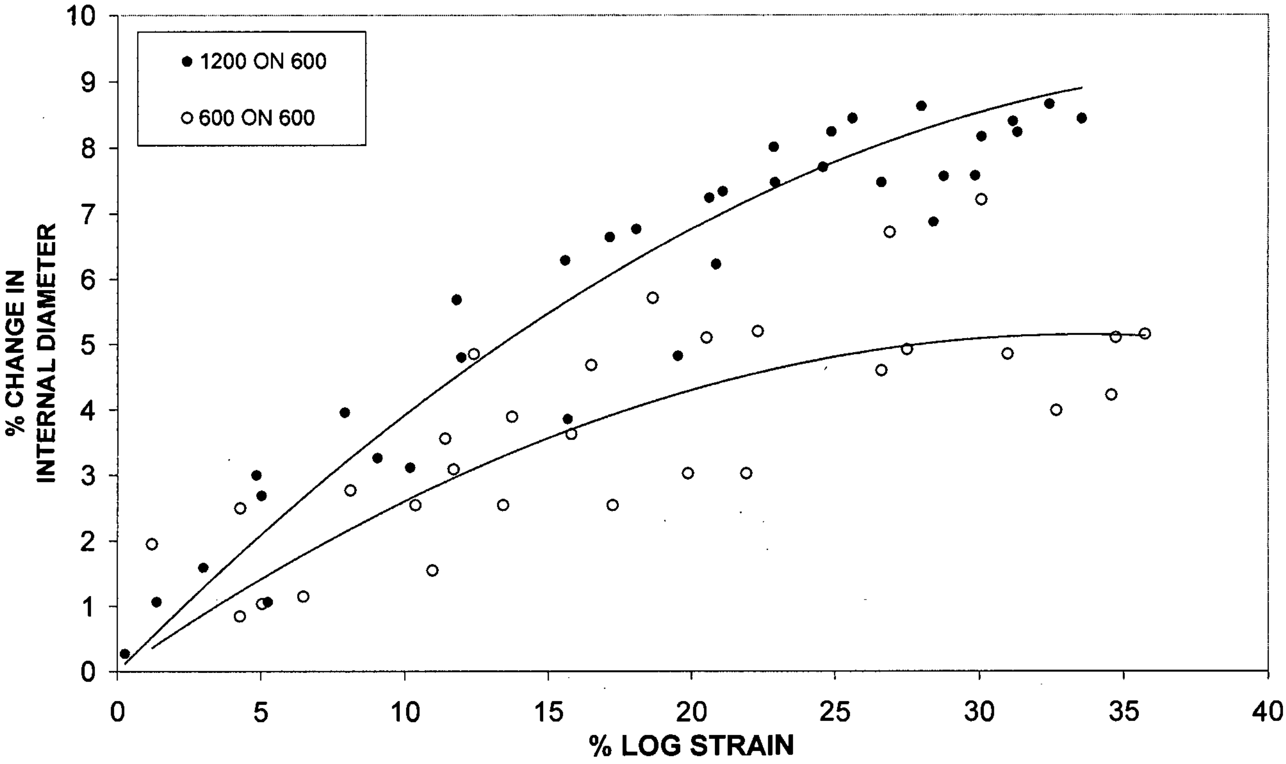

Figure 6.2 Graph of quasi-static ring compression test results for mild steel specimens tested on 600-grit anvils, with least squares 2nd order polynomial fit.

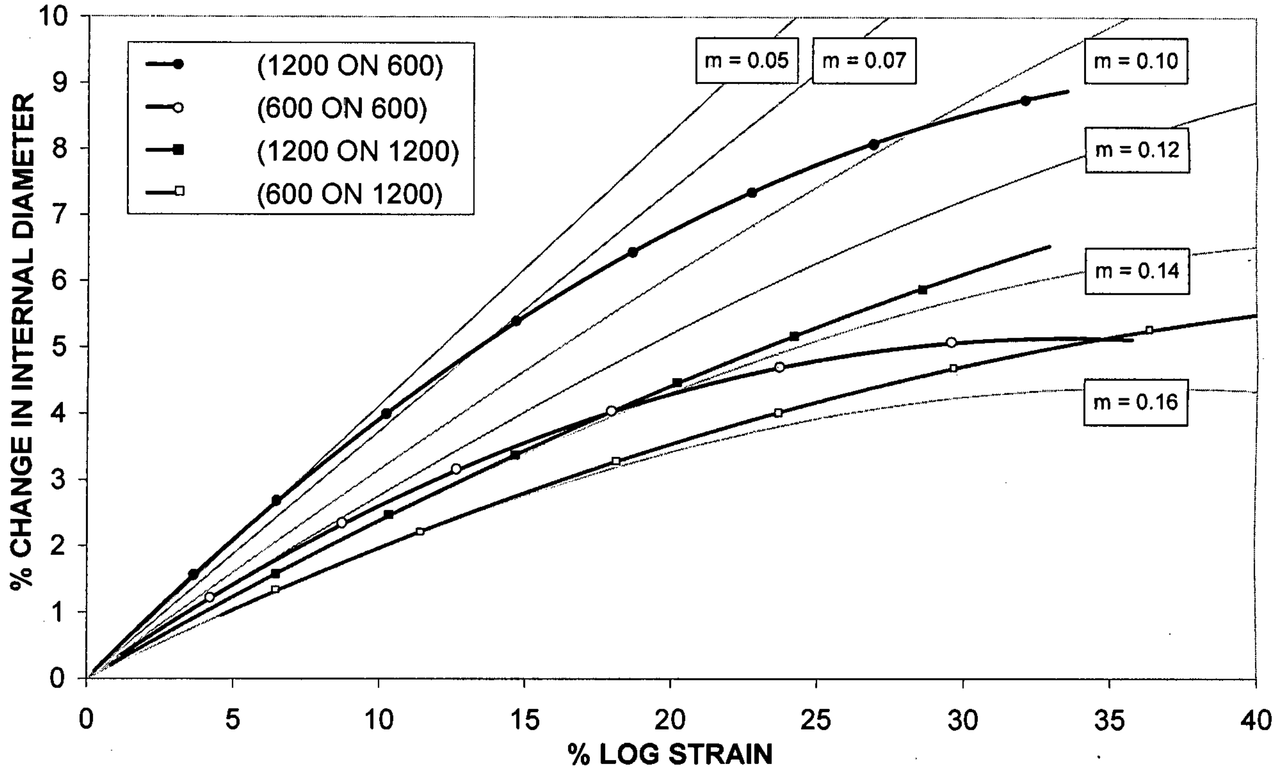

Figure 6.3 Graphical comparison of best fit curves for quasi-static mild steel ring compression test results with theoretical curves according to Avitzur's theory [1].

The lowest friction conditions were obtained for specimens prepared using 1200-grit paper and anvils prepared using 600-grit paper, with friction initially as low as m = 0.05, but rising steadily with increasing strain to an average value of approximately 0.07, as given in *Table 6.1.*

The results from the tests on copper specimens, which were repeated twice, appear in *Figure 6.4*. The test method was the same as that used for the steel specimens, using incremental compression steps between which the specimen was measured and regreased. Friction factors were slightly higher than those of the steel tests with no significant difference emerging across the three different anvil finishes used. The 'm' friction factor for all surface finish combinations was approximately 0.12.

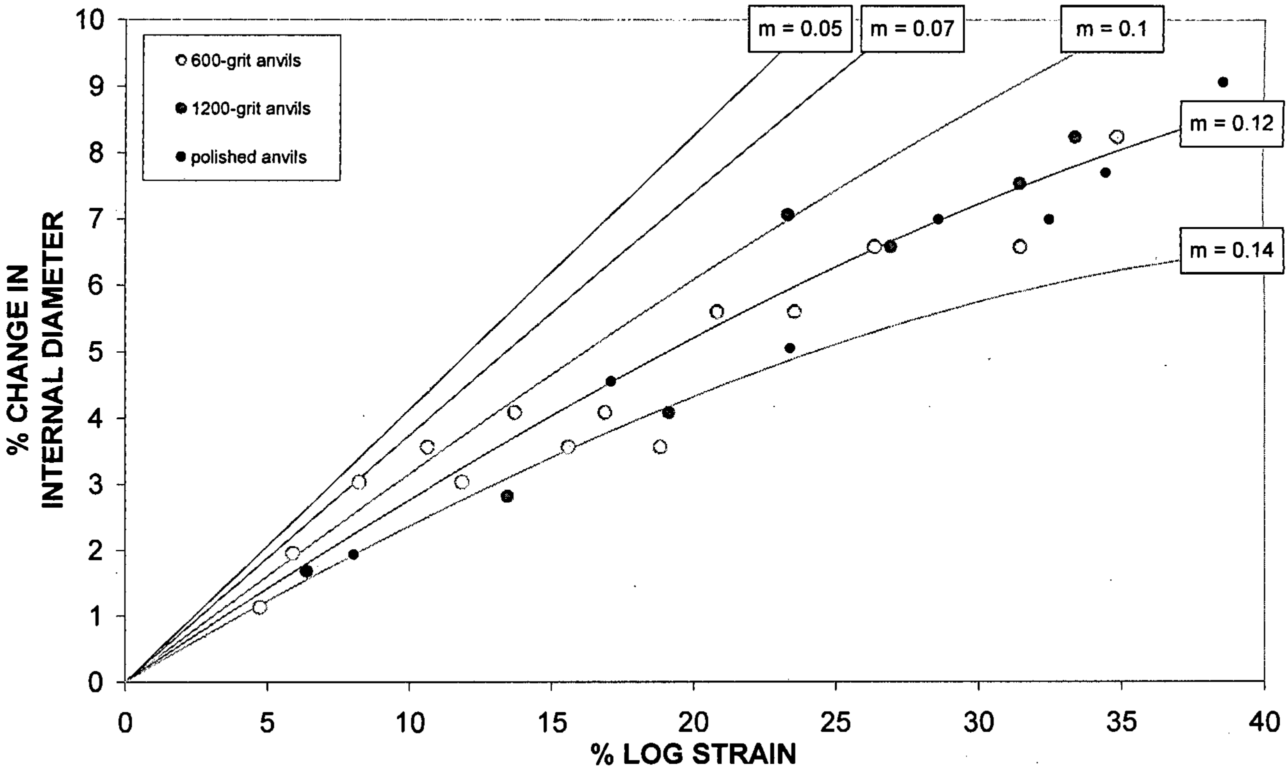

Figure 6.4 Graphical results for 600-grit copper ring compression specimens, tested quasi-statically on three different anvil finishes.

6.3 High Strain Rate Test Results

6.3.1 General Observations

Repeatability and good correlation with the theory was seen in all the experimental results. The consistency was even better than for the quasi-static tests and part of the reason for this may have been the slightly smaller strain range that was covered. Friction factors of m = 0.08 were established as readily repeatable for the specified test conditions. Specimens tested dry demonstrated the necessity for lubrication in preventing excessive friction and the attendant error. A strain rate between 1600s^{-1} and 2100s^{-1} was achieved for the different materials. The specific results for the different materials appear in *Sections 6.3.2, 6.3.3* and *6.3.4.*

6.3.2 Mild steel

Data generated for mild steel specimens appears in *Figures 6.5, 6.6* and *6.7.*

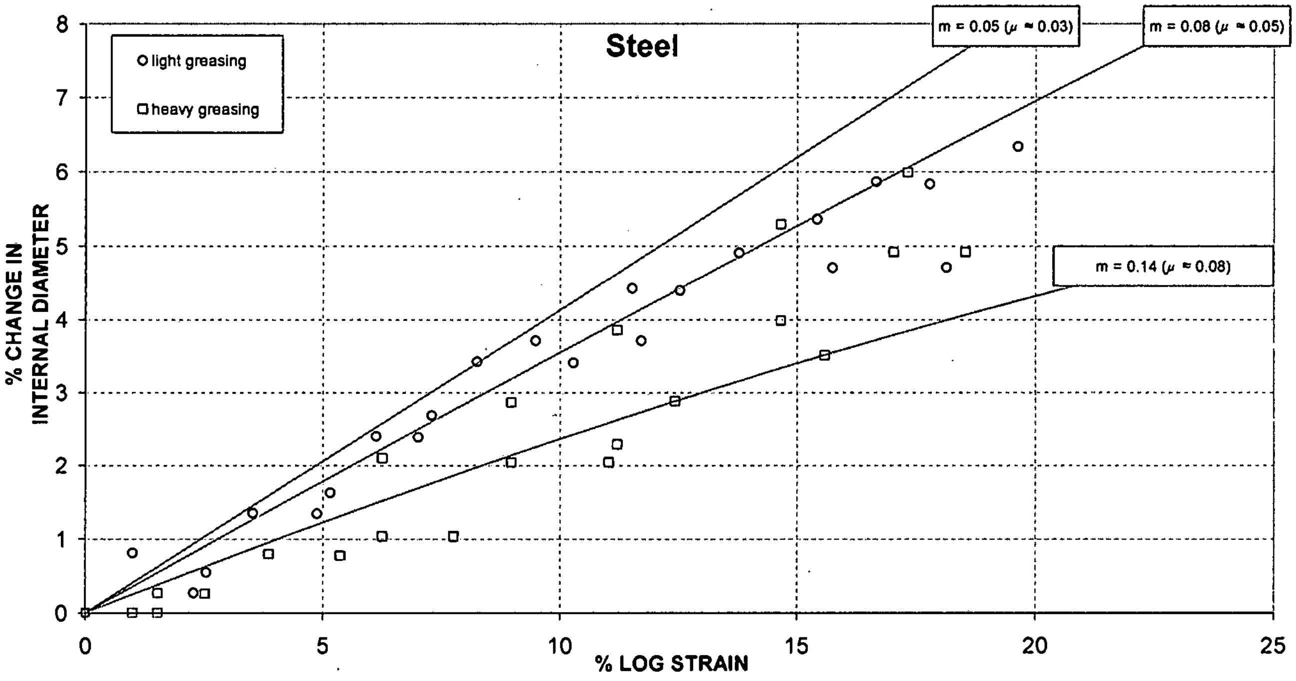

Figure 6.5 Graph of high strain rate ring compression test results for mild steel, with theoretical curves [1].

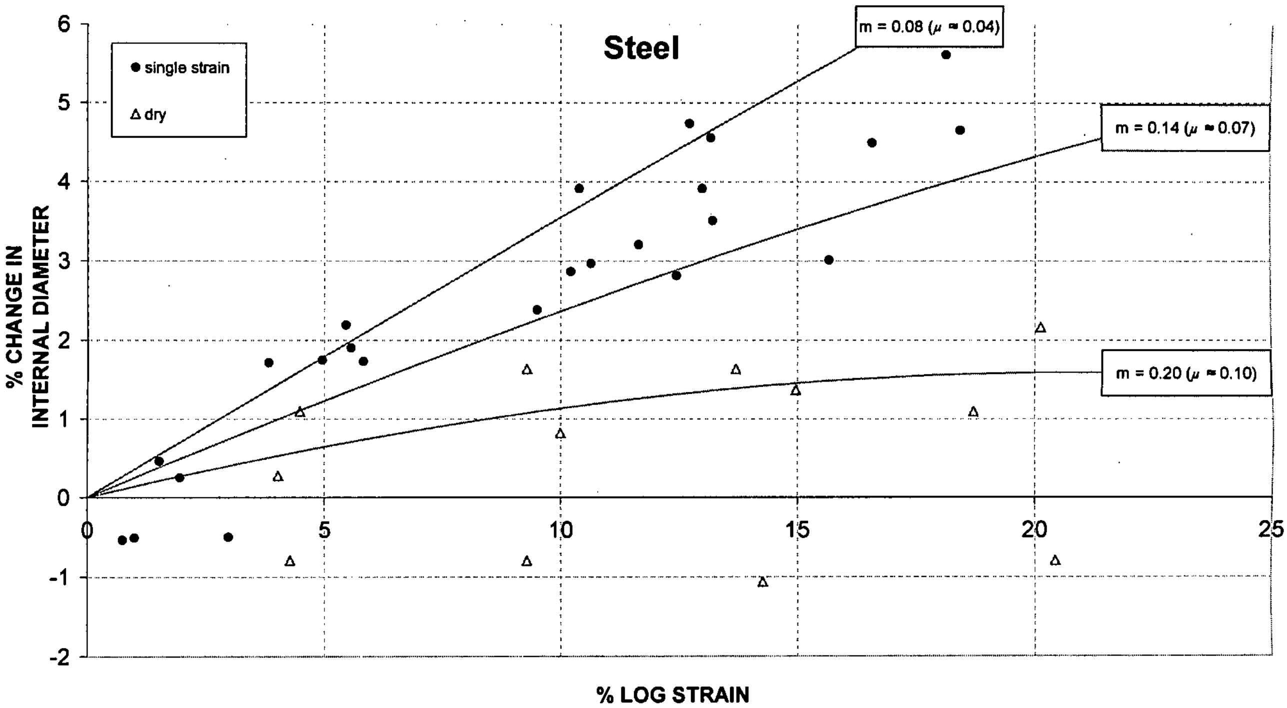

Figure 6.6 Graph of high strain rate ring compression test results for mild steel, with theoretical curves [1].

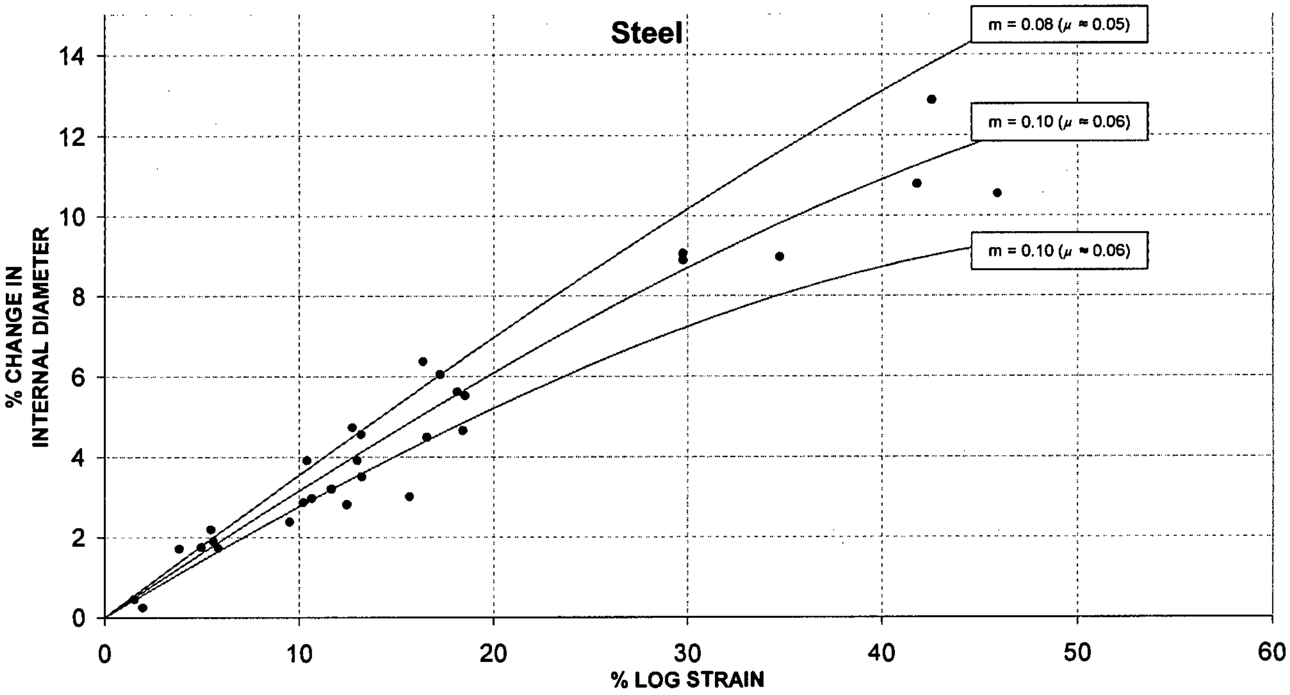

Figure 6.7 Graph of high strain rate ring compression test results for mild steel specimens tested in a single compression, with theoretical curves [1].

Friction factors of m ≈ 0.08 were achieved consistently for specimens subjected to repeated small increments of strain, with regreasing between intervals. Specimens strained only once under similar conditions showed slightly more scatter and measured friction was slightly higher with m ≈ 0.1. Specimens strained up to 45% in three large consecutive compressions fell on the same theoretical friction curve, indicating that the given lubrication conditions and surface preparation can give consistent friction conditions even for large strains. Using more grease appeared to increase friction slightly. The effect on the measured stress-strain data is presented in *Section 6.3.5*. Dry specimens, as expected, experienced a large frictional restraint and indicate the potential for large errors in Hopkinson bar data if no effort is made to actively limit friction.

6.3.3 Copper

Data generated for copper specimens appears in *Figures 6.8, 6.9* and *6.10.*

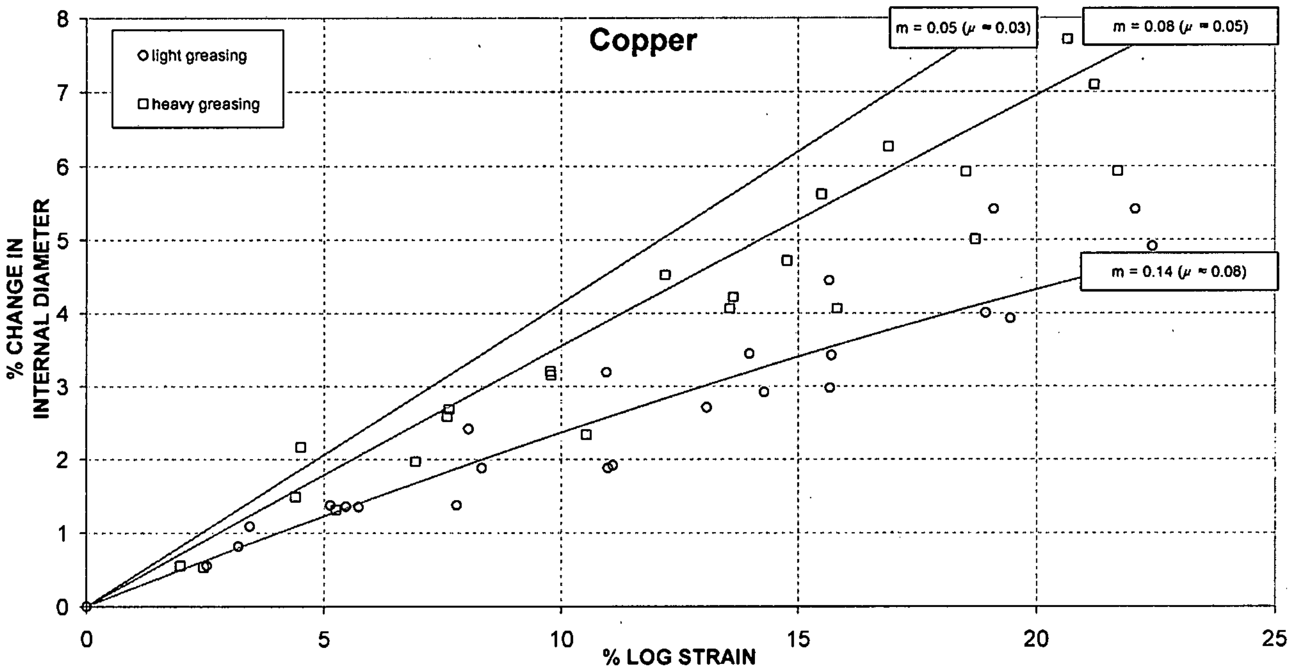

Figure 6.8 Graph of high strain rate ring compression test results for copper, with theoretical curves [1].

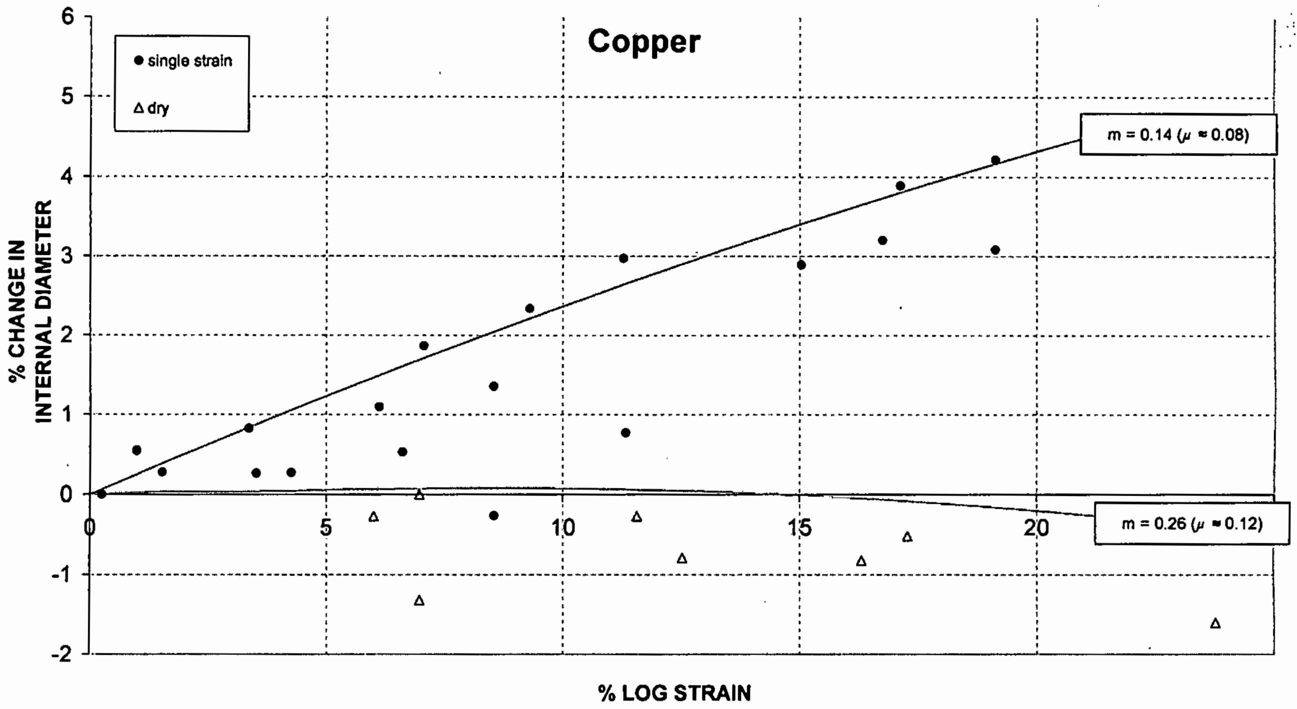

Figure 6.9 Graph of high strain rate ring compression test results for copper, with theoretical curves [1].

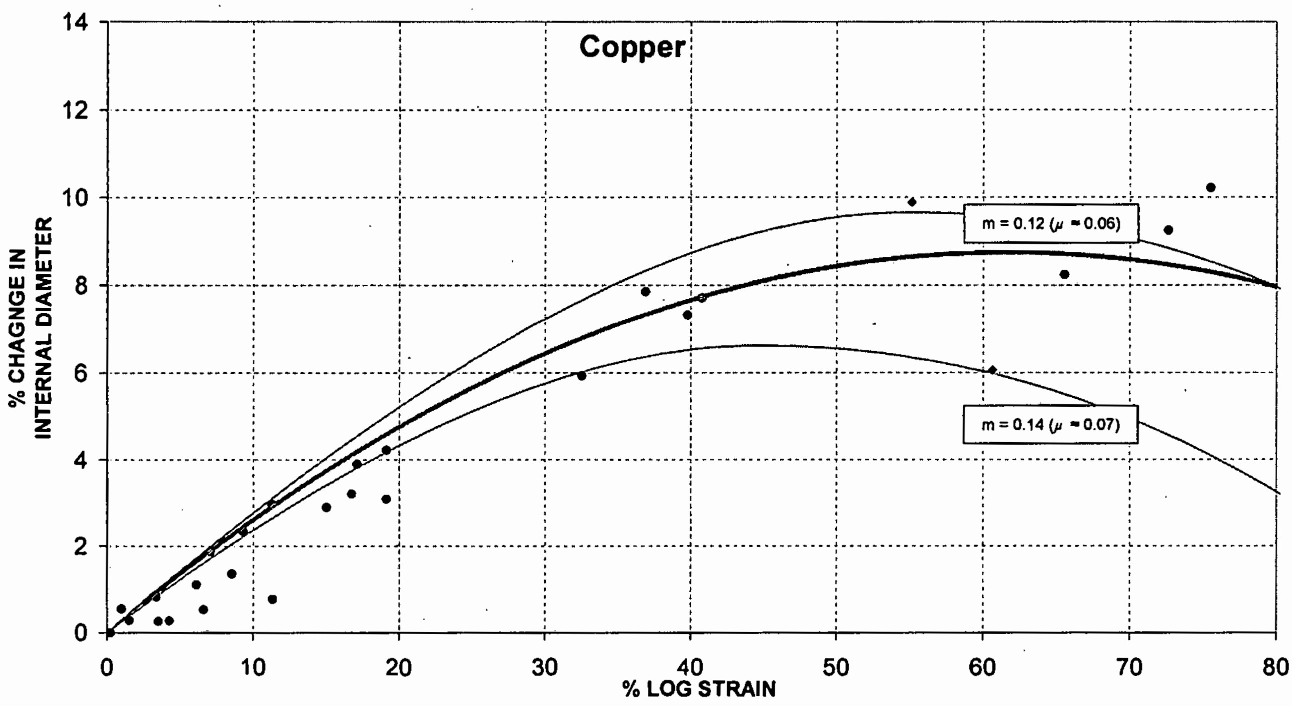

Figure 6.10 Graph of high strain rate ring compression test results for copper specimens tested in a single compression. A 2^{nd} order polynomial best-fit (thick line) is included illustrating the good correlation with the theory [1].

Generally copper showed similar trends to the results for the steel specimens. Friction however was marginally higher for all test scenarios, as was observed in the quasi-static tests. Friction factors were typically around m ≈ 0.1. The specimens tested with heavier greasing consistently recorded lower friction values than the specimens tested with a light layer of grease.

6.3.4 Aluminium

Data generated for aluminium specimens appears in *Figures 6.11*, *6.12* and *6.13*.

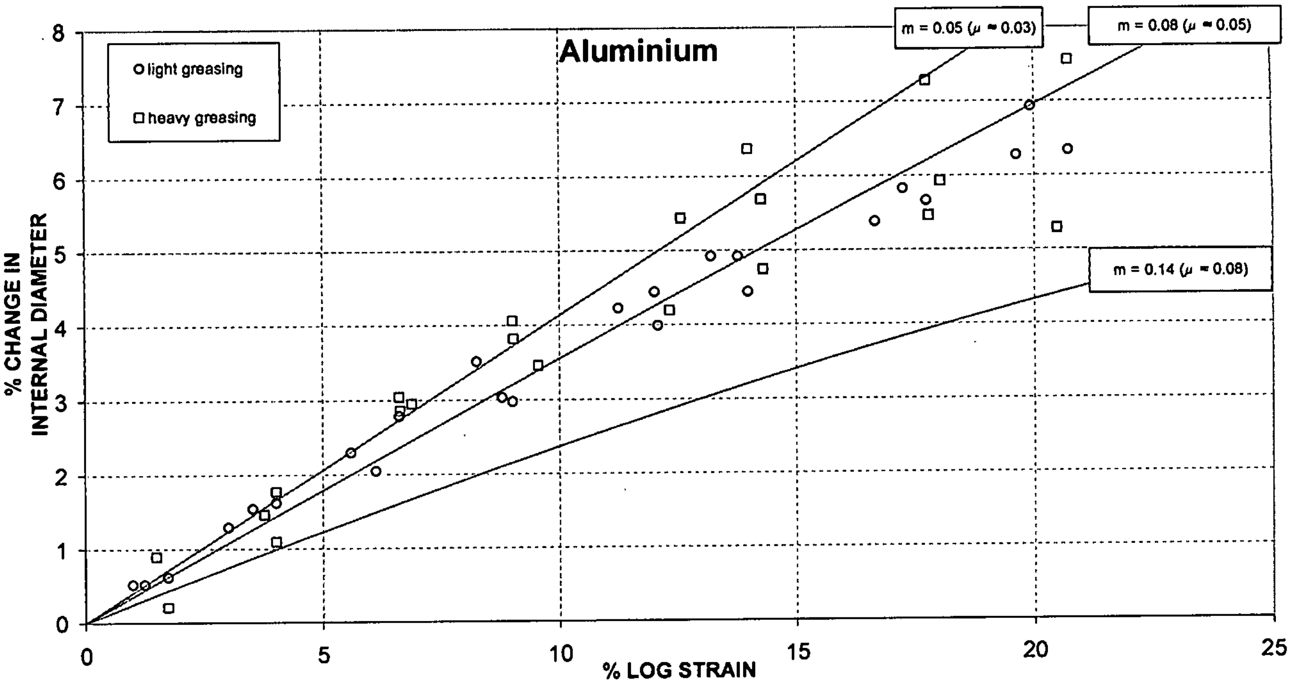

Figure 6.11 Graph of high strain rate ring compression test results for aluminium, with theoretical curves [1].

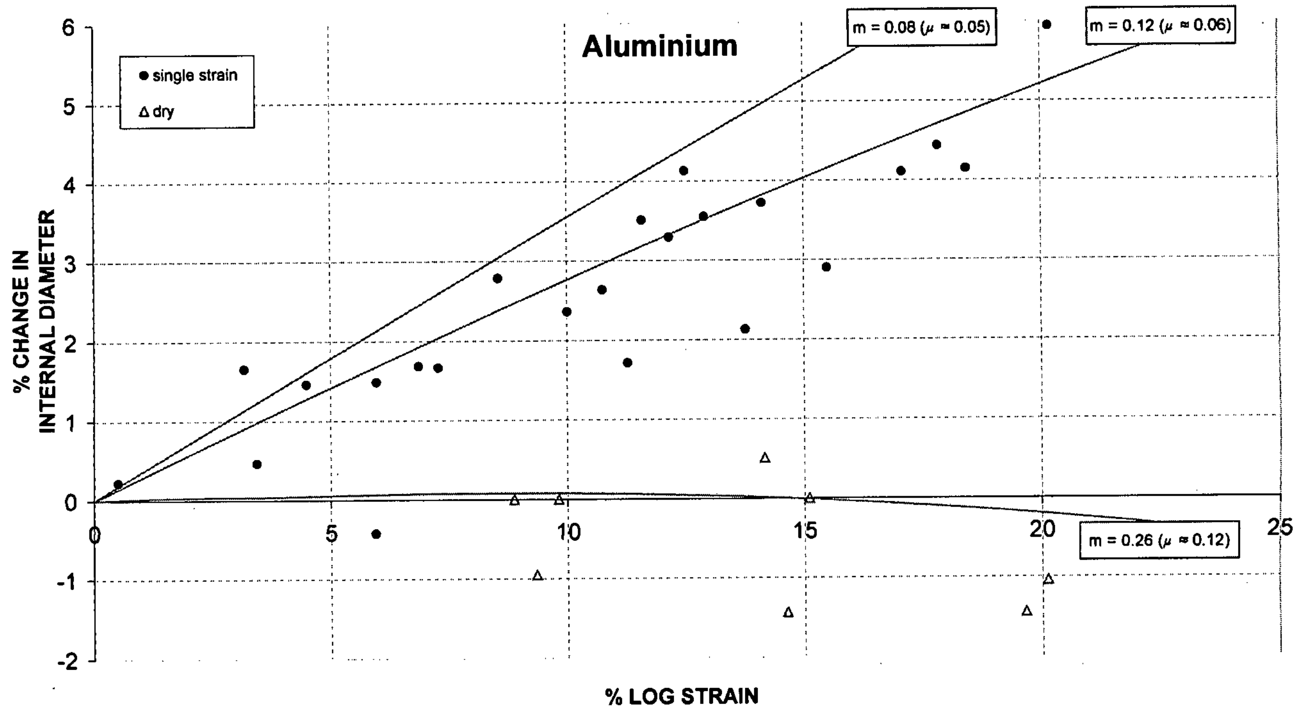

Figure 6.12 Graph of high strain rate ring compression test results for aluminium, with theoretical curves [1].

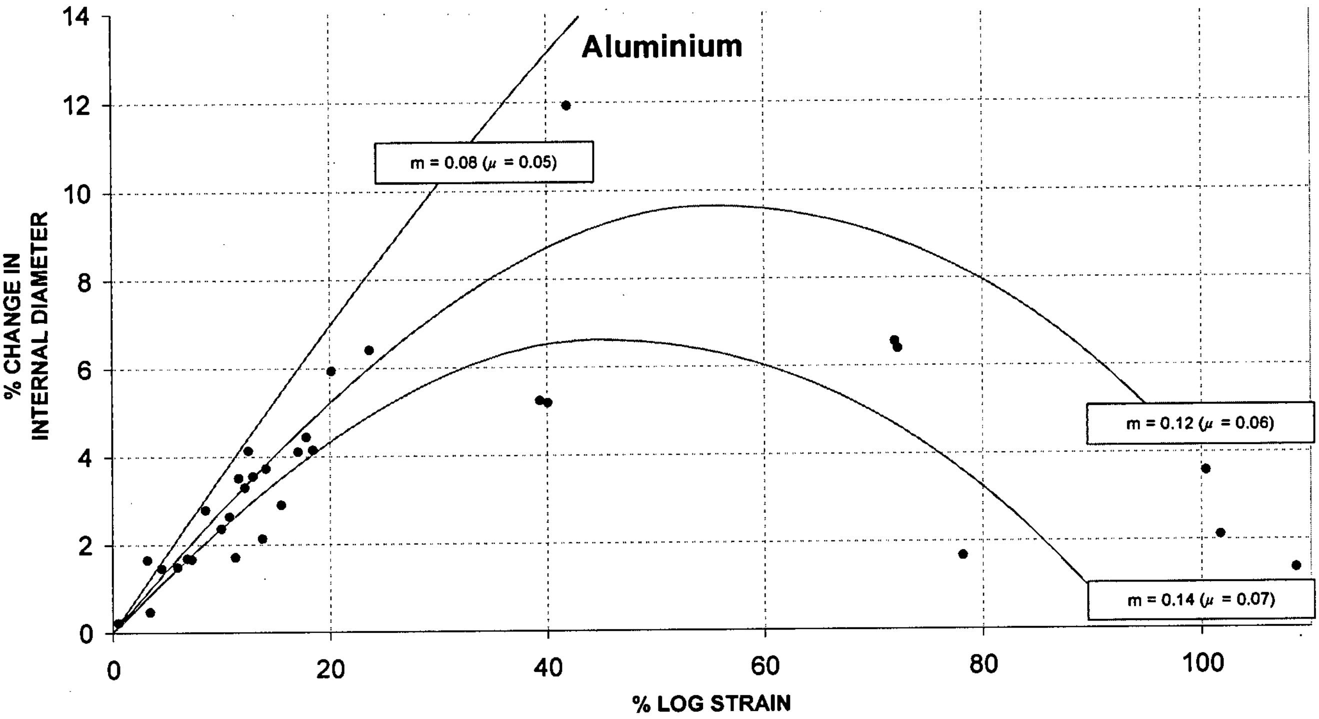

Figure 6.13 Graph of high strain rate ring compression test results for aluminium specimens tested in a single compression, with theoretical curves [1].

The aluminium curves followed trends similar to those of the copper and mild steel specimens. The repeatability at low strains was very good with results falling very close to the theoretical m = 0.08 curve. At higher strains the aluminium seemed to break down on the surface and on the sides of the specimen, with small creases and folds appearing. Large scatter and divergence is seen at the higher strains.

6.3.5 Effects of Lubricant Layer Thickness

Lubricant has been shown through the tests on unlubricated specimens to be essential in reducing friction to acceptable levels. The required thickness of the lubricant layer, however, remains unclear. Follansbee [4] discusses the time delay that can be introduced between the reflected and transmitted pulses by the layer of lubricant on the ends of the specimen, as raised in *Section 3.8*. As mentioned in *Section 5.4* specimens were tested heavily and lightly greased, implying different lubricant film thicknesses. The thickness of the lubricant layer could not be measured but was varied by using either very liberal or only light amounts of grease and by varying the pressure applied when the bars were brought together.

As can be seen in *Figures 6.5 – 6.13* the measured 'm' friction factors were very similar for different amounts of lubricant, with steel exhibiting slightly higher but copper slightly lower friction when more lubricant was used. The optimum lubricant layer thickness may be best obtained through experimentation with the specific lubricant and material.

A distinct time gap was noticed between the transmitted pulses of tests using light greasing and those using heavy greasing, as shown in *Figures 6.14* and *6.15*. The curves compare the recorded voltage-time signals for light and heavily greased mild steel ring compression test specimens, compressed from a thickness of 1.95mm to 1.90mm.

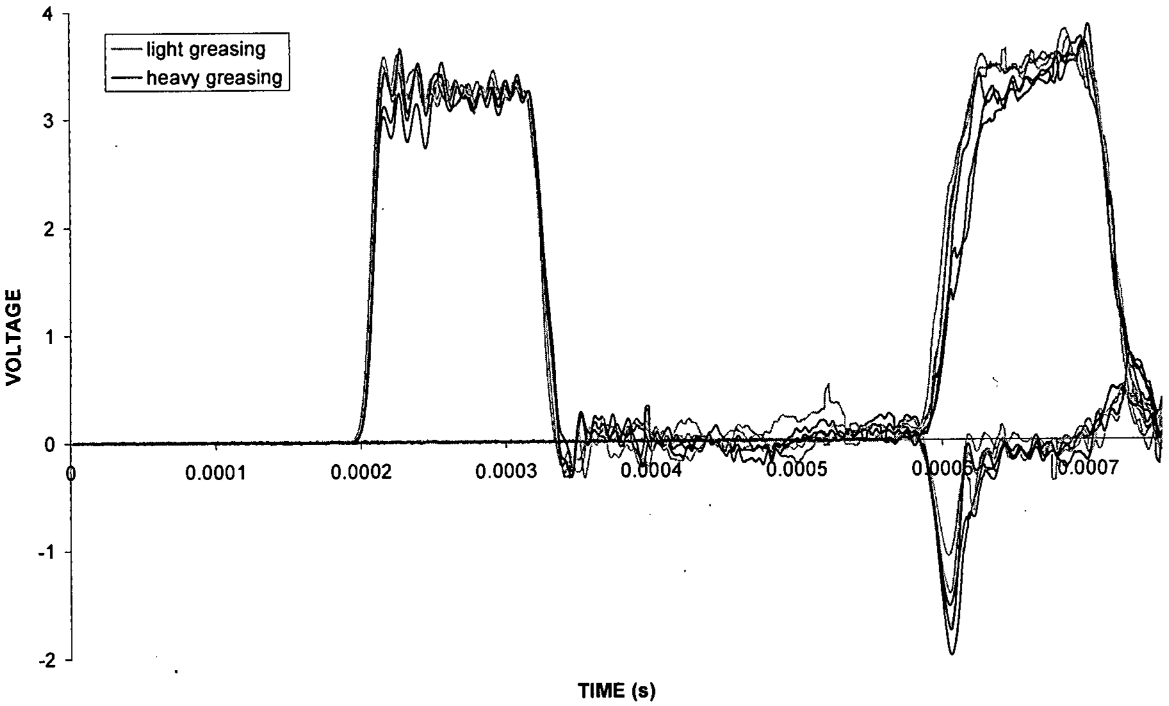

Figure 6.14 Graph showing the recorded voltage-time signals for mild steel ring specimens. The time lag of the transmitted pulse for specimens tested heavily greased is evident, as is the larger reflected pulse.

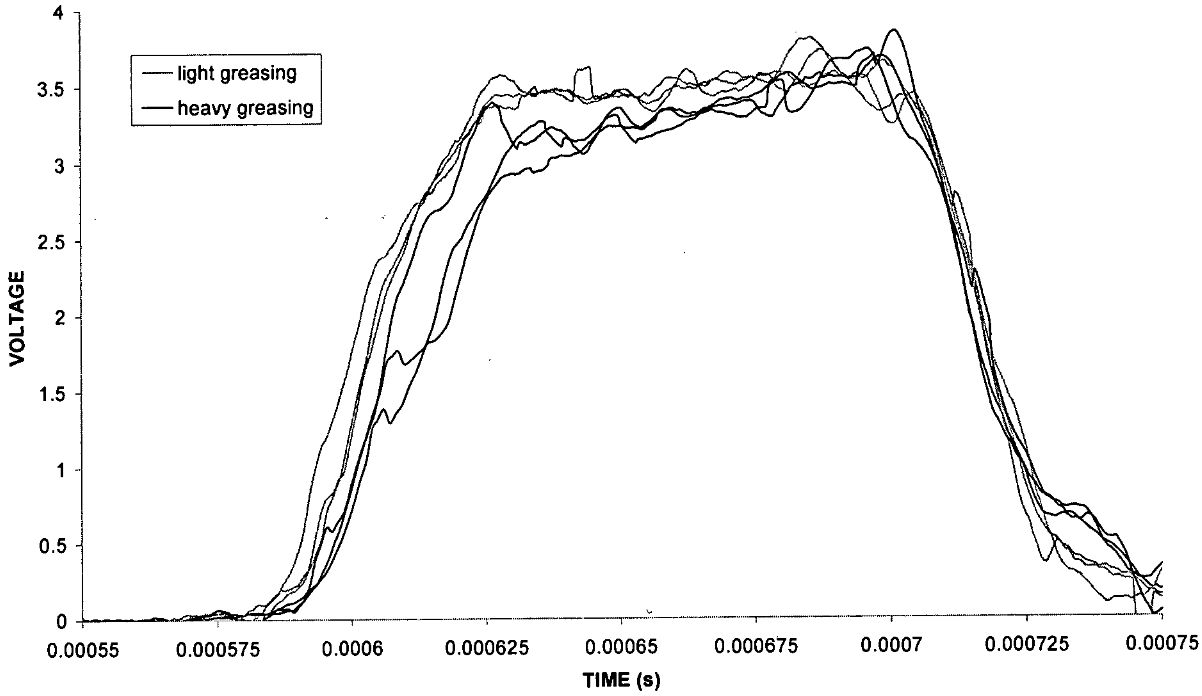

Figure 6.15 Graph of recorded voltage-time signals of the transmitted pulse. Note the time lag of the transmitted pulse for the heavily greased specimens of approximately 5μs, and the slight plateau in the pulse rise.

Figure 6.14 demonstrates that the magnitudes of the incident pulses were identical but the reflected pulses were larger for the heavily greased specimens.

The time difference that can be seen between the two sets of transmitted pulses was approximately 5μs. A slight plateau also appears on the rise of the transmitted pulse for some of the heavily greased tests. This may indicate the point at which the grease is squeezed out or compressed as the bar moves forward to contact the specimen.

The expected time difference in the reflected and transmitted pulses can be calculated by determining the particle velocity in the bar. For a strain rate of $1800s^{-1}$ in a 2mm thick specimen, as was typically obtained for the mild steel specimens, the particle velocity in the bar would be approximately 3.6m/s, from:

$$\dot{\varepsilon} = \frac{v_b}{l_s}$$

where v_b = the particle velocity in the bar (see *Appendix A*).

A lubricant layer of 0.025mm would therefore cause a 6.9μs delay in the reflected and transmitted pulses. This figure agrees with the delay measured from the voltage time signals (*Figure 6.15*). By comparison the incident stress waves generated lasted typically 150μs and had a rise time of approximately 15μs, for the pulse-shaping method used.

7 MICROSTRUCTURAL INVESTIGATION

7.1 Introduction

In previous work on the ring compression test [19] (discussed in *Section 3.7*) a peripheral region was observed around the outer rim on the surface of some of the specimens. Similar observations were mentioned by Gorham *et al* [8] and Walley *et al* [10] and this prompted the recommendation that a microstructural investigation of the deformed grain structure be made. In this chapter the details and results of a microstructural analysis of the tested ring compression specimens are presented and discussed, with reference to some of the experimental results in *Chapter 6*.

7.2 Background

Gorham *et al* [8] provide dimensions for an outer peripheral region that they observed on ring compression test specimens tested at a high strain rate to a strain of about 35% (see *Table 7.1*).

Surface / **Lubricant**	**3μm diamond-polished**	**600 grade SiC**	**Bead-blasted**
Rocol A.S.P.	0.130 (0.03 - 0.07)	0.330 (0.02 – 0.08)	0.500 (0.05 – 0.09)
Rocol J166	0.100 (0.04 – 0.06)	0.065 (0.02 – 0.04)	0.130 (0.05-0.07)
Graphoidal Developments BG15	0.030 (0.01 – 0.07)	0.050 (0.03 – 0.05)	0.100 (0.05 – 0.09)

Table 7.1 Results from Gorham *et al* [8] of outer peripheral region (mm) and the measured friction parameter, m (in brackets).

The formation of this peripheral region was attributed to lubricant breakdown, which is assumed to occur where the interface velocity is greatest. In discussing dynamic friction they quote Schey [17] who suggests that an area of increased roughness at the periphery may actually reduce the overall frictional restraint by trapping grease, preventing complete sticking in localised areas. Test conditions that led to the formation of this peripheral region were considered unsatisfactory and it was inferred that lubricant breakdown had occurred. This could result in conditions of sticking friction over a portion of the specimen surface and hence a non-uniform stress distribution within the specimen. From the above result there appears to be a slight increase in the size of the peripheral region with friction. The specimens tested were reportedly 4mm in diameter and thus the peripheral region, which was generally between 0.05mm and 0.13mm, accounted for between 2.5% and 6.5% of the initial specimen radius.

Walley *et al* [10] mentioned the appearance of a 'fold-over' zone, identified as a smooth region at the perimeter of a typical ring specimen. Through numerical modelling they concluded that during compression specimens typically deform in a flowing or folding manner, rather than by sliding as is generally assumed in the theory, including in the analysis by Avitzur [1]. They suggested that this might explain the appearance of this peripheral region on compression test specimens. The fold-over zone they used to illustrate the phenomenon represented approximately 10% of the initial specimen radius for a coulomb friction coefficient of roughly 0.1. This fold-over zone is described and illustrated by Schey [18].

A distinct region was noted on a number of specimens tested in previous work [19] and on specimens tested at both quasi-static and high strain rates during this investigation. This phenomenon is illustrated on specimens tested quasi-statically and dynamically in *Figure 7.1*.

(a) *(b)*

Figure 7.1 Photographs of specimens tested (a) quasi-statically to about 40% strain and (b) at approximately $1800s^{-1}$ to 30% strain, showing a distinct peripheral region.

7.3 Objectives

Encouraged by the above results and observations and following the appearance of a smooth peripheral region on preliminary quasi-static and dynamic test specimens, a study of the grain structure of tested ring specimens was undertaken.

The objectives of this study were to:

1. **Compare the microstructural behaviour of specimens tested quasi-statically and dynamically.**
2. **Establish whether fold-over was the reason for the appearance of distinct regions on the surface of deformed specimens.**
3. **Establish whether folding was related to the friction conditions.**

7.4 Methodology

The microstructural investigation was conducted using copper specimens from the quasi-static and high strain rate test programs. All specimens were carefully inspected for any sign of a peripheral region or general surface defects. The approximate width of the region was measured, and compared to the percentage strain and the estimated 'm' friction factor for that specimen. Quasi-statically tested specimens and dynamically tested specimens were selected across the range of friction conditions and strains recorded. The specimens were sectioned, etched and examined. The grain structure was studied microscopically to determine whether fold-over had occurred, and if so, to what extent. The degree of fold-over was compared to the value obtained from macroscopic inspection of the surface before sectioning to ascertain whether there was any correlation between the microstructural behaviour and the macroscopic surface evidence.

7.5 Specimen Preparation and Examination

Specimens were sectioned radially and mounted in a clear, thermosetting resin. The samples were abraded on progressively finer grits and then polished to a final finish on 0.25μm diamond polishing pads. Samples were etched at room temperature for 30 seconds using a Ferritic Chloride etchant (5g ferritic chloride ($FeCl_3$) + 50ml hydrochloric acid (HCl) + 100ml water) [24]. The prepared surfaces were viewed and photographed at between 5X and 50X magnification to produce images suitable for establishing the grain structure.

7.6 Results and Discussion

On macroscopic examination approximately 25% of the specimens tested displayed signs of zoning or machining rings on the interfacing surfaces, with aluminium specimens displaying this behaviour most clearly. Distinct regions were typically observable along the specimen outer or inner diameter as areas that appeared smoother than the rest of the specimen surface. On the inner diameter this region was smaller than on the outer diameter, and in many cases was not visible. The size of the region increased consistently with strain and was similar in size and appearance on specimens tested both quasi-statically and dynamically. For larger strains (over 50% log strain) the region was between about 0.3 mm and 0.5 mm, or 10 – 20% of the original specimen radius.

Figure 7.2 shows a scatter plot of m-factor vs. width of peripheral region. The width of the peripheral region is relatively constant for a given m-factor and seems to increase with friction. *Figure 7.3* illustrates the general trend in the size of this region with strain. For specimens tested without lubricant at a high strain rate no peripheral region appeared, despite the large friction factors recorded.

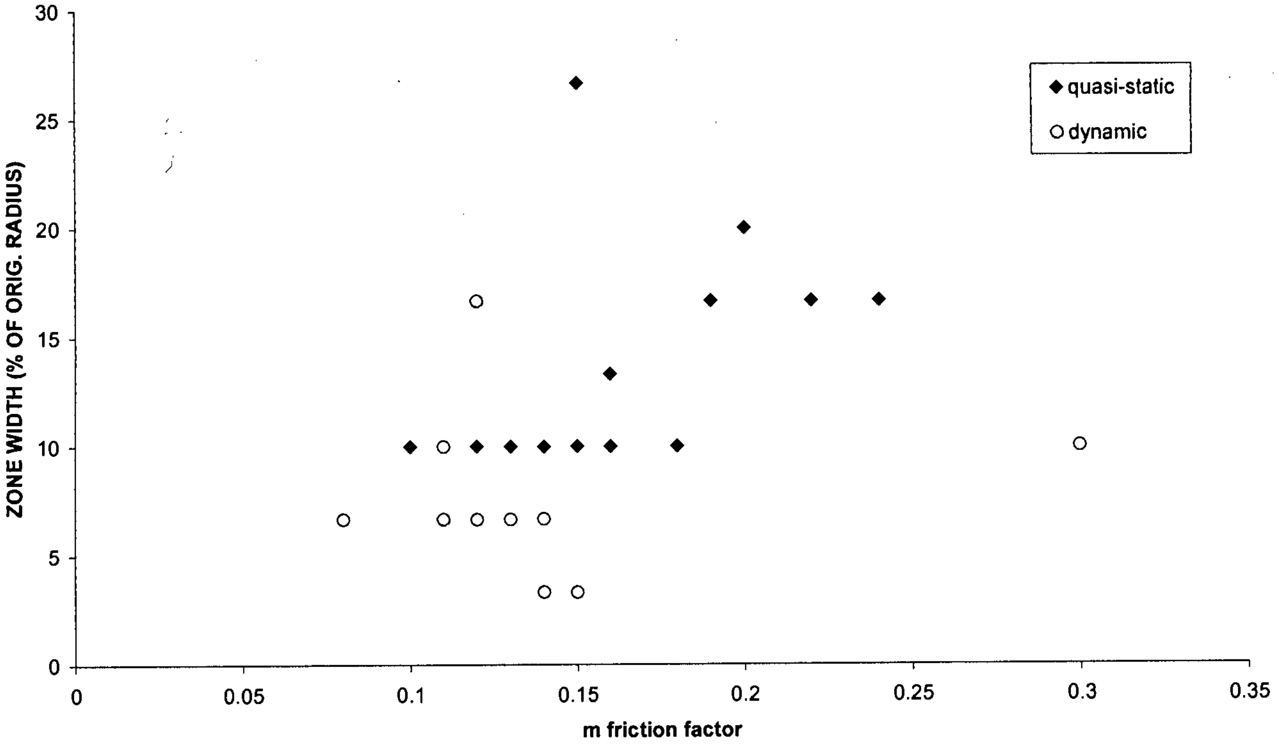

Figure 7.2 Scatter plot of 'm' friction factor against the approximate width of the peripheral region.

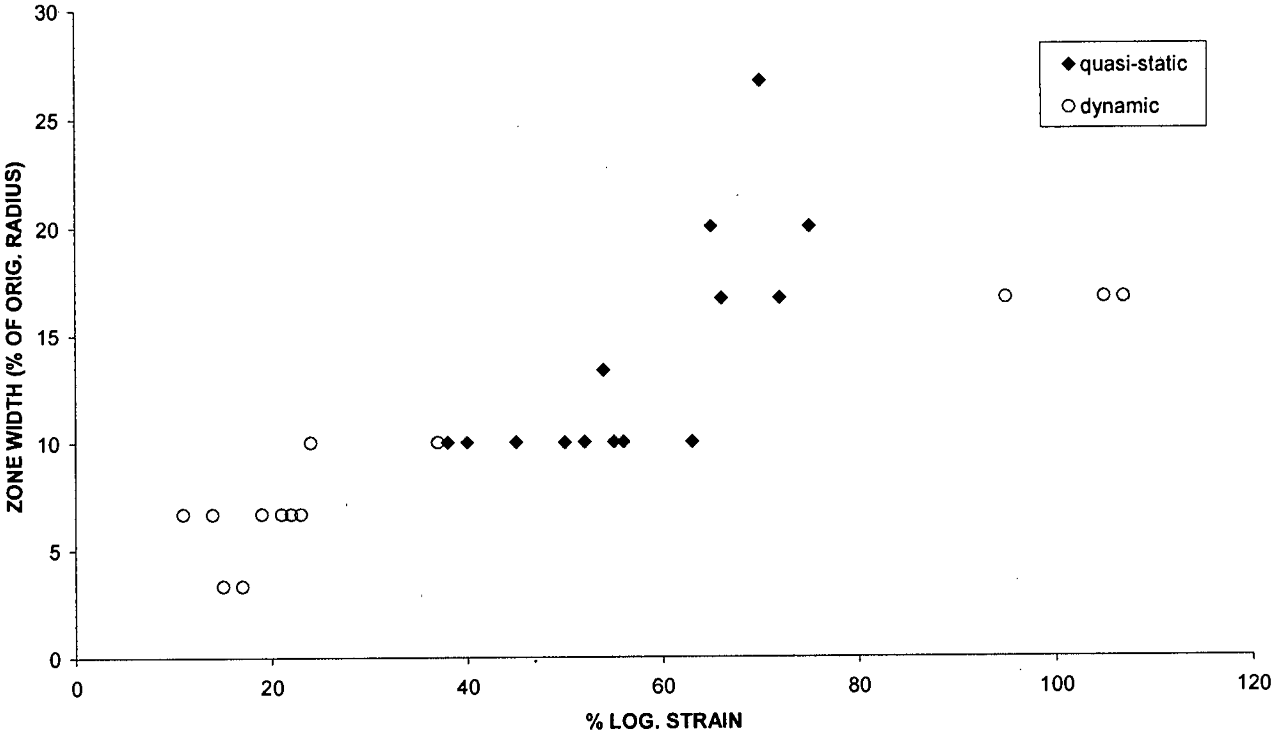

Figure 7.3 Scatter plot showing the approximate change in the width of the peripheral region with increasing strain.

To provide a benchmark for comparison with the micrographs of compressed specimens *Figure 7.4* shows the cross-section of an untested specimen, illustrating the regular grain structure. The grains are elongated in the axial direction, the direction in which the rod was extruded.

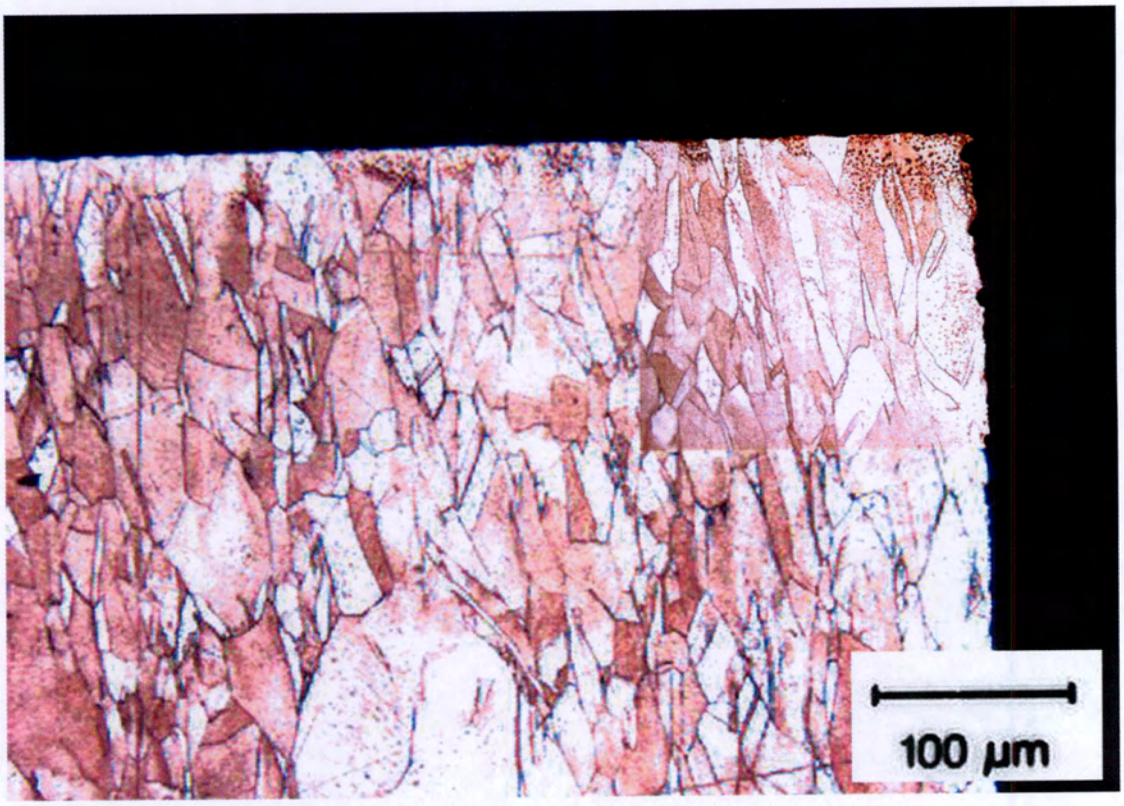

Figure 7.4 Micrograph of cross-section of untested ring compression test specimen showing regular, linear grain structure in corner region.

Figure 7.5 shows one half of the cross section through a typical specimen tested quasi-statically. The specimen was compressed to 60% logarithmic strain. A relatively high 'm' friction factor of 0.24 was measured. An X-shaped region of high strain is evident and the non-uniform grain deformation is exhibited clearly in *Figure 7.6*. This suggests that the stress distribution in the specimen was non-uniform.

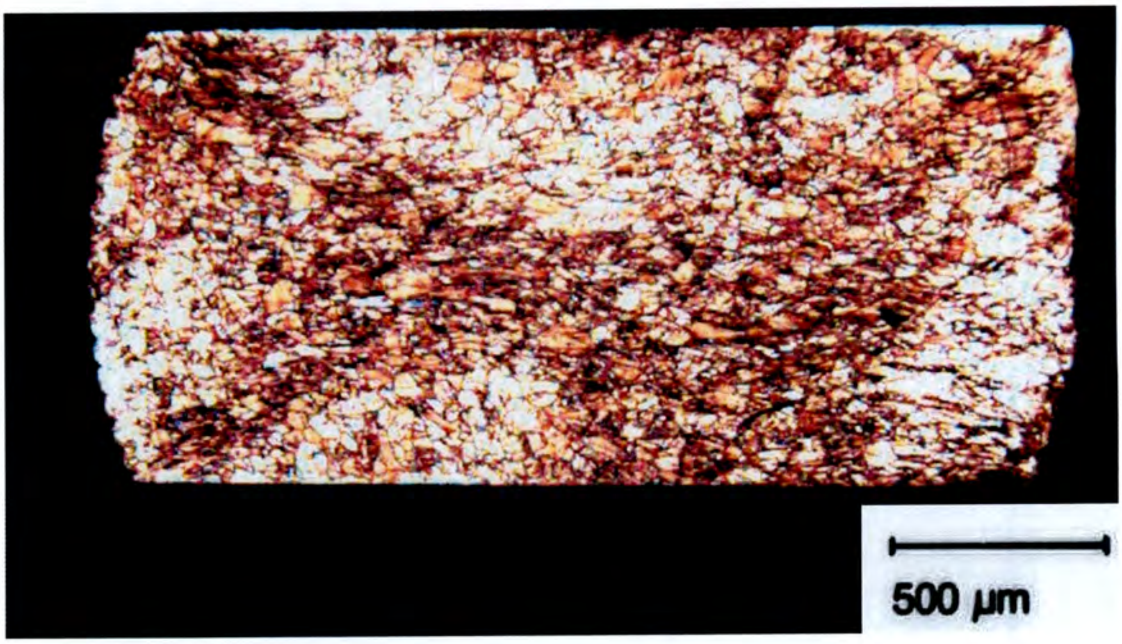

Figure 7.5 Micrograph of half cross-section of quasi-static compression test specimen showing X-shaped high strain regions.

The micrographs taken of specimens tested quasi-statically consistently showed that the cause of the distinct zone on the specimen surface was fold-over. *Figure 7.6* highlights the deformation of the corner of a specimen. The folding behaviour and the formation of the X-shaped high strain region observed in *Figure 7.5* is evident.

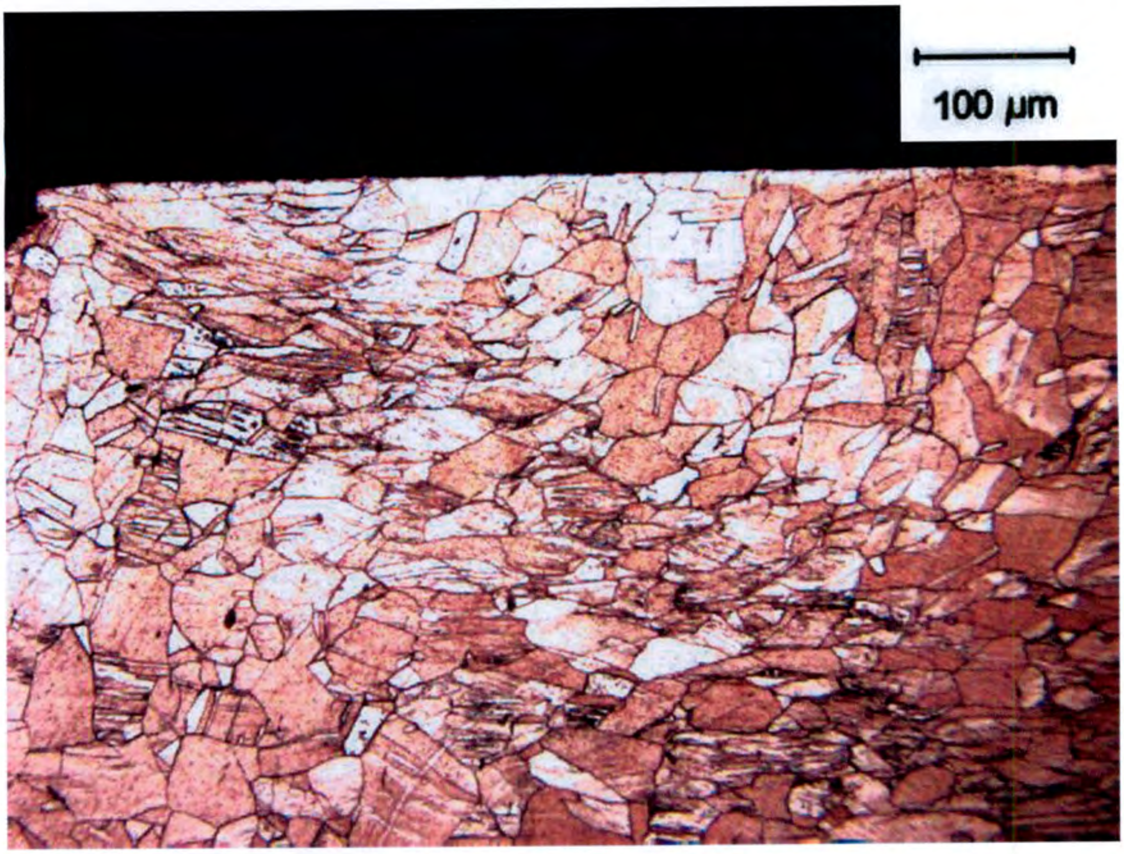

Figure 7.6 Micrograph of cross-section of quasi-static compression test specimen, showing fold-over and grain deformation in corner region.

The outer specimen diameter was produced on a lathe and this left distinctive grooves on the curved surface, as can be seen in the micrograph of the untested specimen in *Figure 7.4*. These grooves were useful in estimating the extent of fold-over as they moved from the sides of the specimen onto the specimen-anvil interface during compression, as indicated in *Figure 7.7*. These grooves and the shape and orientation of the grains in the vicinity of the corner of the specimens were used to estimate the extent of the fold-over, as given in *Table 7.2*.

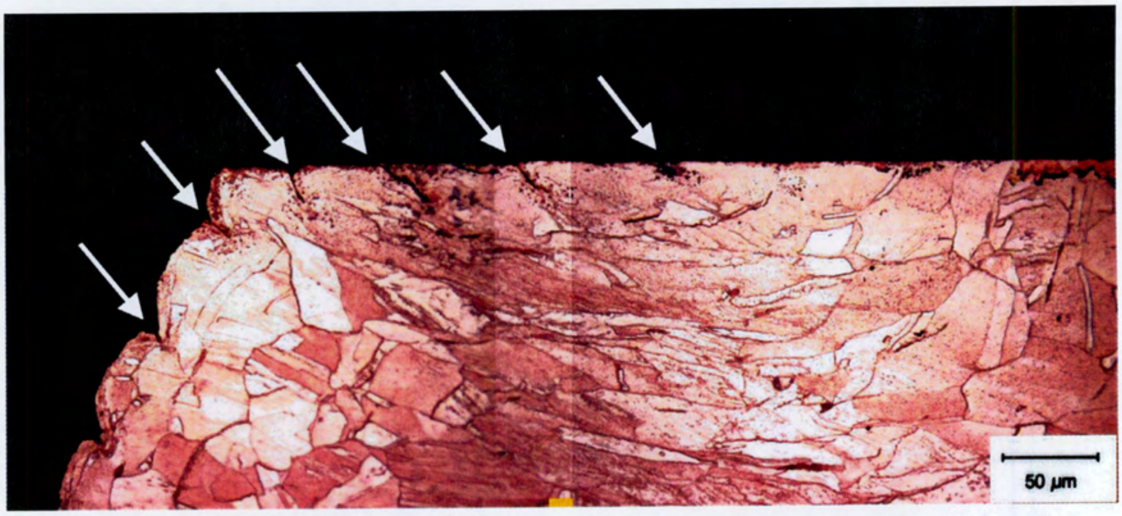

Figure 7.7 Micrograph of quasi-static compression test specimen showing fold-over pattern and movement of machining marks onto interface surface.

Fold-over would cause the relative velocity of the contact surfaces to be significantly lower than that predicted by the theory. Thus more of the forming energy could be used to effect plastic deformation and less to overcome friction than was predicted by Avitzur's solution [1].

Specimens tested at high strain rates had a distinct smooth region around the specimen periphery, as shown in *Figure 7.1.(b)*. However upon microstructural examination very little evidence of fold-over was observed. *Figures 7.8, 7.9, 7.10* and *7.11* illustrate the microstructure of specimens tested at the high strain rate, to steadily greater strain. The final specimen geometry shown in *Figure 7.8* is interesting in that each face appears to be slightly concave.

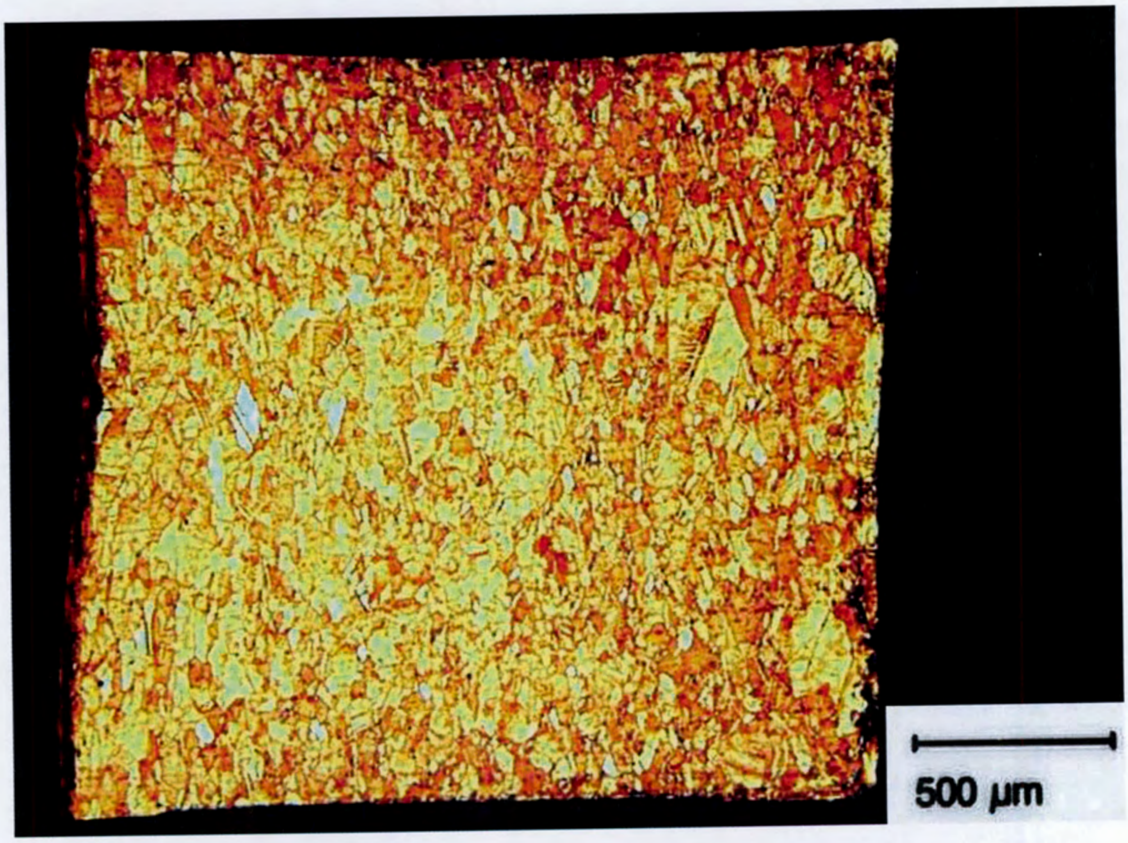

Figure 7.8 Micrograph showing half cross-section of specimen tested at a high strain rate to 21% strain. Theoretical friction parameter m = 0.08. No fold-over evident despite the appearance of a ±0.2mm wide region on the surface.

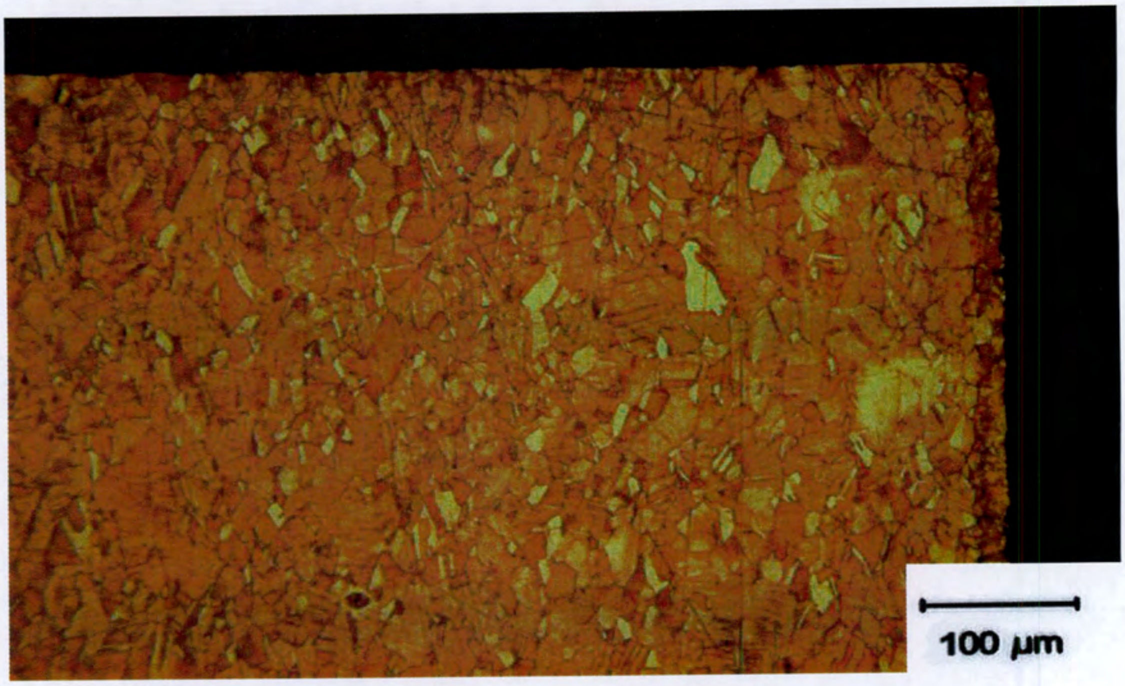

Figure 7.9 Micrograph of corner region of high strain rate specimen compressed to 19% strain with 'm' friction factor ≈0.14. The regular and uniform grain deformation is clear. No fold-over evident despite appearance of an approximately 0.2mm wide peripheral region on the surface.

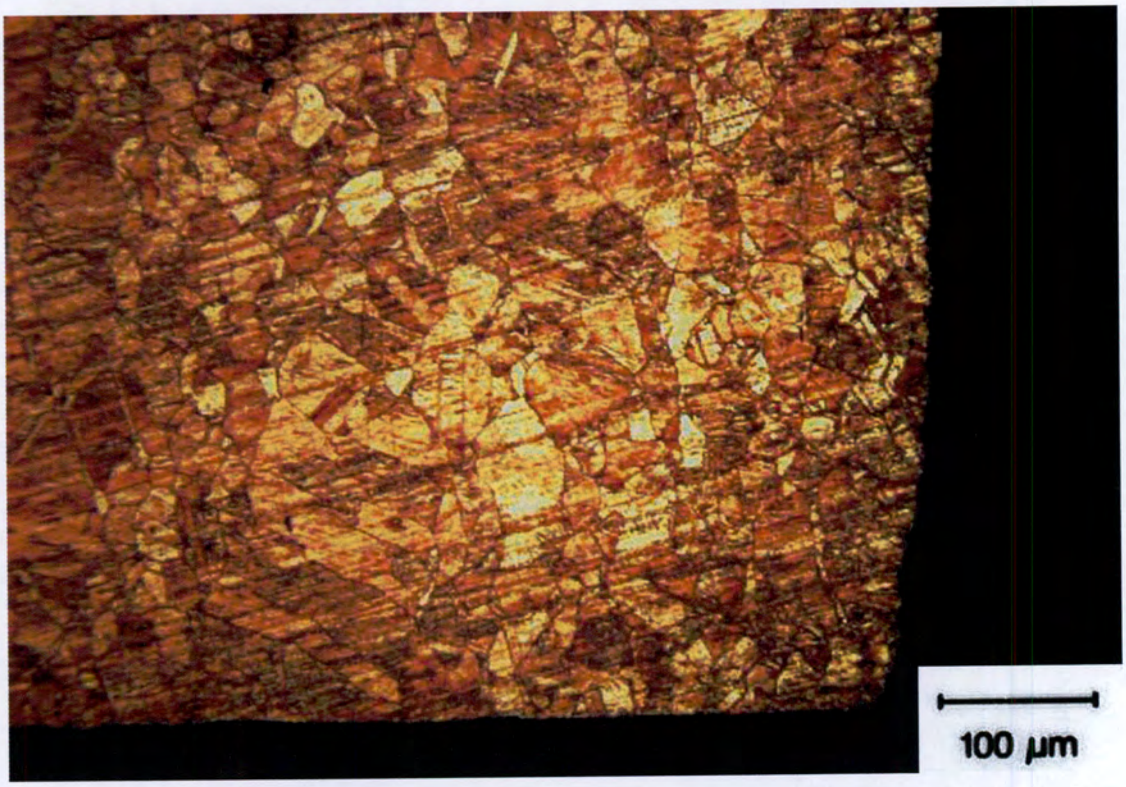

Figure 7.10 Micrograph of corner region of high strain rate specimen tested to 37% strain with 'm' friction factor ≈0.12. The regular and uniform grain deformation is clear. No fold-over evident despite the appearance of an approximately 0.3mm peripheral region on the surface.

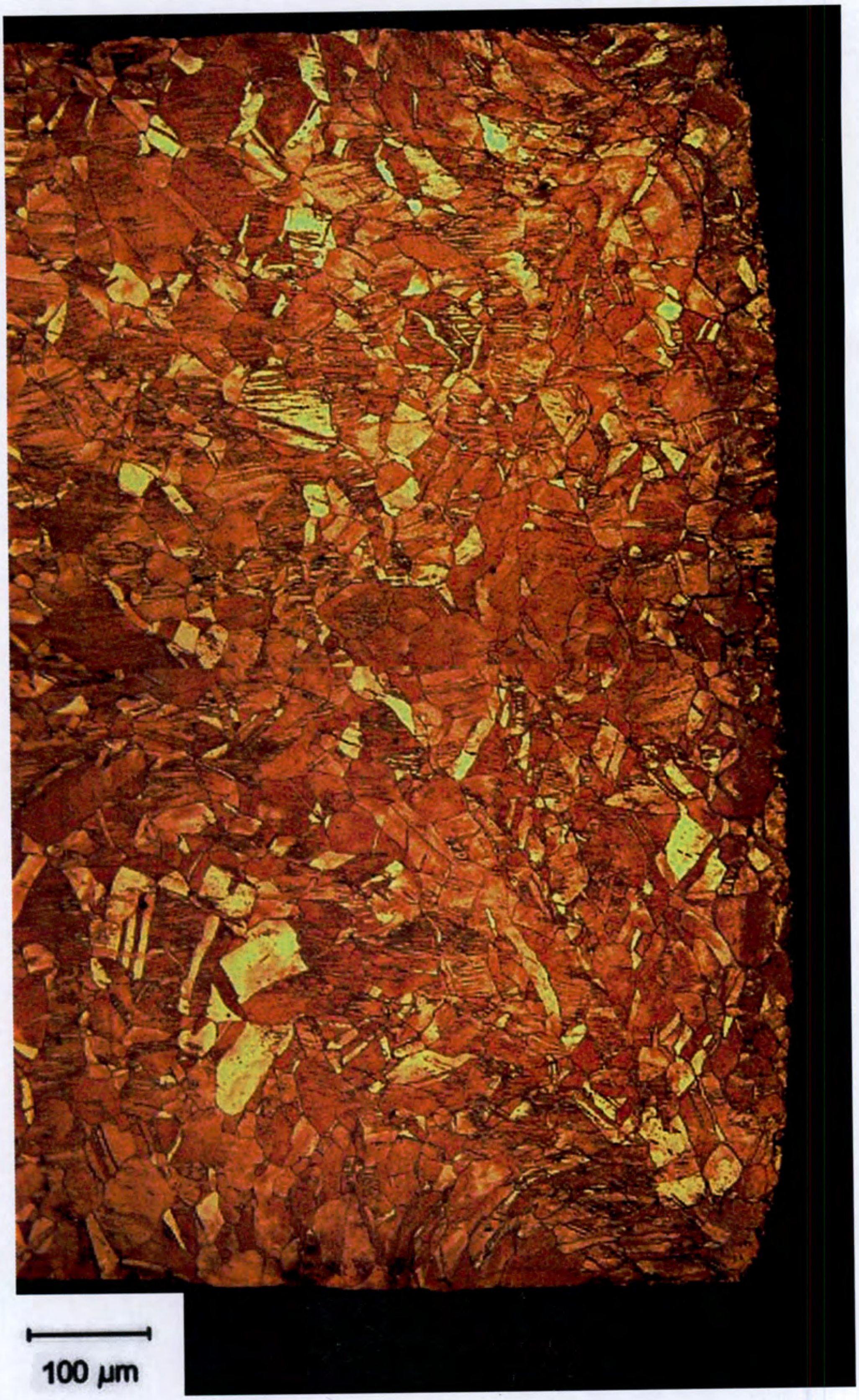

Figure 7.11 Micrograph showing the outer edge of a high strain rate specimen tested to 61% strain with ‘m’ friction factor ≈0.10. Grain deformation is generally uniform although limited fold-over has occurred to about 0.15mm. A 0.3mm peripheral region was visible on the surface.

The ring observed for the high strain rate case may be caused by lubricant breakdown due to the high stresses and velocities experienced during compression, as was suggested by Gorham *et al* [8]. The absence of a peripheral region on specimens tested without lubricant supports this explanation. The ring shown in *Figure 7.1.(b)* was compressed to 32% strain in approximately 0.15ms. During this time the outer diameter changed from 5.94mm to 6.87mm, which, assuming no sticking, fold-over or barrelling, required an average interface velocity of roughly 3.1m/s.

Table 7.2 gives the measurements of the peripheral zone and theoretical friction factor, m, for the copper specimens examined. Where microstructural analysis was conducted the width of the zone as determined from micrographs is included.

Fold-over observed on specimens tested quasi-statically seems to be a consistent indicator of friction for a given strain. Good correlation was found between the peripheral zone measured on the specimen surface and the fold-over region measured from micrographs, as evident in *Table 7.2*.

However at high strain the appearance of a peripheral region cannot be taken as an indication of the extent of fold-over as fold-over generally did not occur, as shown *Figures 7.8, 7.9, 7.10* and *7.11*, for specimens tested to various strains. At 61% logarithmic strain fold-over appeared, to a limited extent, as shown in *Figure 7.11.* It would appear that the peripheral region observed on specimens tested quasi-statically and dynamically are the result of different phenomena and in the case of the high strain rates this zone would appear to be lubricant related. Accurate numerical simulation of ring compression specimens and conventional cylindrical Hopkinson Bar specimens would require models capable of capturing this behaviour.

The deformed grain structure of the specimens tested at the higher strain rate appeared relatively uniform across all the strains considered. This would suggest that the stress state in the specimen is approximately uniform and that the frictional restraint at the specimen surface is either fairly minor or propagated more uniformly through the specimen thickness than during quasi-static testing. This would suggest that the uniform stress state that is assumed to infer high strain rate material data may be closely approximated in ring compression tests specimens.

% LOG. STRAIN	m factor	Measured macroscopically		Measured microscopically	
		Zone width (mm)	Zone % of original radius	Zone width (mm)	Zone % of original radius
QUASI-STATIC					
36	0.12	0.1	*3*	0.1	*3*
38	0.16	0.3	*10*	-	-
40	0.18	0.3	*10*	-	-
45	0.18	0.3	*10*	-	-
50	0.1	0.3	*10*	-	-
52	0.15	0.3	*10*	-	-
54	0.16	0.4	*13*	-	-
55	0.14	0.2	*7*	0.1	*3*
56	0.12	0.3	*10*	-	-
60	0.24	0.3	*10*	0.3	*10*
62	0.2	0.3	*10*	0.25	*8*
63	0.13	0.3	*10*	-	-
65	0.2	0.6	*20*	-	-
66	0.24	0.5	*17*	-	-
66	0.22	0.5	*17*	-	-
70	0.15	0.8	*27*	-	-
72	0.19	0.5	*17*	-	-
75	0.2	0.6	*20*	-	-
DYNAMIC					
11	0.12	0.2	*7*	-	-
14	0.13	0.2	*7*	-	-
15	0.15	0.1	*3*	-	-
17	0.15	0.1	*3*	-	-
17	0.14	0.1	*3*	-	-
19	0.14	0.2	*7*	-	-
19	0.14	0.1	*3*	0	*0*
21	0.08	0.2	*7*	0	*0*
22	0.11	0.2	*7*	0	*0*
22	0.11	0.2	*7*	-	-
23	0.08	0.2	*7*	-	-
24	0.3	0.3	*10*	-	-
37	0.11	0.3	*10*	0	*0*
61	0.12	0.2	*7*	0.1	*3*
95	0.11	0.5	*17*	-	-
105	0.11	0.5	*17*	-	-
107	0.11	0.5	*17*	-	-

Table 7.2 Extent of the fold-over zone estimated by a macroscopic and, where conducted, a microscopic investigation of various copper specimens that displayed such a zone.

8 DISCUSSION

8.1 Introduction

This chapter contains a discussion of the results presented. A comparison of the numerical and experimental results against the analytical solution is made to provide an estimate of the accuracy and reliability of the friction factors obtained.

8.2 Test Results and Interpretation

The conclusions and recommendations arising from previous work [19], as discussed in *Section 3.7.4*, were successfully implemented. The quasi-static tests performed confirmed the sensitivity of the method and provided a good base from which to develop the high strain rate experimentation program, with the results giving an estimate of the level of friction to be expected and the accuracy and repeatability that could be achieved. The surface finish combination of specimens finished to 1200-grit and anvils finished to 600-grit resulted in the lowest measured friction factor for the quasi-static tests and was therefore used for all the high strain rate tests.

The scatter in the results (*Figures 6.1* and *6.2*) can be attributed to the high sensitivity of the test, the difficulties in preparing identical specimens and providing identical lubrication and in the measuring system, which, using a standard micrometer was limited to a resolution of 0.01mm. Each test was repeated identically three times, and in some cases over a period of a few months, and so the reliability and repeatability of the results is considered acceptable.

Valuable experimental data on friction at high strain rates was thereby produced. However the complexity of friction phenomena makes accurate calibration of this data, to the accuracy required for precision material characterisation, very difficult. As mentioned the analytical solution [1] used is based on a number of simplifying assumptions, the validity of which are not always assured in practice. Male & Depierre [14] concluded that Avitzur's solution [1] would at best provide a slight over-estimate of the theoretical friction factors. They assumed that the technique they used of compressing heated wax rings, so that the specimen and anvil were separated by a liquid wax film, would provide almost zero friction. A comparison of these results with the results produced for mild steel specimens tested using the Hopkinson Bar is presented in *Figure 8.1*. The specimens were of the same aspect ratio.

The close correlation between the results and the comparatively small scatter in the mild steel results illustrates the precision of the experimental method used in this investigation. Very similar friction factors are observed for these two scenarios at lower strains. The results for the wax rings follow roughly the friction curve for m ≈ 0.04 as strain is increased, while the steel specimens remain around m ≈ 0.10. The wax ring method is expected to provide noticeably lower friction than the steel specimens that were simply lubricated with grease, even at low strains. The low but measurable friction recorded for the wax rings and the close correlation between the wax and the steel specimens does suggest that factors obtained using Avitzur's analysis [1] could be over-estimates the actual friction conditions.

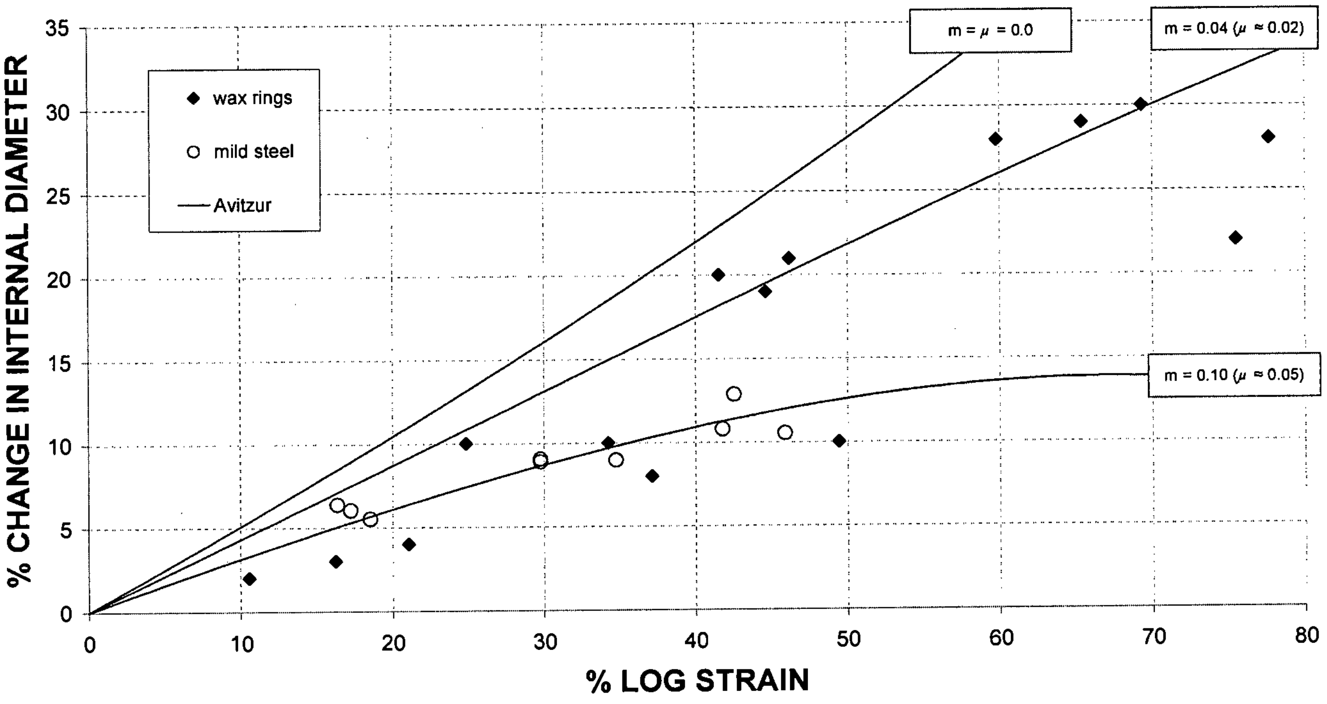

Figure 8.1 Graph of results for tests on wax rings by Male & Depierre [14] and the large strain Hopkinson Bar tests on mild steel specimens from this investigation.

8.3 Barrelling

The effect of barrelling on the results of the ring compression test and the stress distribution in Hopkinson Bar specimens has previously been raised [2] as discussed in *Section 3.8.* Due to barrelling the position at which the internal diameter is measured has been shown numerically to have an effect on the test results. *Figure 8.2* illustrates again the difference in the internal diameter changes at the surface and the mid-line against Avitzur's results [1]. The experimental results for mild steel specimens tested on the Split Hopkinson Bar are added in *Figure 8.3*. In *Chapter 4* it was shown that barrelling only significantly affect the experimental and numerical correlation at strains greater 30% (*Figure 4.10*) and for friction factors greater than μ = 0.06 (*Figure 4.9*).

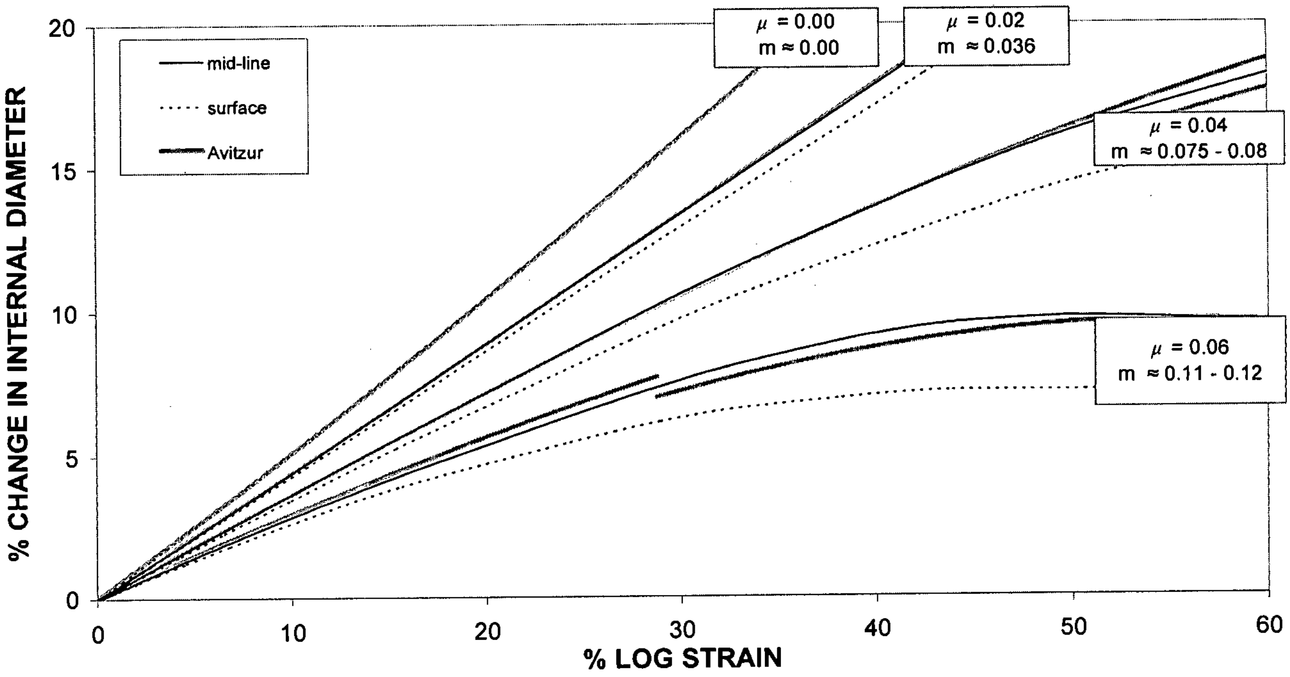

Figure 8.2 Graph showing numerical results, for $\mu = 0$ to $\mu = 0.06$, showing % change in internal diameter at specimen surface and mid-line, with theoretical curves from Avitzur's theory [1].

Figure 8.3 illustrates how close the numerical and analytical solutions lie, when they are considered against the scatter that is typical of the experimental results. Thus although the friction factors predicted using Avitzur's solution [1] and the numerical solution differ, the discrepancy is typically smaller than the resolution of the test method. Friction factors below μ = 0.06 would need to be achieved for Hopkinson Bar tests if the error is to be kept sufficiently small, as shown in *Figure 3.4*. The numerical solution, which incorporates barrelling, and the analytical solution are therefore sufficiently close that the slight error introduced by barrelling when measuring specimens to determine experimental friction factors should not prove significant.

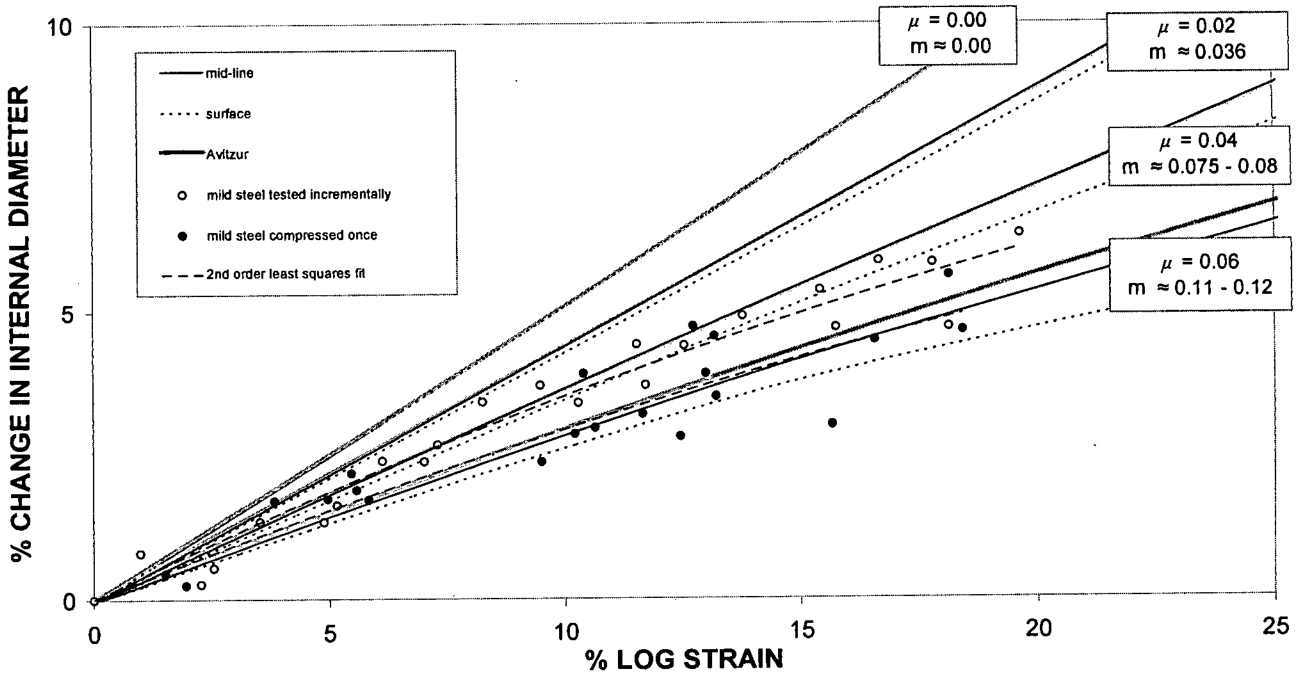

Figure 8.3 Graph showing numerical and experimental results, illustrating that for the low friction and strain considered small discrepancies in numerical and theoretical predictions do not significantly influence the inferred theoretical friction factors.

When considering the behaviour at higher strains the effect of the measurement position and hence barrelling is more evident. In *Figure 8.4* the results from tests on copper specimens to large strains are plotted against the theoretical curves. The numerical result for the change in the internal diameter at the surface with μ = 0.06 is included. The plateau is due to the change from convex to concave barrelling on the inner diameter (as discussed in *Section 4.4*). As can be seen the inferred 'm' friction factor would be 0.13 theoretically while the numerical prediction would put the value at 0.12.

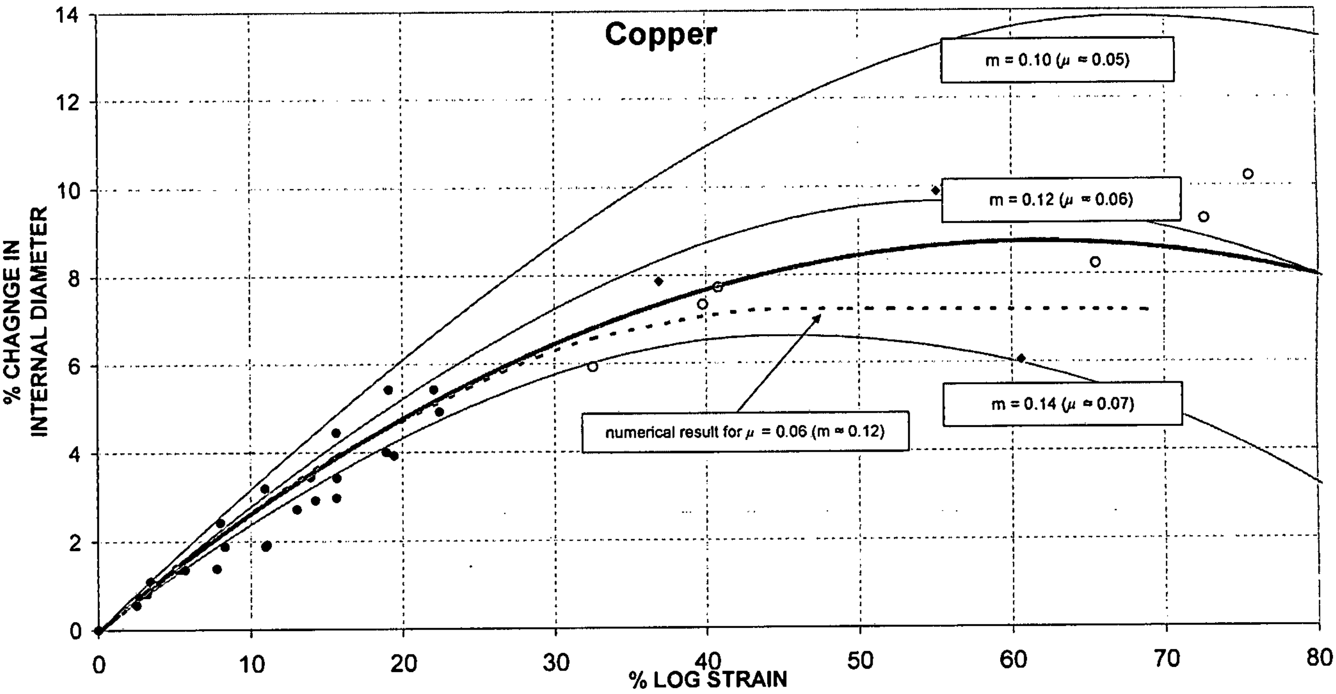

Figure 8.4 Graph showing large strain, high strain rate results for copper specimens with theoretical and numerical geometry predictions.

Barrelling therefore does affect ring compression test results. However when applying this test to the Split Hopkinson Pressure Bar scenario the strain and friction levels required are small enough for barrelling to be neglected. The influence of the position at which the specimen internal diameter measurement is made is therefore also considered negligible.

9 CONCLUSIONS AND RECOMMENDATIONS

This investigation has provided experimental data for assessing the affect of friction on high strain rate tests conducted using the Split Hopkinson Pressure Bar technique. The ring compression test technique worked well and provide a sensitive experimental measure of the friction affecting a given test scenario. Discrimination between the effects of lubricant and surface finish at quasi-static and high strain rates was achieved. The measurement technique used proved to be accurate and practical. The conclusions and recommendations discussed in *Section 3.7* have been adopted and shown to provide useful results. The objectives set have been met.

The technique was simulated numerically and good correlation was observed with the analytical solution of Avitzur [1], as used to infer theoretical friction factors. This suggests that friction factors can be accurately deduced from a comparison of experimental results with numerical simulations rather than analytical solutions, as done in this investigation and in references [8] and [14]. Benefits of this approach would be (a) the incorporation of phenomena such as barrelling and (b) the scope for improvements in the simulation, such as the use of more elaborate friction models. As far as estimating friction factors is concerned, the effect of barrelling was shown to be negligible for the friction and amount of strain in typical Hopkinson Bar tests. The assumptions in Avitzur's analytical solution [1] appear to result in a slight overestimate of the friction conditions. The results presented can therefore be considered conservative or over-estimates of the actual friction. This implies that tests conducted under the specified conditions will be of equal or better accuracy than that determined theoretically in this work.

Specimen preparation and lubrication was successfully investigated, providing an optimum combination of lubricant and specimen and anvil surface condition for general testing of common metals. Highly polished surfaces resulted in greater frictional restraint. Low friction levels were obtained when specimens and compression surfaces were roughened. Specimens abraded using a 1200-grit SiC grinding paper and tested on compression surfaces abraded using a 600-grit paper provided the lowest measured friction factor and it is recommended that this specification be used for Hopkinson Bar testing. Good general agreement was shown between the experimental results and the analytical solution [1] although the results suggest that for higher friction conditions the analytical solution provides slight overestimates of the theoretical friction factors for measured specimen geometry changes.

Measured friction factors fell between $m \approx 0.08$ and $m \approx 0.14$ ($\mu \approx 0.04$ and $\mu \approx 0.08$) for all specimen tested with lubrication. According to Avitzur's solution [1] this level of friction results in an error in Split Hopkinson Bar test data of between 1.5 and 2.5%. Values quoted in the literature of friction factors between $m = 0.05$ and 0.26 give errors of between 1% and 5%. Different materials showed slightly different responses to initial preparation and lubrication, with copper specimens displaying slightly higher friction for given test conditions.

The final specimen appearance has been reported upon. A ring was observed on the specimen surface, as reported in the literature, and the cause investigated microstructurally, as recommended in previous work [19]. The grain behaviour of specimens tested at low strain rates confirmed that predicted in literature on metal forming [18], in that sticking friction occurred and the specimen sides folded-over, explaining the changes in the surface appearance. However the behaviour at high strain rates differed markedly and it was shown that the final surface appearance was not a good indicator of the sub-surface grain behaviour. Fold-over and non-uniformities in grain behaviour were significantly lower at the higher strain rate, suggesting that the surface friction conditions were generally lower and possibly more consistent in time and position. This would also suggest that the stress in the specimen was more uniform.

Throughout this investigation the practical considerations of large-scale, routine high strain rate material testing have been considered. It has been found that, provided careful attention is paid to reducing friction as far as possible by using the correct lubricant, surface finish and specimen aspect ratio, errors of well under 2% may be consistently achieved. As the values obtained in this investigation are considered upper limits on the theoretical friction factors, it appears that errors of the order of 1% may be achieved by using the testing configuration suggested by these results.

The low friction factors and the uniform, regular grain structure of specimens tested at high strain rates suggests that the stress state in the ring specimens tested was approximately uniform. The correlation between the analytical and the numerical solution and the good general agreement with the experimental results indicates that reasonably accurate theoretical friction factors were obtained using the ring compression test. It is therefore recommended that ring compression specimens, rather than cylindrical specimens, be considered as a possible configuration for Split Hopkinson Bar material testing. An advantage of this specimen configuration is that an estimate of the friction experienced can be accurately measured for every test. The accuracy of the result obtained can then be inferred. A more accurate and detailed numerical model could be developed to better capture the specimen behaviour, including barrelling and fold-over, and the stress distribution in the specimen could therefore be estimated numerically. A further advantage of ring-shaped specimens is the greater size for a given surface area and material volume. This makes handling, production and accurate specimen preparation easier. However an increase in the outer diameter of specimens may increase the error due to radial inertia as the maximum velocities and acceleration will be increased. Thus the potential effects of inertia on such a specimen would need to be determined.

It is also recommended that conventional cylindrical Hopkinson Bar specimens are sectioned and examined after testing and that a comparison is made between the deformed grain structures of cylindrical and ring compression test specimens.

Finally it is recommended that, in order to limit the effects of friction in Hopkinson Bar tests and ensure a more uniform stress distribution, specimen surfaces are roughened using a 1200-grit SiC paper, the bar ends are roughened using a 600-grit SiC paper and molybdenum disulphide grease is used for lubrication. These conditions should result in an error in the measured flow stress due to friction of substantially less than 2%. Limited ring compression tests along the lines of those conducted in this investigation can be used to quickly check the friction for specific Hopkinson Bar test conditions and test material and the error can thereby be established.

10 REFERENCES

[1] Avitzur, B., *Forging of Hollow Discs*, Israel Journal of Technology, Vol. 2, No. 3, pp. 295 – 304, 1964.

[2] Tinsley Oden, J., Belytschko, T., Babuska, I., Hughes, T., *Research Directions in Computational Mechanics*, Comput. Methods Appl. Mech. Engrg., 192, pp 913-922, 2003.

[3] G. T. Gray, *Classic Split Hopkinson Pressure Bar Technique*, ASM Volume 8: Mechanical Testing, 1999.

[4] Follansbee, P.S., in *The Hopkinson Bar*, ASM Handbook 10: Mechanical Testing, ASM International, 1984.

[5] Marais, S.T., *Development and Proving of a Split Hopkinson Pressure Bar used for High Strain Rate Materials Testing*, Dissertation in part fulfilment of requirements for the Degree MSc Engineering, Department of Mechanical Engineering, University of Cape Town, August 2001.

[6] Jones, N. *Structural Impact,* Cambridge University Press, 1981

[7] Hibbitt, Karlsson and Sorenson Inc., ABAQUS Reference Manual, ABAQUS, Inc. 2003.

[8] Gorham D. A., Pope P. H. and Cox O., *Sources of error in very high strain rate compression tests*, Mechanical Properties at high rates of strain, 1984: proceedings of the Third Conference on the Mechanical Properties of Materials at High Rates of Strain, held in Oxford, 9 -12 April, 1984, Conference series, no. 70, Institute of Physics, Great Britain, pp. 151 – 158, 1984.

[9] Al-Mousawi M. M., Reid S. R. and Deans W. F., *The use of the split Hopkinson pressure bar techniques in high strain rate materials testing*, J. Mech. Eng. Sci., vol. 221, no. 64, pp. 273 – 292, 1997.

[10] Walley, S.M., Church, P.D., Furth, M., Field, J.E., *A High-Speed Photographic Study of the Rapid Deformation of Metal Annuli: Comparison of Theory with Experiment*, J. Phys IV France 7, 1997.

[11] Bertholf L.D. and Karnes C.H., *Two-dimensional analysis of the split Hopkinson pressure bar system*, J. Mech. Phys. Solids, vol. 23, pp. 1-9, 1975.

[12] Gorham, D. A., *Specimen inertia in high strain-rate compression*, J. Phys. Appl. Phys. vol. 22, pp 1888-1893, 1989.

[13] Bowden, F.P., *Friction,* Anchor/Doubleday New York, 1973.

[14] A. Male and V. Depierre, *The Validity of Mathematical Solutions for Determining Friction From the Ring Compression Test*, Journal of Lubrication Technology, vol. 39, pp. 389 – 397, 1970.

[15] Davies, E. D. H, and Hunter, S. C., *The dynamic compression testing of solids by the method of the split Hopkinson pressure bar*, J. Mech. Phys. Solids, vol. 11, 1963.

[16] Meng, H. and Li, Q. M., *Correlation between the accuracy of SHPB test and the stress uniformity based on numerical experiments*, Int. J. Impact Eng. vol. 28, pp. 537 – 555, 2003.

[17] Schey, J. A., *Tribology in Metalworking: Friction, Lubrication and Wear*, American Society for Metals, Ohio, 1983.

[18] Schey, J. A., *Introduction to Manufacturing Processes*, New York: McGraw-Hill, 1987.

[19] Hartley, R.S., *Characterising Friction Effects using the Ring Compression Test*, Undergraduate Project, Department of Mechanical Engineering, University of Cape Town, November, 2002 (unpublished).

[20] *Personal Communication* with Professor A. Yates. Department of Mechanical Engineering, University of Cape Town, April 2004.

[21] Juvinall, R. C., Marshek, K. M., *Fundamentals of Machine Component Design*, Updated Third Edition , John Wiley & Sons, Inc., 2000.

[22] Hibbitt, Karlsson and Sorenson Inc., ABAQUS Analysis User's Manual, ABAQUS, Inc. 2003.

[23] West Yorkshire Steel Co. Ltd. Sandbeck Works, Sandbeck Industrial Estate, Wetherby, Leeds LS22 7DN U.K. http://www.westyorkssteel.com

[24] ASM Handbook, Materials Park, OH : ASM International, c1984.

[25] Spotts, M. F., *Mechanical Design Analysis*, Prentice-Hall, Inc., 1964.

[26] Window, A.L., Holister, G.S. (ed.), *Strain Gauge Technology,* Applied Science Publishers Ltd., Barking Essex England, 1982.

[27] British Standards Institution, *BS-18: British Standard Method for Tensile testing of metals*, 1987.

APPENDIX A

THEORY OF THE HOPKINSON PRESSURE BAR

A.1 One-dimensional wave propagation theory [25]

Imagine a uniform compressive stress, s, is suddenly applied to the end of a long cylindrical bar of area A and density ρ. The particles at the end of the bar are immediately compressed as they accelerate to velocity v. This compression is communicated along the bar in the form of a stress wave that travels at the sonic velocity, c. Particles are accelerated to velocity v as the stress wave reaches them. After a time t a length ct will be compressed, with all the particles travelling at velocity v.

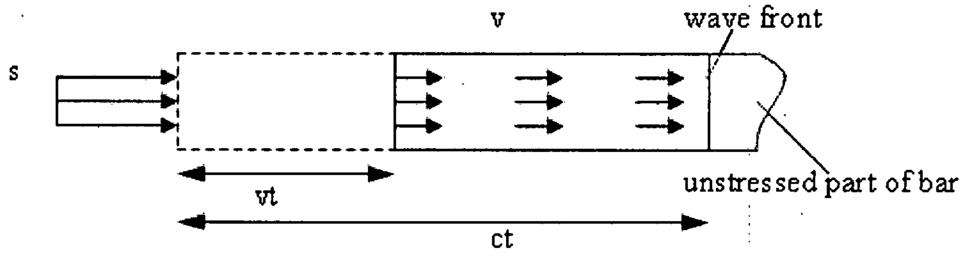

Figure A.1 Schematic diagram of stress wave propagation in a long cylindrical bar

Applying conservation of momentum to this section

$$s.A.t = mass.v$$

$$s.A.t = \rho.c.t.A.v$$

So $$s = \rho.c.v \qquad (A.1)$$

The strain in the stressed portion ct is given by

$$\varepsilon = \frac{\Delta l}{l} = \frac{vt}{ct}$$

So, by
$$\varepsilon = \frac{s}{E}$$

$$v = \frac{sc}{E} \qquad \text{(A.2)}$$

Equating *Equations* (A.1) and (A.2) yields

$$c = \sqrt{\frac{E}{\rho}} \qquad \text{(A.3)}$$

Consider an impact between two cylindrical bars of cross-sectional areas A_b and A_s, with the one bar stationary and the other travelling at velocity v_o, for example a striker bar and a Hopkinson bar. It is assumed that contact is made over the entire area of the smaller bar and that the bars remain in contact for the duration of the impact. Compressive waves are set up in both bars and move away from the interface. When the compressive wave in the striker reaches the free (left-hand) end, it reflects as a tensile wave. Once this wave arrives back at the interface it causes the striker to move away from the Hopkinson Bar, effectively ending the impact. The total duration of the impact is therefore twice the time taken for a stress wave to travel through the striker bar and hence the stress wave produced in the Hopkinson Bar is twice the length of the striker.

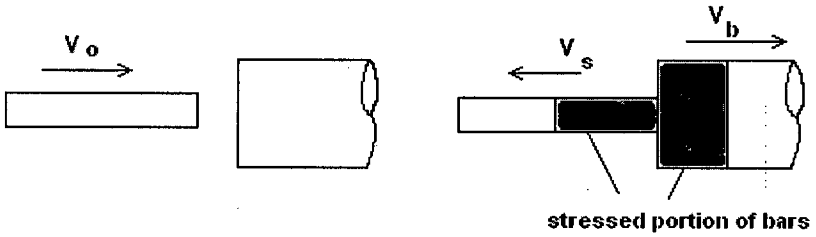

Figure A.2 Schematic diagram of particle velocities upon impact of a smaller striker bar with a large stationary cylindrical bar

Assuming the bars are of the same material and hence have the same density, ρ, and sonic velocity, c:

$$v_s = \frac{\sigma_s}{c\rho} \text{ to the left in the striker}$$

and $$v_b = \frac{\sigma_b}{c\rho} \text{ to the right in the bar}$$

The particle velocity associated with the compressive stress wave set up in the striker is sufficient to reduce the initial velocity, v_o, to the interface velocity, which is the same as v_b, so we can write (taking all quantities as positive)

$$v_0 - v_s = v_b$$

so $$v_0 = \frac{\sigma_s}{c\rho} + \frac{\sigma_b}{c\rho}$$

Equilibrium at the interface requires that

$$\sigma_s A_s = \sigma_b A_b$$

from which we can determine the resulting stresses in the bars in terms of the incident velocity and the cross-sectional area ratio

$$\sigma_s = \frac{A_b}{A_s + A_b} c\rho v_0$$

and $$\sigma_b = \frac{A_s}{A_s + A_b} c\rho v_0 \tag{A.4}$$

A.2 Split Hopkinson Pressure Bar theory [3]

Cauchy's equation of motion states that

$$\frac{\partial T_{ji}}{\partial x_j} + \rho b_i = \rho a_i$$

Assuming no body forces and a uniform, uniaxial stress state i.e. $T_{ji} = 0 \mid T_{11} \neq 0$

$$\frac{\partial T_{11}}{\partial x} = \rho \frac{\partial^2 u}{\partial t^2} \tag{A.5}$$

Assuming a linearly elastic bar material

$$T_{11} = E_y E_{11} \qquad T_{22} = 0 \qquad T_{33} = 0$$

where E_y is the elastic modulus of the bar material and E is the elasticity tensor.

Substituting into *Equation* (A.5)

$$E_y \frac{\partial E_{11}}{\partial x} = \rho \frac{\partial^2 u}{\partial t^2} \tag{A.6}$$

From the equations of linear elasticity

$$E_{11} = \frac{1}{E_y}[(1+\nu)T_{11} - \nu T_{11}\delta_{11}]$$

$$E_{11} = \frac{T_{11}}{E_y} \qquad E_{22} = -\frac{\nu T_{11}}{E_y} \qquad E_{33} = -\frac{\nu T_{11}}{E_y}$$

and

$$E_{ij} = \frac{1}{2}[\frac{\partial u_i}{\partial x_j} + \frac{\partial u_j}{\partial x_i}]$$

so

$$E_{11} = \frac{\partial u}{\partial x}$$

Substituting into *Equation* (A.6)

$$E_y \frac{\partial^2 u}{\partial x^2} = \rho \frac{\partial^2 u}{\partial t^2}$$

Thus using *Equation* (A.3):

$$c = \sqrt{\frac{E}{\rho}}$$

we arrive at the well known one dimensional wave equation:

$$\frac{\partial^2 u}{\partial x^2} = \frac{1}{c^2}\frac{\partial^2 u}{\partial t^2} \qquad \text{(A.7)}$$

The solution of the wave equation is of the form:

$$u = f(x-ct) + g(x+ct) = u_i + u_r \qquad \text{(A.8)}$$

as it applies to a Hopkinson Pressure Bar where u_i and u_r are the displacements of particles due to the incident and reflected pulses respectively, and f and g are functions describing the incident and reflected wave shapes.

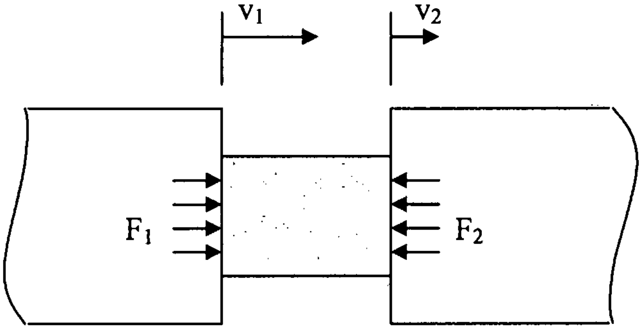

Figure A.3 Schematic diagram of specimen and bar ends, illustrating interface velocities and forces acting between the bars and the specimen.

Now by definition $\varepsilon = \frac{\partial u}{\partial x}$ and $v = \frac{\partial u}{\partial t}$

So differentiating *Equation* (A.8) with respect to x gives

$$\varepsilon = f' + g' = \varepsilon_i + \varepsilon_r$$

and with respect to t gives

$$v_1 = c(-f' + g') = c(-\varepsilon_i + \varepsilon_r)$$

For the transmitter bar (A.8) takes the form,

$$u = h(x-ct) = u_t \qquad \text{(A.9)}$$

where h describes the transmitted wave shape and u_t the particle velocity in the transmitted bar.

And so

$$\varepsilon = h' = \varepsilon_t$$

$$v_2 = c(-h') = -c\varepsilon_t$$

The particle velocities at the ends of the bar, which are assumed to be in contact with the specimen, can thus be determined and used to calculate the strain rate in the specimen:

$$\dot{\varepsilon} = \frac{v_1 - v_2}{l_s}$$

or

$$\dot{\varepsilon} = \frac{c}{l_s}(-\varepsilon_i + \varepsilon_r + \varepsilon_t) \qquad \text{(A.10)}$$

The instantaneous specimen length is found by:

$$l_s(t) = l_o - \int_{t=o}^{t} v_1 - v_2 dt$$

It is assumed, after some initial 'ring up' period (a period during which stress waves are reflected within the specimen), that:

1. The specimen is in force equilibrium.
2. The specimen is deforming uniformly.

Thus

$$F_1 = F_2$$

The forces acting on the specimen can be determined from the material properties of the bars, since, by definition

$$F_1 = AE(\varepsilon_i + \varepsilon_r)$$

$$F_2 = AE(\varepsilon_t)$$

Then

$$\varepsilon_i + \varepsilon_r = \varepsilon_t$$

Substituting this relation into *Equation* (A.9) allows the strain rate to be determined using only the reflected strain.

$$\dot{\varepsilon} = \frac{2c\varepsilon_r}{l_s} \tag{A.11}$$

The true strain in the sample is determined by integration of *Equation* (A.11).

The true stress in the sample is

$$\sigma(t) = \frac{AE\varepsilon_t}{A_s} \tag{A.12}$$

where the instantaneous area, A_s, can only be calculated if the specimen material can be assumed to be incompressible, i.e. $A_o l_o = A_s l_s$. Determination of the true stress and strain for materials that are compressible can only be achieved using additional sensors or techniques such as high speed photography, to track the actual specimen length with time.

Analysis by *Equations* (A.11) and (A.12) allows generation of the true stress-strain curve for the material and is termed a one-wave analysis.

Two-wave and three-wave analyses can also be performed using

2-wave: $$\sigma(t) = \frac{AE(\varepsilon_i + \varepsilon_r)}{A_s}$$

3-wave: $$\sigma(t) = \frac{AE(\varepsilon_i + \varepsilon_r + \varepsilon_t)}{2A_s}$$

All analyses cannot be correct in the initial ring-up period before force equilibrium is achieved and are also only accurate as long as the volume remains constant and the sample is free of barrelling [3].

APPENDIX B

THE THEORETICAL ANALYSIS BY AVITZUR

B.1 A Summary of the Analysis and Results

Avitzur considered the compression of hollow circular discs between flat, rigid anvils. The changes in the inner and outer diameters were determined as well as an upper bound on the pressure required to cause plastic flow.

The method used was the minimum power or energy approach. A lower upper bound solution was sought for a hollow disc and for the special case of a solid disc.

The material was assumed to obey the Lévy-Mises plasticity model implying no elastic deformation and no strain-hardening or strain rate sensitivity. The constant shear factor (m-factor) approach was used to model friction between the specimen and the anvils, expressed as:

$$\tau = m\frac{\sigma_y}{\sqrt{3}} \tag{B.1}$$

The problem was effectively reduced to two-dimensions by using an axi-symmetric formulation. The upper anvil was assumed to move at constant velocity toward the lower platen. Velocity was assumed to vary linearly between the anvils. Planes normal to the axis of symmetry were assumed to remain plane and normal to this axis. These assumptions effectively preclude barrelling. The assumed velocity field is thus:

$$\begin{aligned} \dot{U}_\theta &= 0 \\ \dot{U}_Z &= \frac{Z}{T}\dot{U} \\ \dot{U}_R &= \dot{U}_R(R,Z) \end{aligned} \tag{B.2}$$

Applying the constant volume assumption to the derived strain rate field yields:

$$\dot{U}_R = -\frac{1}{2}\frac{\dot{U}}{T}R + \frac{B(Z)}{R} \qquad \text{(B.3)}$$

Applying a zero velocity boundary condition at the neutral radius, R_n, to the above velocity field yields B(Z) in terms of R_n, so that:

$$\dot{U}_R = -\frac{1}{2}\frac{\dot{U}}{T}R\left[1-\left(\frac{R_n}{R}\right)^2\right] \qquad \text{(B.4)}$$

The Lévy-Mises plasticity model can be expressed as,

$$\sigma_{ij}' = \lambda\dot{\varepsilon}_{ij} \qquad \frac{2}{3}\sigma_y^2 = \sigma_{ij}'\cdot\sigma_{ij}' = \lambda^2\dot{\varepsilon}_{ij}\cdot\dot{\varepsilon}_{ij}$$

which can be used to write the work of plastic deformation as

$$\dot{W}_d = -\frac{2}{\sqrt{3}}\sigma_y\int\sqrt{\frac{1}{2}\dot{\varepsilon}_{ij}\cdot\dot{\varepsilon}_{ij}}\,dV = -2\pi\sigma_y\dot{U}\int_{R=R_i}^{R_o}\sqrt{R+\frac{1}{3}R_n^4}\,\frac{dR}{R}$$

$$\text{(B.5)}$$

Expressing the friction power loss as

$$\dot{W}_f = -\int_S \tau\left|\Delta v\right|ds \qquad \text{where } \left|\Delta v\right| = \left|\dot{U}_R\right| \qquad \text{(B.6)}$$

and integrating across the contact surface yields two different expressions, depending on whether R_n is greater or smaller than the inner radius R_i.

For Rn ≤ Ri

$$\dot{W}_f = -\frac{2\pi m\sigma_y}{3\sqrt{3}}\frac{\dot{U}}{T}R_n^3\left[\left(\frac{R_o}{R_n}\right)^3-\left(\frac{R_i}{R_n}\right)^3-3\left(\frac{R_o}{R_n}-\frac{R_i}{R_n}\right)\right] \qquad \text{(B.7)}$$

and for Rn > Ri

$$\dot{W}_f = -\frac{2\pi m \sigma_y}{3\sqrt{3}} \frac{\dot{U}}{T} R_n^3 \left[4 + \left(\frac{R_o}{R_n} \right)^3 + \left(\frac{R_i}{R_n} \right)^3 - 3 \left(\frac{R_o}{R_n} + \frac{R_i}{R_n} \right) \right] \qquad \text{(B.8)}$$

The sum of these two work rate terms yields the total power required for deformation. R_n is assumed to minimise this total work rate, W_T. Solving

$$\frac{\partial \dot{W}_T}{\partial R_n} = 0 \qquad \text{(B.9)}$$

yields, for $R_n \le R_i$

$$\left(\frac{R_n}{R_o} \right)^2 = \frac{\sqrt{3}}{2} \frac{1 - \left(\frac{R_i}{R_o} \right)^4 x^2}{\sqrt{x(x-1) \left[1 - \left(\frac{R_i}{R_o} \right)^4 x \right]}} \qquad \text{(B.10)}$$

where $$x = \left[\frac{R_o}{R_i} e^{-m \frac{R_o}{T} \left(1 - \frac{R_i}{R_o} \right)} \right]^2$$

and for $R_n > R_i$

$$2 \left(m \frac{R_o}{T} \right) \left(1 + \frac{R_i}{R_o} - 2 \frac{R_n}{R_o} \right) + \ln \left| \left(\frac{R_i}{R_o}^2 \right) \frac{\left(\frac{R_n}{R_o} \right)^2 + \sqrt{3 + \left(\frac{R_n}{R_o} \right)^4}}{\left(\frac{R_n}{R_o} \right)^2 + \sqrt{3 \left(\frac{R_i}{R_o} \right)^4 + \left(\frac{R_n}{R_o} \right)^4}} \right| = 0 \qquad \text{(B.11)}$$

which cannot be solved explicitly and so R_n has to found by successive approximations.

The criteria for selecting between *Equations* (B.10) and (B.11) was found by assuming $R_n = R_i$. This leads to

$$m\frac{R_o}{T} = \frac{1}{2\left(1-\frac{R_i}{R_o}\right)}\ln\left|\frac{3\left(\frac{R_o}{R_i}\right)^2}{1+\sqrt{1+3\left(\frac{R_o}{R_i}\right)^4}}\right| \tag{B.12}$$

Equation (B.10) is valid when the left hand side of *Equation* (B.12) is smaller and *Equation* (B.11) is valid when the left hand side is greater.

The solutions for P_{ave}/σ_o are, for $R_n \leq R_i$

$$\frac{P_{ave}}{\sigma_o} = \frac{1}{1-\left(\frac{R_i}{R_o}\right)^2}\left\{\sqrt{1+\frac{1}{3}\left(\frac{R_n}{R_o}\right)^4} - \sqrt{\left(\frac{R_i}{R_o}\right)^4+\frac{1}{3}\left(\frac{R_n}{R_o}\right)^4} + \frac{2}{3\sqrt{3}}m\frac{R_o}{T}\left[1-\left(\frac{R_i}{R_o}\right)^3\right]\right\} \tag{B.13}$$

and for $R_n > R_i$

$$\frac{P_{ave}}{\sigma_o} = \frac{1}{1-\left(\frac{R_i}{R_o}\right)^2}\left\{\sqrt{1+\frac{1}{3}\left(\frac{R_n}{R_o}\right)^4} - \sqrt{\left(\frac{R_i}{R_o}\right)^4+\frac{1}{3}\left(\frac{R_n}{R_o}\right)^4} + \frac{2}{3\sqrt{3}}m\frac{R_o}{T}\left[1+\left(\frac{R_i}{R_o}\right)^3-2\left(\frac{R_n}{R_o}\right)^3\right]\right\} \tag{B.14}$$

B.2 Application of the Solution

Implementing the above solutions to find the dimension changes and average surface pressure was achieved by building a spreadsheet of the following form (as recommended by Avitzur [1]).

Theoretical Friction Factor $\boxed{m = 0.02}$

R_i	1.5 mm	*(inner radius)*	Δt	1 s	*(time increment between solution values)*
R_o	3.0 mm	*(outer radius)*	U	-0.01667 mm/s	*(compression rate)*
T	2.0 mm	*(thickness)*	so ΔT =	-0.01667 mm	*(incremental change in thickness)*
m	0.020	*(friction factor)*			
U	0.0167 mm/s	*(compression rate)*			

(1)	(2)	(3)	(4)	(5)	(6)	(7)	(8)	(9)	(10)	(11)	(12)	(13)	(14)	(15)
No	X or seek	R_i	R_o	R_i/R_o	T	mR_o/T	R_n/R_o	R_n	ΔR_o	ΔR_i	P_{ave}/σ	$dR_{R=Ro}$	$dR_{R=Ri}$	TEST
		mm	mm		mm		eq (B.11)	mm						
1	3.8818	1.5000	3.0000	0.5000	2.000	0.0300	0.1316	0.3949	0.0123	0.0058	1.013	0.0123	0.0058	0.4055
2	3.8820	1.5058	3.0123	0.4999	1.983	0.0304	0.1324	0.3989	0.0124	0.0059	1.013	0.0124	0.0059	0.4054
3	3.8822	1.5117	3.0247	0.4998	1.967	0.0308	0.1332	0.4030	0.0126	0.0060	1.014	0.0126	0.0060	0.4054
...	...	...	...	...	...	...	...	...	...	...	...	...	...	...

The equations are solved to fill the spreadsheet as follows:

(3) and (4) are the results of the previous step.

(5) is found from (3) and (4).

(6) is calculated from the previous step as T + ΔT.

(7) is then calculated.

At this point it needs to be determined whether the neutral radius is greater or less than the inner radius, to decide whether *Equation* (B.10) or (B.11) should be used. The right hand side of *Equation* (B.12) is calculated in (15).

While (15) is greater than (7) (2) can be found as $x = \left[\frac{R_o}{R_i} e^{-m\frac{R_o}{T}\left(1-\frac{R_i}{R_o}\right)} \right]^2$

$$\text{or } (2) = [1/(5).e^{-(7).(1-(5))}]^2$$

(2) is then used in *Equation* (B.10) to find (8).

Once (7) exceeds (15) *Equation* (B.11) must be used. *Equation* (B.11) cannot be solved explicitly and therefore requires an iterative approach. The Microsoft Excel

'GoalSeek' function was used to find the value of (8) for which *Equation* (B.11) had a zero value, calculated in (2).

Using the value in (8), (9) can then be calculated.

Now that the neutral radius has been found the velocities of the outer and inner radii can be determined from the velocity field in *Equation* (B.4) and entered in (13) and (14). The incremental change in the inner and outer radii (10) and (11) are simply the respective dR x Δt and are used to update (3) and (4) in the next step.

Lastly (12) is found using *Equation* (B.13) or *Equation* (B.14) according to the same criteria used above.

APPENDIX C

RESULTS OF PREVIOUS WORK

This appendix contains the results of a previous investigation [19] that proved useful in developing the test methodology followed in the current work. The ring compression test was used quasi-statically to investigate a variety of surface finishes and to verify the need for lubrication. Difficulties and potential pitfalls that may be encountered when using the ring compression test were uncovered and solutions proposed.

C.1 Oval deformation

The desired specimen surface roughness was achieved by grinding on a rotating grinding wheel, fitted with the specified Silicon-Carbide (SiC) paper. The circular motion of the grinding paper resulted in all the surface scratches lying uniformly in the tangential direction. During testing it was noticed that specimens were deforming in a non-uniform or 'oval' manner. Trial tests were conducted to establish the cause. Specimens were specifically prepared with an alignment on the surface by grinding in one direction with a rough grinding paper. Compression of these specimens resulted in the distinct oval shape depicted in *Figure C.1* below. Thus it was concluded that care must be taken to ensure a uniform 'anisotropic' surface finish, to ensure uniform deformation of the specimen. Non-uniform deformation prevents accurate measurement of the final internal diameter, making the extraction of useful friction factors virtually impossible.

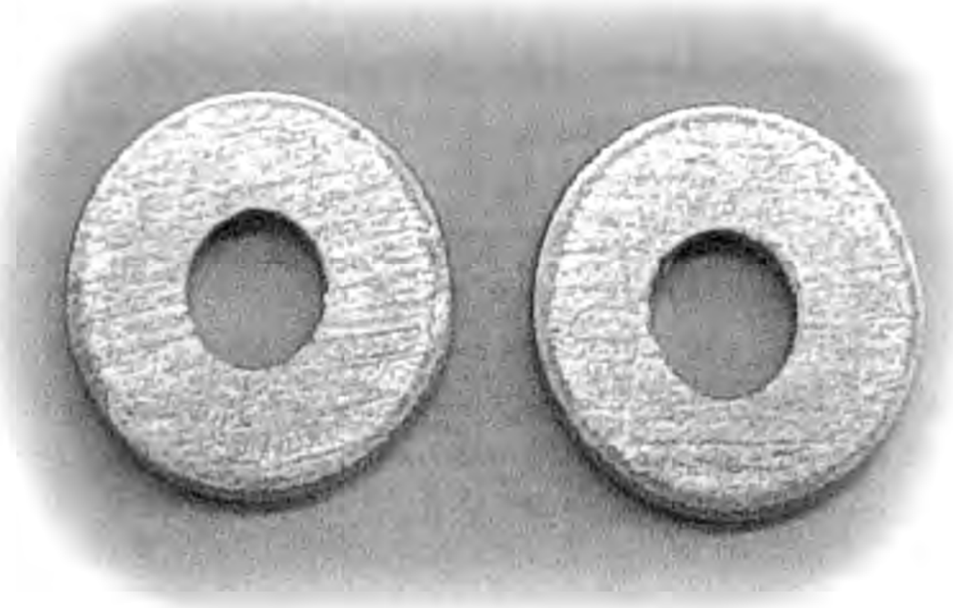

Figure C.1 Oval deformation of specimens due to linear scratches induced on the abraded surface. Specimens clearly deformed more readily against the induced grain, resulting in an oval internal hole. This was problematic for the measurement technique used, and prevented reliable comparison with theoretical predictions.

C.2 Scatter

The scatter in the results (see *Figure C.2*) was initially large and made extraction of useful friction parameters very difficult. The sensitivity of the test is such that great care is required in ensuring consistent friction conditions for otherwise identical tests. Testing a given scenario several times and developing a precise test methodology helps to establish a confidence limit in the results. It is clear from the chart below that the extraction of useful theoretical friction factors is not always possible.

Experimentation during previous work and in the current investigation led to a refinement of the experimental technique, tighter quality control on the selection of specimens and greater care being taken in the grinding and measuring of the specimens. Based on these results it was also decided to repeat all tests three times so that a reasonable level of confidence could be achieved (as mentioned in *Section 5.2*).

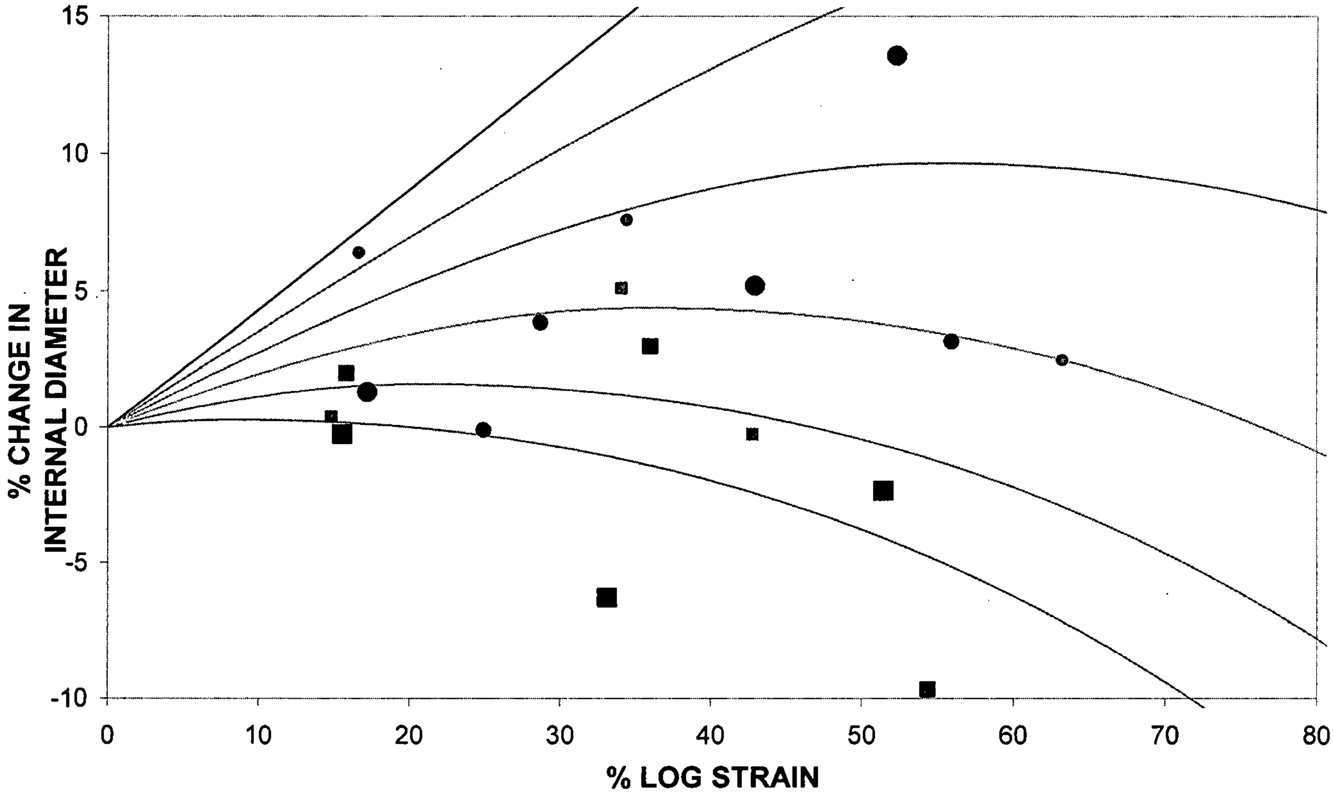

Figure C.2 Plot against theoretical curves [1] showing the scatter in the results of tests on 1200-grit steel specimens compressed using various anvil finishes. A larger marker indicates a rougher anvil.

C.3 Surface Finish

A highly polished specimen surface finish gave unpredictable results and often indicated relatively high friction, as is discussed in *Section 3.7* and can be seen in *Figure C.3* below.

Polished finishes were briefly used in the current work but the attempt was soon abandoned as similar scatter, high friction factors and generally unpredictable results occurred. Therefore only specimens and anvils prepared using 600-grit and 1200-grit SiC grinding papers were used.

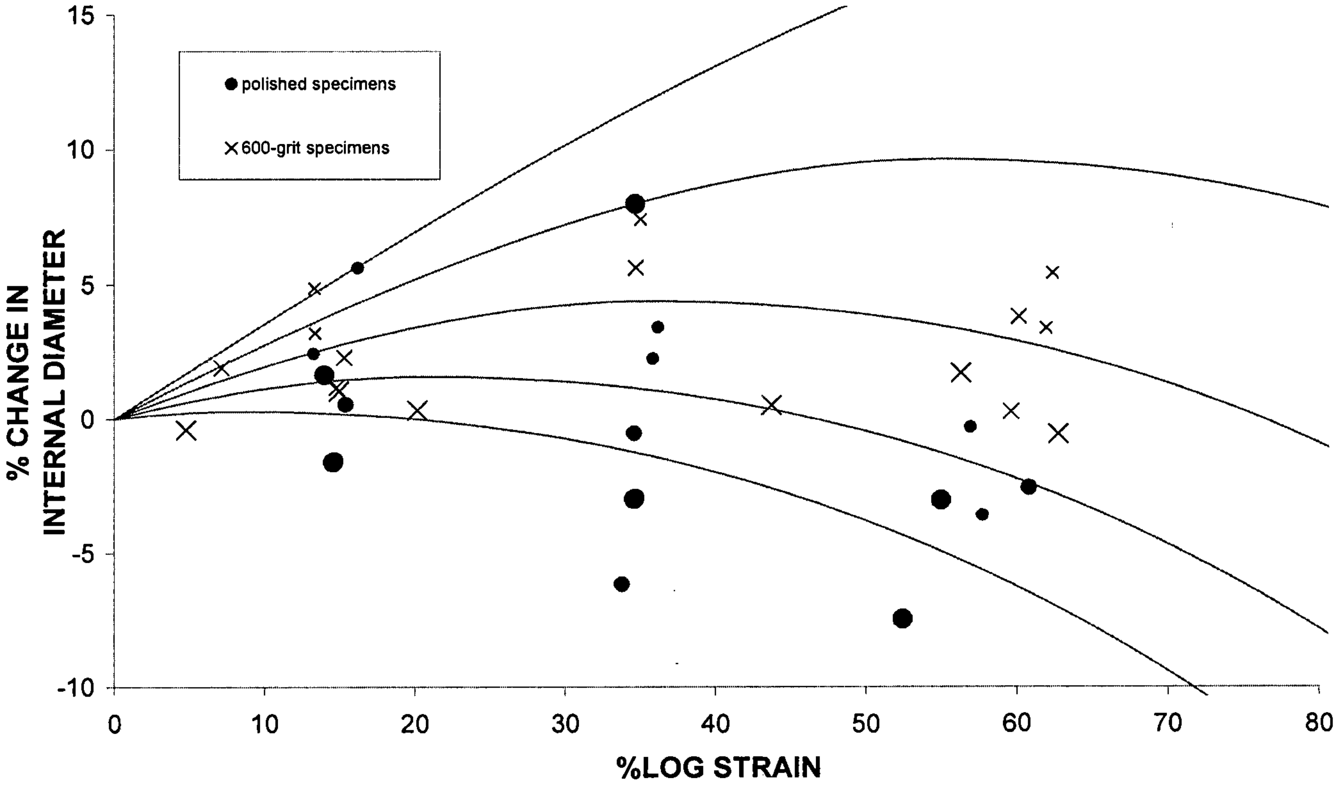

Figure C.3 Plot against the analytical result by Avitzur [1] showing the results from tests of 600-grit specimens (crosses) and polished specimen (dots) on various anvil finishes. A larger marker indicates a rougher anvil. Note the scatter and the relatively high friction that results when testing polished specimens.

C.4 Lubrication

Lubrication was found to be vital in reducing interface friction as shown below in *Figure C.4*. Lubricant was observed to squeeze out from under the specimens and it could therefore be assumed that friction conditions were not consistent.

The effects of lubrication were further investigated in the current work.

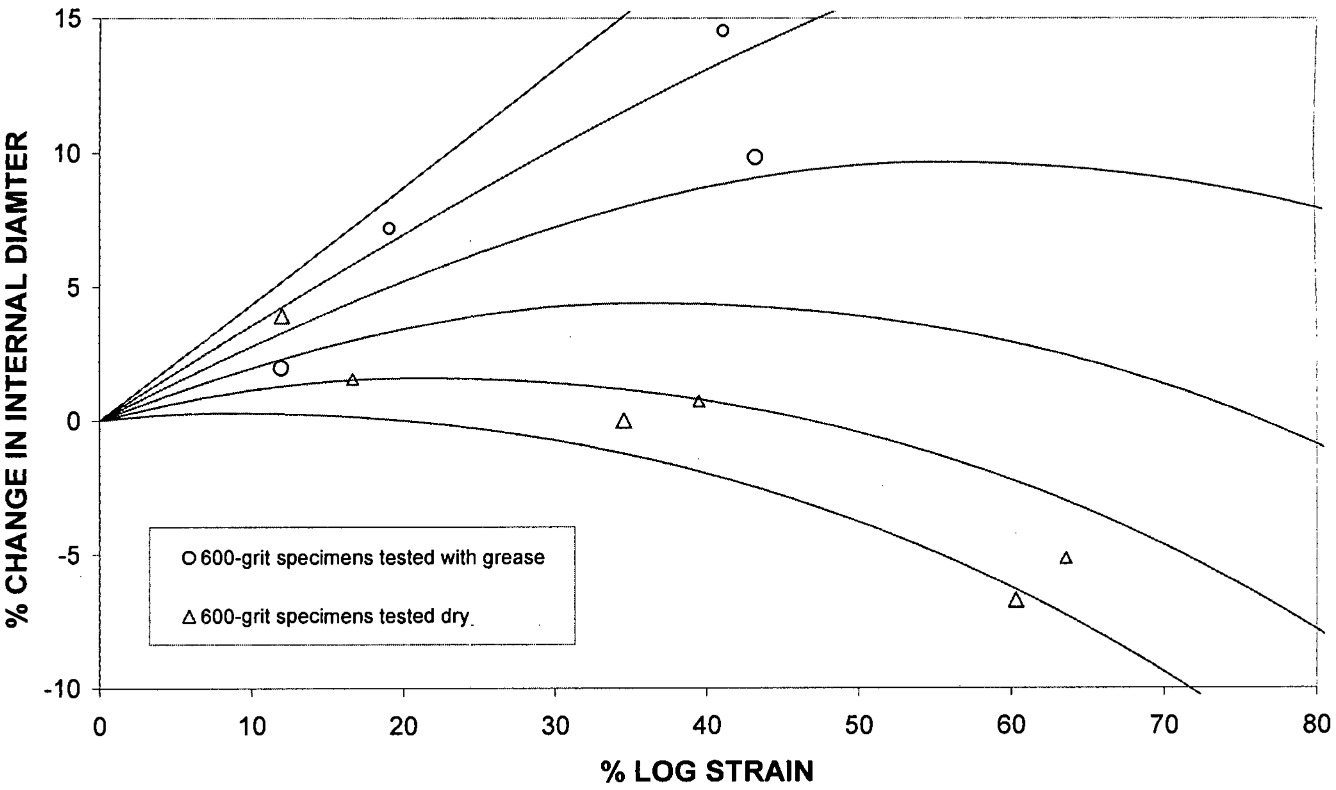

Figure C.4 Plot of greased and dry copper test specimens, for various anvil surface finishes. The smaller markers indicate 1200-grit anvils and the larger markers, 600-grit anvils. Lubrication clearly has an effect many times greater that of the surface roughness. The curves are from the analytical solution by Avitzur [1].

C.5 Changing Friction Conditions

Friction seemed to change during a single compression, as suggested by Schey [18]. The experimental results shown below illustrate this trend in a general sense in that the experimental results drop off from the theoretical curves (see *Figure C.5*) after a given strain, indicating that the actual conditions no longer follow the initial constant theoretical friction factor. The specimen surface finish, which was initially visibly roughened, appeared to have been smoothed as the specimen flowed plastically. The results at higher strains, however, are of limited reliability due to excessive barrelling, uneven deformation and the effects of strain hardening.

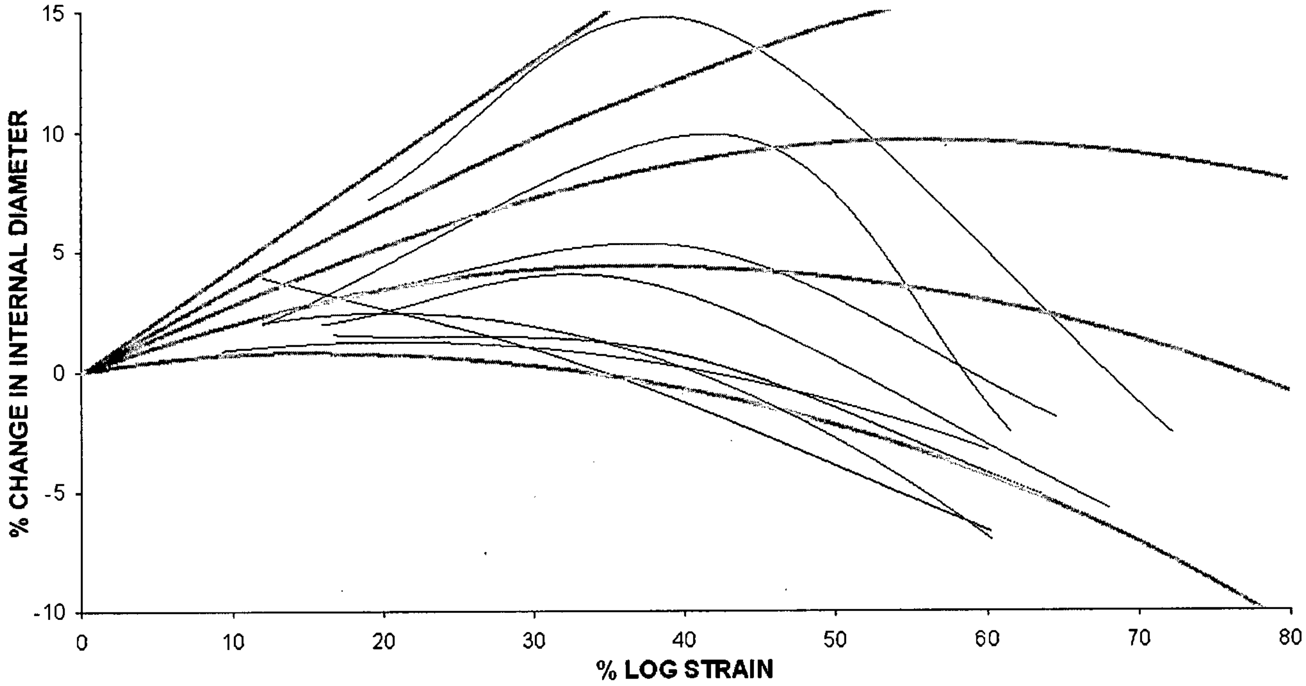

Figure C.5 Plot of best-fit curves for a range of experimental results against the analytical curves by Avitzur [1] showing the general tendency of the theoretical friction factor to increase as the test progresses beyond 40% strain.

C.6 Different Materials

Responses across the different materials were similar and the composition and microstructure of the metal did not seem to play a large role in the friction experienced, as can be seen from the results in *Table C.1*

C.7 Peripheral Zone

A distinct zone as discussed by *Gorham et al* [8] and *Walley et al* [10] was observed on the specimen periphery after testing as can be seen in the photograph in *Figure C.6*.

This distinct zone was also observed on specimens tested in the current work, and this, along with the numerical behaviour discussed in *Chapter 4*, prompted the microstructural investigation described in *Chapter 6*.

Figure C.6 Photographs of copper and aluminium specimens showing distinct peripheral zone or ring after testing to 40% log strain.

C.8 General Results

The table below gives the friction factors that could be reasonably extracted from the quasi-static tests performed. Blank spaces indicate conditions for which no reasonable friction factor could be extracted from the results obtained.

SPECIMEN FINISH	***ANVIL FINISH***	***Copper***	***Aluminium***	***Mild Steel***
DRY				
600	600		0.14	
600	1200	0.20		
600	polished			0.14
GREASED				
600	600	0.18	0.24	
600	1200	0.08	0.24	0.16
600	polished			0.06
DRY				
1200	600	0.20		
1200	1200	0.18	0.15	0.18
1200	polished	0.10		
GREASED				
1200	600	0.15	0.14	
1200	1200		0.18	0.18
1200	polished			0.06
DRY				
polished	600			0.28
polished	1200			
polished	polished		0.22	0.16
GREASED				
polished	600	0.26	0.14	
polished	1200		0.04	0.22
polished	Polished	0.18		0.06

Table C.1 Approximate m friction factors extracted from previous work [19].

APPENDIX D

SPLIT HOPKINSON PRESSURE BAR CALIBRATION

D.1 Bar Material Properties

Accurate material properties for the bars are required for the calibration methods used. The sonic velocity, c, was determined using the length of the bar and the period of a stress wave, which was measured from the signal recorded from the incident bar during the first calibration test. The density was determined by weighing and measuring the bar. These two measurements provide an accurate means of determining the elastic modulus, E, using one-dimensional wave theory.

From *Equation* (A.3)

$$c = \sqrt{E/\rho}$$

so

$$E = c^2\rho$$

Bar properties

Mass	9.88 kg
Length	2m
Diameter	20mm
Density	7866 kg/m^3
Incident wave transit time	0.3862 ms
sonic velocity, c	5179 m/s
Elastic Modulus, E	211 GPa

Table D.1 Silver-steel bar material properties, determined as described above.

D.2 Calibration Methods

The theoretical calibration factor is found by [26]

$$\sigma = \frac{4Ee_{out}}{AKFe_{in}}$$

For which F = 2.11
K = 2
A = 1000 (amplification)

where F is the gauge factor for the strain gauges used, as supplied by the manufacturer.
K is a factor used to account for the bridge configuration used.
A is the gain on the amplifiers, as described in *Section 5.4.2.*

Therefore

$$\sigma = e_{out}\left(\frac{4E}{4220e_{in}}\right)$$

So for a bridge excitation voltage of 5V, as was used throughout this investigation

$$\sigma = 40.10^{6} e_{out}$$

The theoretical calibration factor is thus $40\text{x}10^{6}$ and depends only on the bar elastic modulus and the bridge excitation voltage.

One dimensional wave theory

By applying simple one-dimensional stress wave propagation theory to the impact of the striker (denoted $_s$) and the bar (denoted $_b$) (*see Appendix A.1*) the stress generated in the bar for a measured striker velocity and known bar material properties can be determined.

Thus the stress induced in the bar for measured input conditions and material properties is determined and compared to the average of the measured voltage to determine the calibration factor, K.

$$K = \frac{\sigma_b^{\max}}{V_{out}^{\max}}$$

From one-dimensional wave theory (*see Appendix A.1*) the maximum stress in the incident wave is

$$\sigma_b = \frac{A_s}{A_s + A_b} c\rho v_0$$

$$v_0 = \frac{d}{t} = \frac{0.081}{t}$$

$$\therefore \sigma_b = \frac{0.081}{t} \frac{A_s}{A_s + A_b} c\rho$$

Momentum Balance

The total momentum of the striker before impact can be determined from the mass and the impact velocity. The momentum of the striker after impact can be calculated using the rebound velocity, which can be simply determined using one-dimensional wave theory as:

$$v_{striker}^{reb} = \frac{v_0\left(\frac{A_s}{A_b} - 1\right)}{\left(\frac{A_s}{A_b} + 1\right)}$$

The total impulse transferred to the incident bar, I, is thus

$$I = m_s(v_s - v_{reb})$$

The equation of motion states that

$$dI = Fdt$$

Hence

$dI = A\sigma.dt$ (assuming A and σ constant)

Therefore
$$
\begin{aligned}
I &= \int_0^T A\sigma(t).dt \\
&= A \int_0^T \sigma(t).dt \\
&= A \int_0^T K.v(t)dt \\
&= A\,K \int_0^T v(t)dt
\end{aligned}
$$

The voltage signal is integrated using the trapezoidal rule and K is determined from

$$K = \frac{m_s(v_s - v_{reb})}{A\int_0^T v dt}$$

D.3 Calibration Results

A typical curve used for calibrating the system is shown in *Figure D.1*. An example of the calculations and results appears below. If the error between the three different calibration methods was less than 5% the system was considered to be functioning correctly.

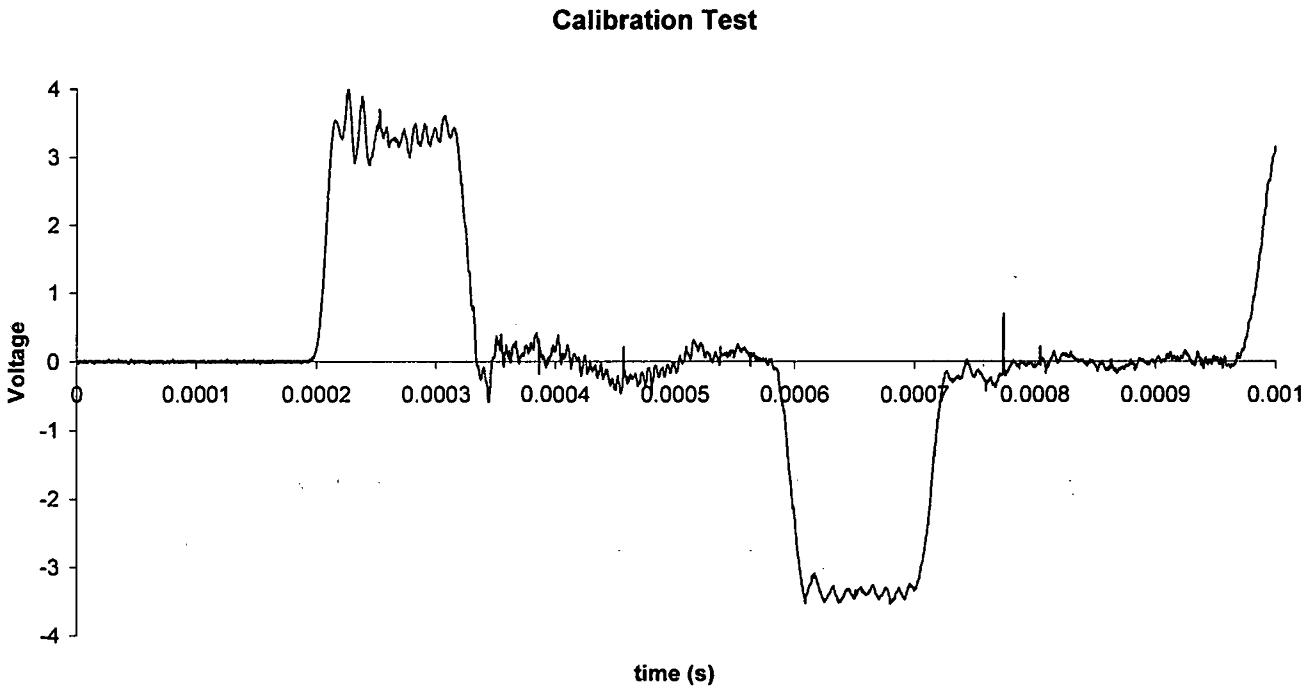

Figure D.1 Typical calibration curve as used in the calculations in *Table D.2*.

CONSTANTS

striker velocity (m/s)	*bar velocity (m/s)*	*rebound velocity (m/s)*	*bar density* (kg/m^3)	*bar elastic modulus (GPa)*	*wave speed (m/s)*	*striker length (mm)*	*speed trap (ms)*
12.66	3.350	-5.956	7866	2.110E+11	5179.219	300	6.4

bar diameter (mm)	*striker diameter (mm)*	*area of striker* A_s (mm^2)	*area of bar* A_b *(mm)*	A_s/A_b	*bridge voltage*	*striker mass (g)*	*speed trap length (mm)*
20	12	0.000113097	0.000314159	0.36	5	267	81

1. Theoretical Factor from strain gauge theory

40000000 MPa/V

2. Stress in the input bar from one dimensional wave theory

max stress (Pa)	*average voltage (V)*	*calibration factor (MPa/V)*
136485601	3.378	**40410018.16**

3. Momentum

total momentum (kg.m/s)	*rebound momentum (kg.m/s)*	*integral of voltage (V.s)*	*bar area x voltage integral* $A\int vdt$	*calibration factor (MPa/V)*
3.37778976	1.589548124	0.000394526	1.23944E-07	**40077316.43**

1. Theoretical	**2. Stress**	**3. Momentum**
(MPa/V) **40000000**	***(MPa/V)*** **40410018.16**	***(MPa/V)*** **40077316.43**
Error [%]	***1.025***	***0.193***

Table D.2 Results of the calibration for the Split Hopkinson Pressure bars used.

APPENDIX E

NUMERICAL MODELLING

All modelling was performed using an axi-symmetric configuration. The effects of different elements types and mesh densities were investigated initially to establish a suitable model. Six separate, similar tests were then simulated for which six different coulomb coefficients between 0.00 and 0.10 were assumed. Barrelling was then investigated by removing the barrel geometrically at increments during the simulation. Different loading rates were also simulated, using similar models. A typical input data file for a coulomb coefficient of 0.06 appears below. This is followed by the model used during the investigation of the effects of barrelling. An extract from a typical spreadsheet used to generate the theoretical curves based on Avitzur's analytical solution [1] is then included. The constant 'm' friction factor and the range of equivalent coulomb factors, μ, are shown. These values were used to compare the numerical and analytical results.

E.1 Input Data File for μ = 0.06

```
*Heading
 60 second reduced quadratic mu = 006
** Job name: 006-60sec-red-273 Model name: 006Friction
*Preprint, echo=NO, model=NO, history=NO, contact=NO
**
** PARTS
**
*Part, name=Specimen
*End Part
*Part, name=bott_anvil
*End Part
*Part, name=top_anvil
*End Part
**
** ASSEMBLY
**
*Assembly, name=Assembly
**
*Instance, name=bott_anvil-1, part=bott_anvil
*Node
      1,           0.,           0.,           0.
*Nset, nset=bott_anvil-1-RefPt_, internal
1,
*Surface, type=SEGMENTS, name=Surf_bott_anvil
START,           0.,           0.
```

```
 LINE, 0.00999999999999979,          0.
*Rigid Body, ref node=bott_anvil-1-RefPt_, analytical
surface=Surf_bott_anvil
*End Instance
**
*Instance, name=Specimen-1, part=Specimen
*Node
```

The code automatically assigns node coordinates. The full definitions have not been included.

```
*Element, type=CAX8R
```

Element connectivity has not been included.

```
*Nset, nset=Specimen, generate
    1,  4961,     1
*Elset, elset=Specimen, generate
    1,  1600,     1
** Region: (Section-1:Picked)
*Elset, elset=_PickedSet6, internal, generate
    1,  1600,     1
** Section: Section-1
*Solid Section, elset=_PickedSet6, material=copper
1.,
*End Instance
**
*Instance, name=top_anvil-1, part=top_anvil
          0., 0.00200000000000022,          0.
*Node
      1,           0.,           0.,           0.
*Nset, nset=top_anvil-1-RefPt_, internal
1,
*Surface, type=SEGMENTS, name=Surf_top_anvil
START, 0.00999999999999979,           0.
 LINE,          0.,           0.
*Rigid Body, ref node=top_anvil-1-RefPt_, analytical
surface=Surf_top_anvil
*End Instance
*Nset, nset=_G35, internal, instance=Specimen-1
    6,    7,    8,  143,  144,  145,  146,  147,  148,  149,  150,
151,  152,  153,  154,  155
  156,  157,  158,  159,  160,  161,  162,  163,  164,  165,  166,
167,  168,  169,  170,  171
  172,  173,  174,  175,  176,  177,  178,  179,  180, 4882, 4885,
4887, 4889, 4891, 4893, 4895
 4897, 4899, 4901, 4903, 4905, 4907, 4909, 4911, 4913, 4915, 4917,
4919, 4921, 4923, 4925, 4927
 4929, 4931, 4933, 4935, 4937, 4939, 4941, 4943, 4945, 4947, 4949,
4951, 4953, 4955, 4957, 4959
 4961,
*Elset, elset=_G35, internal, instance=Specimen-1, generate
 1561,  1600,     1
*Nset, nset=_G38, internal, instance=Specimen-1
    2,    3,   28,   29,   30,   31,   32,   33,   34,   35,   36,
37,   38,   39,   40,   41
   42,   43,   44,   45,   46,   47,   48,   49,   50,   51,   52,
53,   54,   55,   56,   57
```

```
   58,   59,   60,   61,   62,   63,   64,   65,   66, 1741, 1782,
1823, 1864, 1905, 1946, 1987
 2028, 2069, 2110, 2151, 2192, 2233, 2274, 2315, 2356, 2397, 2438,
2479, 2520, 2561, 2602, 2643
 2684, 2725, 2766, 2807, 2848, 2889, 2930, 2971, 3012, 3053, 3094,
3135, 3176, 3217, 3258, 3299
 3340,
*Elset, elset=_G38, internal, instance=Specimen-1, generate
  20,  800,   20
*Nset, nset=Set-bott_anvil, instance=bott_anvil-1
 1,
*Nset, nset=Set-top_anvil, instance=top_anvil-1
 1,
*Nset, nset=Set-top_points, instance=Specimen-1, generate
 6,  8,  1
*Nset, nset=Set-mid_points, instance=Specimen-1
 1, 4, 5
*Nset, nset=Set-top_surfaces, instance=Specimen-1
    6,    7,    8,  143,  144,  145,  146,  147,  148,  149,  150,
151,  152,  153,  154,  155
  156,  157,  158,  159,  160,  161,  162,  163,  164,  165,  166,
167,  168,  169,  170,  171
  172,  173,  174,  175,  176,  177,  178,  179,  180, 4882, 4885,
4887, 4889, 4891, 4893, 4895
 4897, 4899, 4901, 4903, 4905, 4907, 4909, 4911, 4913, 4915, 4917,
4919, 4921, 4923, 4925, 4927
 4929, 4931, 4933, 4935, 4937, 4939, 4941, 4943, 4945, 4947, 4949,
4951, 4953, 4955, 4957, 4959
 4961,
*Elset, elset=Set-top_surfaces, instance=Specimen-1, generate
 1561,  1600,     1
*Elset, elset=_Surf_spec_top_S3, internal, instance=Specimen-1,
generate
 1561,  1600,     1
*Surface, type=ELEMENT, name=Surf_spec_top
_Surf_spec_top_S3, S3
*Elset, elset=_Surf_spec_bott_S2, internal, instance=Specimen-1,
generate
  20,  800,   20
*Surface, type=ELEMENT, name=Surf_spec_bott
_Surf_spec_bott_S2, S2
*Elset, elset=__PickedSurf93_S2, internal, instance=Specimen-1,
generate
  840,  1600,    40
*Elset, elset=__PickedSurf93_S4, internal, instance=Specimen-1,
generate
  801,  1561,    40
*Surface, type=ELEMENT, name=_PickedSurf93, internal
__PickedSurf93_S2, S2
__PickedSurf93_S4, S4
*Elset, elset=__PickedSurf95_S1, internal, instance=Specimen-1,
generate
  1,  20,   1
*Elset, elset=__PickedSurf95_S3, internal, instance=Specimen-1,
generate
 781,  800,    1
*Surface, type=ELEMENT, name=_PickedSurf95, internal
__PickedSurf95_S1, S1
__PickedSurf95_S3, S3
*End Assembly
**
```

```
** MATERIALS
**
*Material, name=copper
*Density
8870.,
*Elastic
 1.1e+11, 0.3
*Plastic
 2.73e+08,0.
 2.73e+08,2.
**
** INTERACTION PROPERTIES
**
*Surface Interaction, name=Fricition006
1.,
*Friction, slip tolerance=0.005
 0.06,
**
** BOUNDARY CONDITIONS
**
** Name: BC-bott Type: Symmetry/Antisymmetry/Encastre
*Boundary
Set-bott_anvil, ENCASTRE
** Name: BC-top Type: Symmetry/Antisymmetry/Encastre
*Boundary
Set-top_anvil, XSYMM
**
** INTERACTIONS
**
** Interaction: Int-bott
*Contact Pair, interaction=Fricition006, adjust=0.001
Surf_spec_bott, bott_anvil-1.Surf_bott_anvil
** Interaction: Int-top
*Contact Pair, interaction=Fricition006, adjust=0.001
Surf_spec_top, top_anvil-1.Surf_top_anvil
** Interaction: Lower-sides
*Contact Pair, interaction=Fricition006, adjust=0.0
_PickedSurf95, bott_anvil-1.Surf_bott_anvil
** Interaction: Upper-sides
*Contact Pair, interaction=Fricition006, adjust=0.0
_PickedSurf93, top_anvil-1.Surf_top_anvil
** ----------------------------------------------------------------
**
** STEP: Compression
**
*Step, name=Compression, nlgeom=YES, amplitude=STEP, inc=300
Quasi-static compression at 1mm/min for 1min
*Static
0.0001, 60., 1e-05, 60.
**
** BOUNDARY CONDITIONS
**
** Name: Velocity Type: Velocity/Angular velocity
*Boundary, type=VELOCITY
Set-top_anvil, 2, 2, -1.66667e-05
**
** OUTPUT REQUESTS
**
*Restart, write, frequency=1
**
** FIELD OUTPUT: F-Output-1
```

```
**
*Output, field
*Node Output
TF, U, V
*Element Output
LE, PE, PEEQ, PEMAG, S
*Contact Output
CDISP, CSTRESS
**
** FIELD OUTPUT: CSTRESSTOP
**
*Contact Output, nset=Set-top_surfaces
CSTRESS,
**
** HISTORY OUTPUT: H-Output-1
**
*Output, history, variable=PRESELECT
**
** HISTORY OUTPUT: mid_displ
**
*Output, history
*Node Output, nset=Set-mid_points
U1, U2
**
** HISTORY OUTPUT: top_displ
**
*Node Output, nset=Set-top_points
U1, U2
**
** HISTORY OUTPUT: top_CSTRESS
**
*Element Output, elset=Set-top_surfaces
INV3, MISES, PRESS, S11, S12, S13, S22, S23, S33, SP, TRESC
*Contact Output, nset=Set-top_surfaces
CAREA, CSTRESS
**
** HISTORY OUTPUT: top_PRESS
**
*Element Output, elset=Set-top_surfaces
PRESS,
*El Print, freq=999999
*Node Print, freq=999999
*End Step
** ----------------------------------------------------------------
**
** STEP: Remove Contact
**
*Step, name="Remove Contact", nlgeom=YES, amplitude=STEP
Remove Contact
*Static
0.1, 10., 0.0001, 1.
**
** BOUNDARY CONDITIONS
**
** Name: Velocity Type: Velocity/Angular velocity
*Boundary, type=VELOCITY
Set-top_anvil, 2, 2, 0.000166667
**
** INTERACTIONS
**
** Interaction: Int-top
```

```
*Model Change, type=CONTACT PAIR, remove
Surf_spec_top, top_anvil-1.Surf_top_anvil
** Interaction: Upper-sides
*Model Change, type=CONTACT PAIR, remove
_PickedSurf93, top_anvil-1.Surf_top_anvil
**
** OUTPUT REQUESTS
**
*Restart, write, frequency=1
**
** FIELD OUTPUT: F-Output-1
**
*Output, field
*Node Output
TF, U, V
*Element Output
LE, PE, PEEQ, PEMAG, S
*Contact Output
CDISP, CSTRESS
**
** FIELD OUTPUT: CSTRESSTOP
**
*Contact Output, nset=Set-top_surfaces
CSTRESS,
**
** HISTORY OUTPUT: H-Output-1
**
*Output, history, variable=PRESELECT
**
** HISTORY OUTPUT: mid_displ
**
*Output, history
*Node Output, nset=Set-mid_points
U1, U2
**
** HISTORY OUTPUT: top_displ
**
*Node Output, nset=Set-top_points
U1, U2
**
** HISTORY OUTPUT: top_CSTRESS
**
*Element Output, elset=Set-top_surfaces
PRESS, S11, S12, S22, SP,
*Contact Output, nset=Set-top_surfaces
CAREA, CSTRESS
**
** HISTORY OUTPUT: top_PRESS
**
*Element Output, elset=Set-top_surfaces
PRESS,
*End Step
```

E.2 Input Data File for Barrelling Investigation

```
*Heading
 18
** Job name: bar008-18 Model name: Barrelling008-18
*Preprint, echo=NO, model=NO, history=NO, contact=NO
**
** PARTS
**
*Part, name=Specimen
*End Part
*Part, name=bott_anvil
*End Part
*Part, name=top_anvil
*End Part
**
** ASSEMBLY
**
*Assembly, name=Assembly
**
*Instance, name=bott_anvil-1, part=bott_anvil
*Node
      1,           0.,           0.,           0.
*Nset, nset=bott_anvil-1-RefPt_, internal
1,
*Surface, type=SEGMENTS, name=Surf_bott_anvil
START,           0.,           0.
 LINE, 0.00999999999999979,           0.
*Rigid Body, ref node=bott_anvil-1-RefPt_, analytical
surface=Surf_bott_anvil
*End Instance
**
*Instance, name=Specimen-1, part=Specimen
*Node
```

The code automatically assigns node coordinates. The full definitions have not been included.

```
*Element, type=CAX8R
```

Element connectivity has not been included.

```
*Nset, nset=Specimen, generate
    1,  4961,     1
*Elset, elset=Specimen, generate
    1,  1600,     1
** Region: (Section-1:Specimen)
** Section: Section-1
*Solid Section, elset=Specimen, material=copper
1.,
*End Instance
**
*Instance, name=top_anvil-1, part=top_anvil
          0., 0.00114999999999998,           0.
*Node
      1,           0.,           0.,           0.
*Nset, nset=top_anvil-1-RefPt_, internal
1,
*Surface, type=SEGMENTS, name=Surf_top_anvil
```

```
START, 0.00999999999999979,           0.
 LINE,            0.,             0.
*Rigid Body, ref node=top_anvil-1-RefPt_, analytical
surface=Surf_top_anvil
*End Instance
*Nset, nset=_G35, internal, instance=Specimen-1
    1,     2,     3,     4,     5,     6,     7,     8,     9,    10,    11,
12,    13,    14,    15,    16
   17,    18,    19,    20,    21,    22,    23,    24,    25,    26,    27,
28,    29,    30,    31,    32
   33,    34,    35,    36,    37,    38,    39,    40,    41, 1682, 1686,
1689, 1692, 1695, 1698, 1701
 1704, 1707, 1710, 1713, 1716, 1719, 1722, 1725, 1728, 1731, 1734,
1737, 1740, 1743, 1746, 1749
 1752, 1755, 1758, 1761, 1764, 1767, 1770, 1773, 1776, 1779, 1782,
1785, 1788, 1791, 1794, 1797
 1800,
*Elset, elset=_G35, internal, instance=Specimen-1, generate
  1,  40,   1
*Nset, nset=_G38, internal, instance=Specimen-1
 1641, 1642, 1643, 1644, 1645, 1646, 1647, 1648, 1649, 1650, 1651,
1652, 1653, 1654, 1655, 1656
 1657, 1658, 1659, 1660, 1661, 1662, 1663, 1664, 1665, 1666, 1667,
1668, 1669, 1670, 1671, 1672
 1673, 1674, 1675, 1676, 1677, 1678, 1679, 1680, 1681, 4882, 4885,
4887, 4889, 4891, 4893, 4895
 4897, 4899, 4901, 4903, 4905, 4907, 4909, 4911, 4913, 4915, 4917,
4919, 4921, 4923, 4925, 4927
 4929, 4931, 4933, 4935, 4937, 4939, 4941, 4943, 4945, 4947, 4949,
4951, 4953, 4955, 4957, 4959
 4961,
*Elset, elset=_G38, internal, instance=Specimen-1, generate
 1561,  1600,     1
*Nset, nset=Set-bott_anvil, instance=bott_anvil-1
 1,
*Nset, nset=Set-top_anvil, instance=top_anvil-1
 1,
*Nset, nset=Set-TopREF, instance=Specimen-1
  1, 41
*Nset, nset=Set-top_surface, instance=Specimen-1
    1,     2,     3,     4,     5,     6,     7,     8,     9,    10,    11,
12,    13,    14,    15,    16
   17,    18,    19,    20,    21,    22,    23,    24,    25,    26,    27,
28,    29,    30,    31,    32
   33,    34,    35,    36,    37,    38,    39,    40,    41, 1682, 1686,
1689, 1692, 1695, 1698, 1701
 1704, 1707, 1710, 1713, 1716, 1719, 1722, 1725, 1728, 1731, 1734,
1737, 1740, 1743, 1746, 1749
 1752, 1755, 1758, 1761, 1764, 1767, 1770, 1773, 1776, 1779, 1782,
1785, 1788, 1791, 1794, 1797
 1800,
*Elset, elset=Set-top_surface, instance=Specimen-1, generate
  1,  40,   1
*Nset, nset=Set-MID_IR, instance=Specimen-1
 861,
*Nset, nset=Set-MID_OR, instance=Specimen-1
 821,
*Nset, nset=Set-MIDOutput, instance=Specimen-1
 821, 861
*Nset, nset=Set-INNER, instance=Specimen-1
```

```
   41,   82,  123,  164,  205,  246,  287,  328,  369,  410,  451,
492,  533,  574,  615,  656
  697,  738,  779,  820,  861,  902,  943,  984, 1025, 1066, 1107,
1148, 1189, 1230, 1271, 1312
 1353, 1394, 1435, 1476, 1517, 1558, 1599, 1640, 1681, 1801, 1882,
1963, 2044, 2125, 2206, 2287
 2368, 2449, 2530, 2611, 2692, 2773, 2854, 2935, 3016, 3097, 3178,
3259, 3340, 3421, 3502, 3583
 3664, 3745, 3826, 3907, 3988, 4069, 4150, 4231, 4312, 4393, 4474,
4555, 4636, 4717, 4798, 4879
 4960,
*Elset, elset=Set-INNER, instance=Specimen-1, generate
   40,  1600,    40
*Elset, elset=_Surf_spec_top_S1, internal, instance=Specimen-1,
generate
  1,  40,   1
*Surface, type=ELEMENT, name=Surf_spec_top
_Surf_spec_top_S1, S1
*Elset, elset=_Surf_spec_bott_S3, internal, instance=Specimen-1,
generate
 1561,  1600,     1
*Surface, type=ELEMENT, name=Surf_spec_bott
_Surf_spec_bott_S3, S3
*Elset, elset=__PickedSurf214_S2, internal, instance=Specimen-1,
generate
  840,  1600,    40
*Elset, elset=__PickedSurf214_S4, internal, instance=Specimen-1,
generate
  801,  1561,    40
*Surface, type=ELEMENT, name=_PickedSurf214, internal
__PickedSurf214_S2, S2
__PickedSurf214_S4, S4
*Elset, elset=__PickedSurf215_S2, internal, instance=Specimen-1,
generate
  40,  800,   40
*Elset, elset=__PickedSurf215_S4, internal, instance=Specimen-1,
generate
   1,  761,   40
*Surface, type=ELEMENT, name=_PickedSurf215, internal
__PickedSurf215_S2, S2
__PickedSurf215_S4, S4
*End Assembly
**
** MATERIALS
**
*Material, name=copper
*Density
8870.,
*Elastic
 1.1e+11, 0.3
*Plastic
 9e+07,0.
 9e+07,2.
**
** INTERACTION PROPERTIES
**
*Surface Interaction, name=Fricition008
1.,
*Friction, slip tolerance=0.005
 0.08,
**
```

```
** BOUNDARY CONDITIONS
**
** Name: BC-bott Type: Symmetry/Antisymmetry/Encastre
*Boundary
Set-bott_anvil, ENCASTRE
** Name: BC-top Type: Symmetry/Antisymmetry/Encastre
*Boundary
Set-top_anvil, XSYMM
**
** INTERACTIONS
**
** Interaction: Int-bott
*Contact Pair, interaction=Fricition008, adjust=0.001
Surf_spec_bott, bott_anvil-1.Surf_bott_anvil
** Interaction: Int-top
*Contact Pair, interaction=Fricition008, adjust=0.001
Surf_spec_top, top_anvil-1.Surf_top_anvil
** Interaction: Lower-sides
*Contact Pair, interaction=Fricition008
_PickedSurf214, bott_anvil-1.Surf_bott_anvil
** Interaction: Upper-sides
*Contact Pair, interaction=Fricition008
_PickedSurf215, top_anvil-1.Surf_top_anvil
** ----------------------------------------------------------------
**
** STEP: Compression
**
*Step, name=Compression, nlgeom=YES, amplitude=STEP, inc=300
Quasi-static compression at 1mm/min
*Static
0.0001, 3., 1e-05, 3.
**
** BOUNDARY CONDITIONS
**
** Name: Velocity Type: Velocity/Angular velocity
*Boundary, type=VELOCITY
Set-top_anvil, 2, 2, -1.66667e-05
**
** OUTPUT REQUESTS
**
*Restart, write, frequency=1
**
** FIELD OUTPUT: F-Output-1
**
*Output, field, variable=PRESELECT
**
** FIELD OUTPUT: CSTRESSTOP
**
*Output, field
*Contact Output, nset=Set-top_surface
CSTRESS,
**
** HISTORY OUTPUT: H-Output-1
**
*Output, history, variable=PRESELECT
**
** HISTORY OUTPUT: His-U1-inner
**
*Output, history
*Node Output, nset=Set-INNER
U1,
```

```
**
** HISTORY OUTPUT: MidOutput
**
*Node Output, nset=Set-MIDOutput
U1, U2
**
** HISTORY OUTPUT: TopREFOut
**
*Node Output, nset=Set-TopREF
U1, U2
**
** HISTORY OUTPUT: TOPCSTRESS
**
*Element Output, elset=Set-top_surface
SP,
*Contact Output, nset=Set-top_surface
CAREA, CSTRESS
*El Print, freq=999999
*Node Print, freq=999999
*End Step
```

E.3 Calculation of Equivalent Coulomb Coefficients

An extract from the spreadsheet used to generate a portion of Avitzur's analytical solution [1] and to find the equivalent coulomb coefficients for given constant friction 'm' factors is shown below. The range of equivalent coulomb coefficients, μ, across the strain considered, for the given 'm' friction factor of 0.10, appear in the right-most column. These values were used in a step-wise manner to compare curves based on the two different friction models.

INITIAL CONDITIONS		
R_i	1.5	mm
R_o	3.0	mm
h	2.0	mm
m	0.100	*(constant)*

Δt	1	s
anvil speed, U	-0.01667	mm/s
Δh	-0.01667	mm

R_i	R_o	R_i/R_o	h	ΔR_o	ΔR_i	P_{ave}/σ_o	***% LOG***	***% CHANGE IN***	***EQUIVALENT***
(mm)	***(mm)***		***(mm)***	***(mm)***	***(mm)***		***STRAIN***	***INT. DIAMETER***	μ
1.500	3.000	0.500	2.000	0.011	0.004	1.062	*0.00*	*0.00*	**0.054**
1.504	3.011	0.499	1.983	0.012	0.004	1.063	*0.84*	*0.27*	**0.054**
1.508	3.023	0.499	1.967	0.012	0.004	1.064	*1.68*	*0.54*	**0.054**
1.512	3.035	0.498	1.950	0.012	0.004	1.064	*2.53*	*0.82*	**0.054**
1.516	3.046	0.498	1.933	0.012	0.004	1.065	*3.39*	*1.09*	**0.054**
1.520	3.058	0.497	1.917	0.012	0.004	1.066	*4.26*	*1.37*	**0.054**

1.525	3.070	0.497	1.900	0.012	0.004	1.067	*5.13*	*1.64*	**0.054**
1.529	3.083	0.496	1.883	0.012	0.004	1.067	*6.01*	*1.92*	**0.054**
1.533	3.095	0.495	1.867	0.013	0.004	1.068	*6.90*	*2.20*	**0.054**
1.537	3.107	0.495	1.850	0.013	0.004	1.069	*7.80*	*2.48*	**0.054**
1.541	3.120	0.494	1.833	0.013	0.004	1.070	*8.70*	*2.76*	**0.054**
1.546	3.133	0.493	1.817	0.013	0.004	1.071	*9.61*	*3.04*	**0.054**
1.550	3.146	0.493	1.800	0.013	0.004	1.072	*10.54*	*3.32*	**0.054**
1.554	3.159	0.492	1.783	0.013	0.004	1.072	*11.47*	*3.60*	**0.054**
1.558	3.172	0.491	1.767	0.013	0.004	1.073	*12.41*	*3.88*	**0.054**
1.563	3.186	0.490	1.750	0.014	0.004	1.074	*13.35*	*4.17*	**0.054**
1.567	3.199	0.490	1.733	0.014	0.004	1.075	*14.31*	*4.45*	**0.054**
1.571	3.213	0.489	1.717	0.014	0.004	1.076	*15.28*	*4.73*	**0.054**
1.575	3.227	0.488	1.700	0.014	0.004	1.077	*16.25*	*5.02*	**0.054**
1.580	3.241	0.487	1.683	0.014	0.004	1.078	*17.24*	*5.30*	**0.054**
1.584	3.255	0.486	1.667	0.014	0.004	1.079	*18.23*	*5.59*	**0.054**
1.588	3.270	0.486	1.650	0.015	0.004	1.080	*19.24*	*5.87*	**0.053**
1.592	3.285	0.485	1.633	0.015	0.004	1.081	*20.25*	*6.15*	**0.053**
1.597	3.300	0.484	1.617	0.015	0.004	1.082	*21.28*	*6.44*	**0.053**
1.601	3.315	0.483	1.600	0.015	0.004	1.083	*22.31*	*6.72*	**0.053**
1.605	3.330	0.482	1.583	0.015	0.004	1.084	*23.36*	*7.00*	**0.053**
1.609	3.345	0.481	1.567	0.016	0.004	1.085	*24.42*	*7.28*	**0.053**
1.613	3.361	0.480	1.550	0.016	0.004	1.086	*25.49*	*7.56*	**0.053**
1.618	3.377	0.479	1.533	0.016	0.004	1.088	*26.57*	*7.84*	**0.053**
1.622	3.393	0.478	1.517	0.016	0.004	1.089	*27.66*	*8.12*	**0.053**
1.626	3.410	0.477	1.500	0.017	0.004	1.090	*28.77*	*8.40*	**0.053**
1.630	3.426	0.476	1.483	0.017	0.004	1.091	*29.89*	*8.67*	**0.053**
1.634	3.443	0.475	1.467	0.017	0.004	1.093	*31.02*	*8.95*	**0.053**
1.638	3.460	0.473	1.450	0.017	0.004	1.094	*32.16*	*9.22*	**0.053**
1.642	3.477	0.472	1.433	0.018	0.004	1.095	*33.31*	*9.48*	**0.053**
1.646	3.495	0.471	1.417	0.018	0.004	1.097	*34.48*	*9.75*	**0.053**
1.650	3.513	0.470	1.400	0.018	0.004	1.098	*35.67*	*10.01*	**0.053**
1.654	3.531	0.468	1.383	0.018	0.004	1.099	*36.87*	*10.27*	**0.053**
1.658	3.549	0.467	1.367	0.019	0.004	1.101	*38.08*	*10.52*	**0.052**
1.662	3.568	0.466	1.350	0.019	0.004	1.102	*39.30*	*10.77*	**0.052**
1.665	3.587	0.464	1.333	0.019	0.004	1.104	*40.55*	*11.01*	**0.052**
1.669	3.606	0.463	1.317	0.020	0.004	1.106	*41.80*	*11.25*	**0.052**
1.672	3.626	0.461	1.300	0.020	0.003	1.107	*43.08*	*11.49*	**0.052**
1.676	3.646	0.460	1.283	0.020	0.003	1.109	*44.37*	*11.72*	**0.052**
1.679	3.666	0.458	1.267	0.021	0.003	1.111	*45.68*	*11.94*	**0.052**
1.682	3.686	0.456	1.250	0.021	0.003	1.112	*47.00*	*12.15*	**0.052**
1.685	3.707	0.455	1.233	0.021	0.003	1.114	*48.34*	*12.35*	**0.052**
1.688	3.728	0.453	1.217	0.022	0.003	1.116	*49.70*	*12.55*	**0.052**
1.691	3.750	0.451	1.200	0.022	0.003	1.118	*51.08*	*12.74*	**0.052**
1.694	3.772	0.449	1.183	0.022	0.002	1.120	*52.48*	*12.91*	**0.052**
1.696	3.794	0.447	1.167	0.023	0.002	1.122	*53.90*	*13.07*	**0.051**
1.698	3.817	0.445	1.150	0.023	0.002	1.124	*55.34*	*13.23*	**0.051**

1.700	3.840	0.443	1.133	0.024	0.002	1.126	*56.80*	*13.36*	**0.051**
1.702	3.864	0.441	1.117	0.024	0.002	1.128	*58.28*	*13.49*	**0.051**
1.704	3.887	0.438	1.100	0.024	0.001	1.130	*59.78*	*13.60*	**0.051**
1.705	3.912	0.436	1.083	0.025	0.001	1.133	*61.31*	*13.69*	**0.051**
1.706	3.937	0.433	1.067	0.025	0.001	1.135	*62.86*	*13.76*	**0.051**
1.707	3.962	0.431	1.050	0.026	0.000	1.138	*64.44*	*13.81*	**0.051**
1.708	3.988	0.428	1.033	0.026	0.000	1.140	*66.04*	*13.84*	**0.051**
1.708	4.014	0.425	1.017	0.027	0.000	1.143	*67.66*	*13.84*	**0.051**
1.707	4.041	0.423	1.000	0.027	0.000	1.145	*69.31*	*13.83*	**0.050**
1.707	4.068	0.420	0.983	0.028	-0.001	1.148	*71.00*	*13.81*	**0.050**
1.706	4.097	0.417	0.967	0.029	-0.001	1.151	*72.70*	*13.76*	**0.050**
1.706	4.125	0.413	0.950	0.030	-0.001	1.154	*74.44*	*13.70*	**0.050**
1.704	4.155	0.410	0.933	0.030	-0.001	1.157	*76.21*	*13.62*	**0.050**
1.703	4.185	0.407	0.917	0.031	-0.002	1.160	*78.02*	*13.52*	**0.050**
1.701	4.216	0.403	0.900	0.032	-0.002	1.164	*79.85*	*13.40*	**0.050**
1.699	4.248	0.400	0.883	0.033	-0.003	1.168	*81.72*	*13.26*	**0.049**
1.696	4.281	0.396	0.867	0.034	-0.003	1.171	*83.62*	*13.09*	**0.049**
1.693	4.314	0.393	0.850	0.034	-0.003	1.175	*85.57*	*12.90*	**0.049**
1.690	4.349	0.389	0.833	0.035	-0.004	1.180	*87.55*	*12.68*	**0.049**
1.686	4.384	0.385	0.817	0.036	-0.004	1.184	*89.57*	*12.42*	**0.049**
1.682	4.421	0.381	0.800	0.038	-0.005	1.189	*91.63*	*12.14*	**0.049**
1.677	4.458	0.376	0.783	0.039	-0.005	1.193	*93.73*	*11.82*	**0.048**
1.672	4.497	0.372	0.767	0.040	-0.006	1.199	*95.89*	*11.45*	**0.048**

APPENDIX F

QUASI-STATIC TENSILE TESTS ON COPPER

Standard tensile tests as per BS-18 [27] were performed to obtain the quasi-static yield strength for the copper used for the ring compression test specimens. A Zwick Universal Testing Machine was used to obtain the force – crosshead displacement data at a strain rate of $0.002s^{-1}$. From these tests the 0.2% offset yield strength for the commercially pure as-received copper used was found to be 273MPa and the ultimate tensile strength approximately 330MPa. These values were used in the numerical model and to estimate the forces required during the Hopkinson Bar tests for different friction conditions.

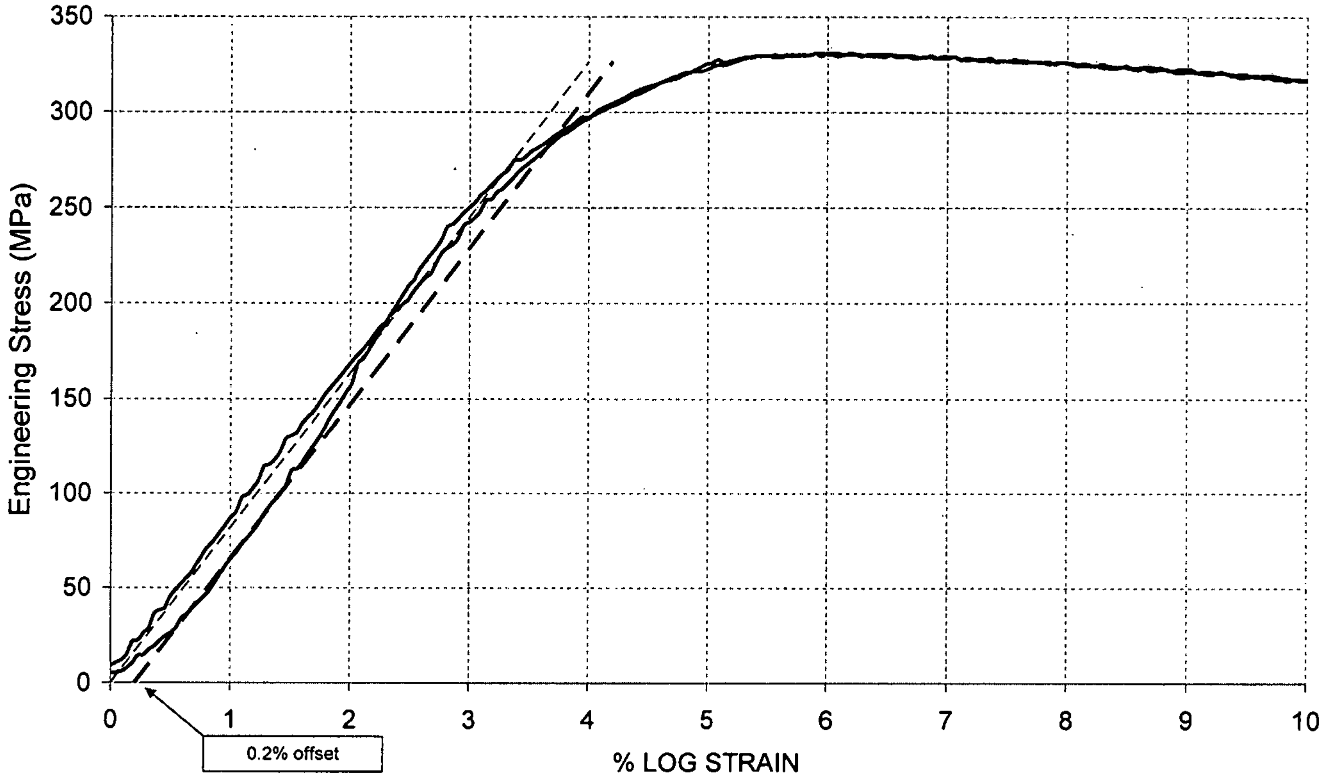

Figure F.1 Tensile test results for two copper tensile test specimens. The 0.2% offset yield was found to be approximately 273MPa and the ultimate tensile strength approximately 330MPa.

APPENDIX G

MATERIAL DENSITY CALCULATIONS

D.1 Copper

	Diameter (mm) **top**	**middle**	**base**	**Height (mm)**	**Mass (g)**
1	9.675	9.675	9.675	13.210	8.6155
2	9.675	9.670	9.670	13.215	8.6156
3	9.670	9.670	9.675	13.212	8.6157
	Average		9.675 ± 0.005	13.215 ± 0.005	8.6156 ± 0.0001

Volume	**971.3 mm^3**
Density	**8870 kg/mm^3**

D.2 Aluminium

Diameter		**Height (mm)**	**Mass (g)**
Average	10.00 ± 0.005	10.035 ± 0.005	2.1132 ± 0.0001

Volume	**788.2 mm^3**
Density	**2681 kg/mm^3**

D.3 Steel

Diameter		**Height (mm)**	**Mass (g)**
Average	10.01 ± 0.005	9.805 ± 0.005	6.0143 ± 0.0001

Volume	**771.6 mm^3**
Density	**7794 kg/mm^3**

APPENDIX I

DRAWINGS

Drawing Number	**Description**
RH-SPECIMEN-MS-001	Mild steel ring compression test specimen
RH-SPECIMEN-CU-001	Copper ring compression test specimen
RH-SPECIMEN-AL-001	Aluminium ring compression test specimen
RH-ANVIL-001	Compression anvil
RH-COLLAR-L-001	Large limit-collars
RH-COLLAR-S-001	Small limit-collars

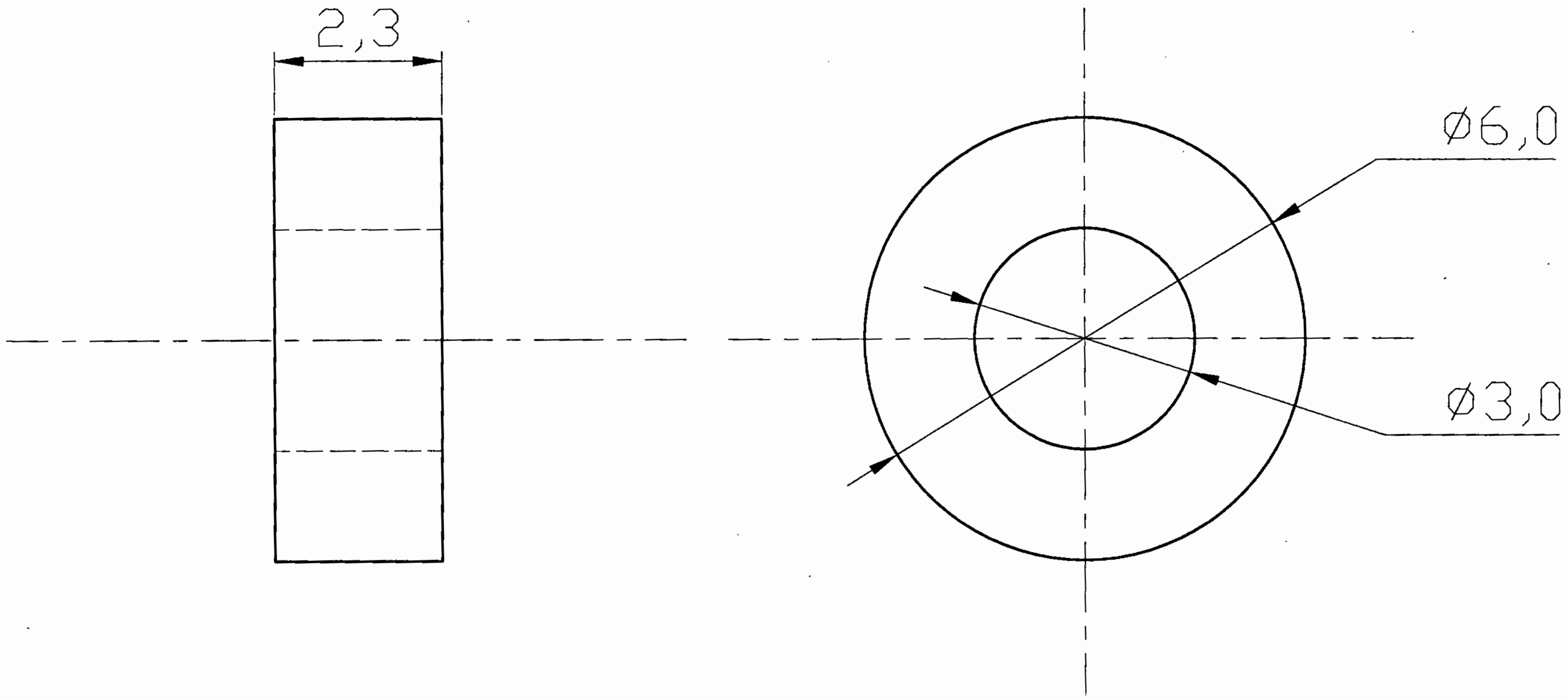

1	6:3:2 Steel Specimen	MILD STEEL	60
PT. NO.	DESCRIPTION	MATERIAL	NO. OFF

UNIVERSITY OF CAPE TOWN
Department of Mechanical Engineering

6:3:2 STEEL SPECIMEN

Dimensions in mm	SCALE 10:1	DATE 17-03-2004	SHEET 1 OF 1
Tolerance unless otherwise stated +-0.1mm	DRAWN BY R. S. HARTLEY		DRAWING NO RH-SPECIMEN MS-001

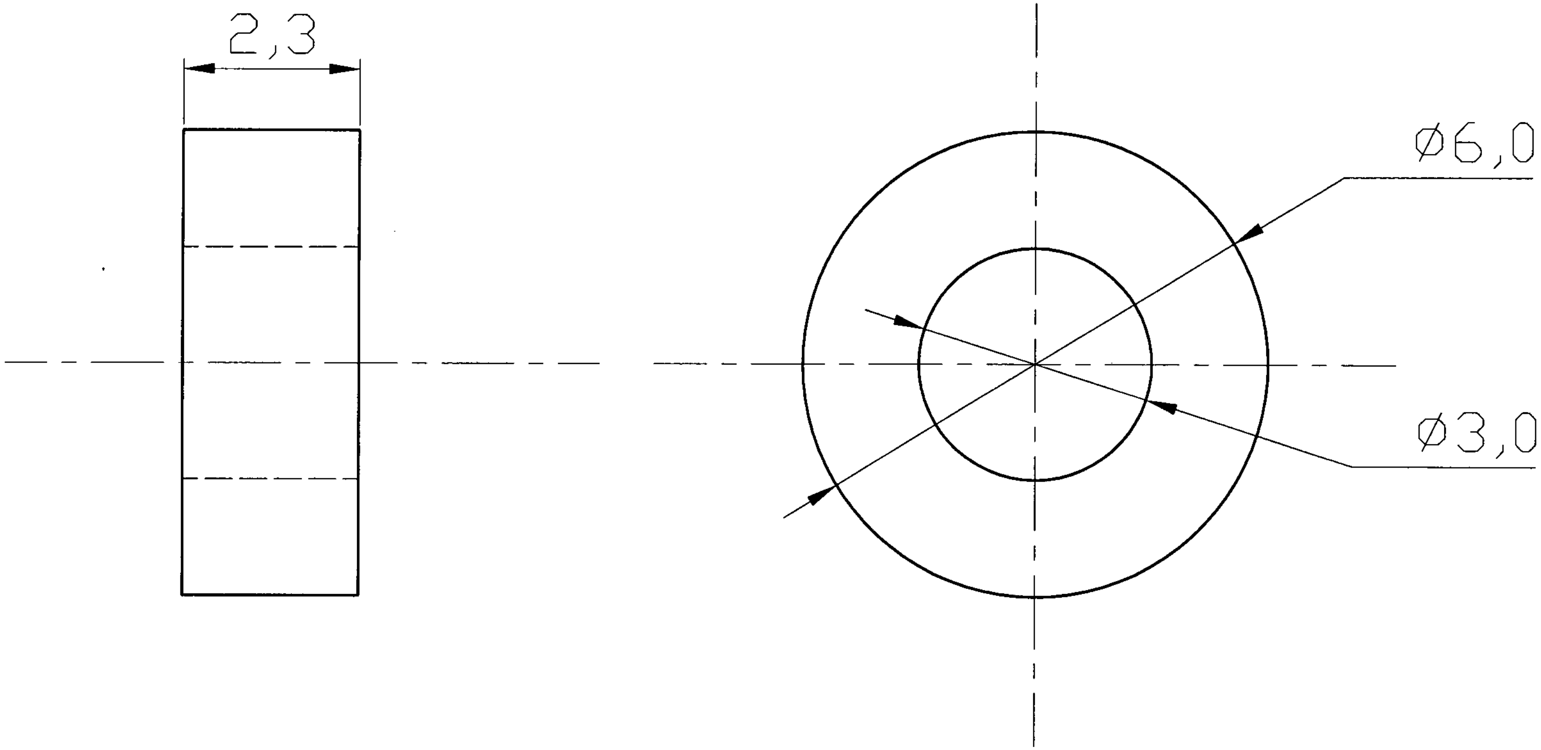

1	6:3:2 Copper Specimen	COPPER	60
PT. NO.	DESCRIPTION	MATERIAL	NO. OFF

UNIVERSITY OF CAPE TOWN
Department of Mechanical Engineering

6:3:2 COPPER SPECIMEN

Dimensions in mm	SCALE 10:1	DATE 23-04-2004	SHEET 1 OF 1
Tolerance unless otherwise stated +-0,1mm	DRAWN BY R. S. HARTLEY		DRAWING NO RH-SPECIMEN CU-001

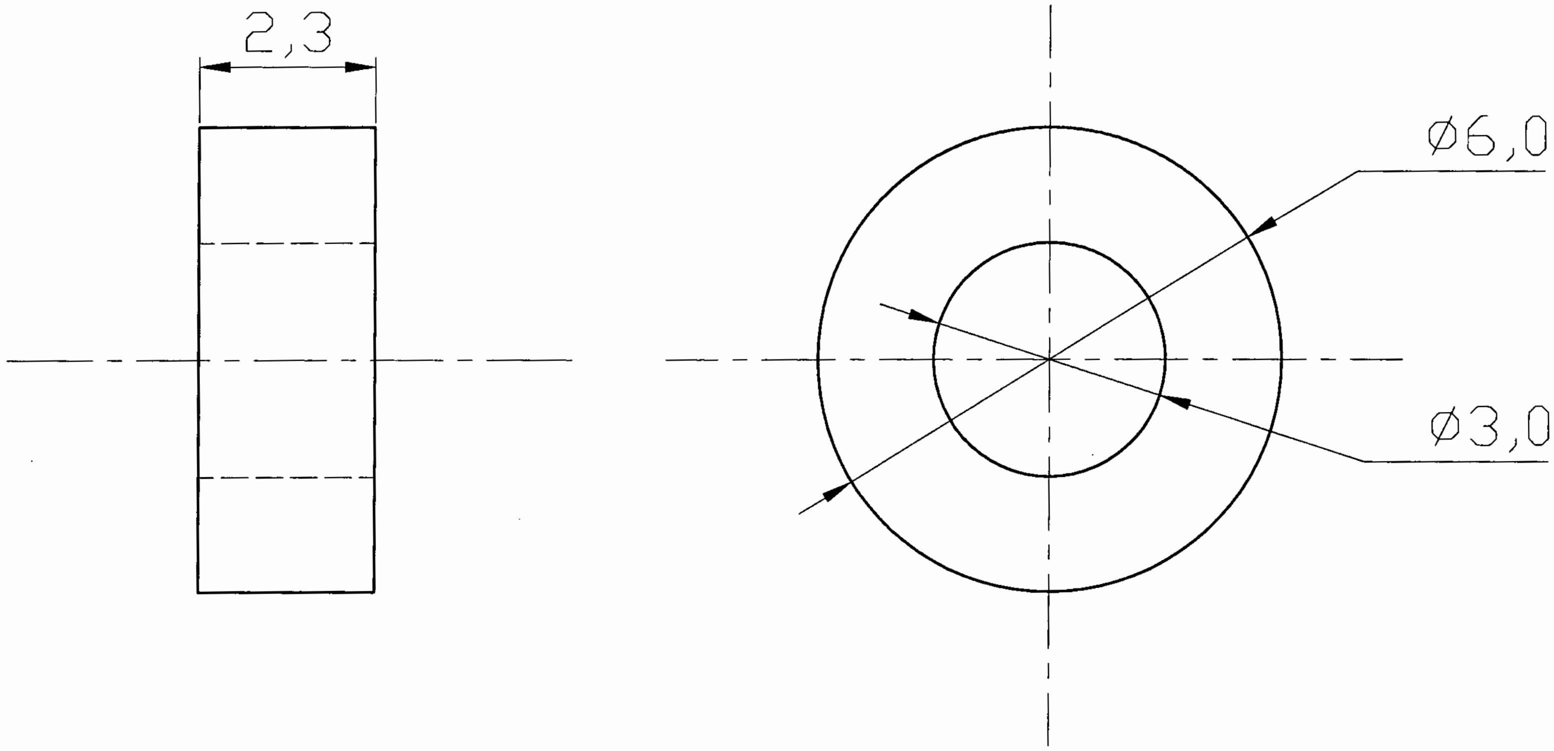

1	6:3:2 Aluminium Specimen	ALUMINIUM	60
PT. NO.	DESCRIPTION	MATERIAL	NO. OFF

UNIVERSITY OF CAPE TOWN
Department of Mechanical Engineering

6:3:2 ALUMINIUM SPECIMEN

Dimensions in mm	SCALE 10:1	DATE 26-04-2004	SHEET 1 OF 1
Tolerance unless otherwise stated +-0.1mm	DRAWN BY R. S. HARTLEY		DRAWING NO RH-SPECIMEN AL-001

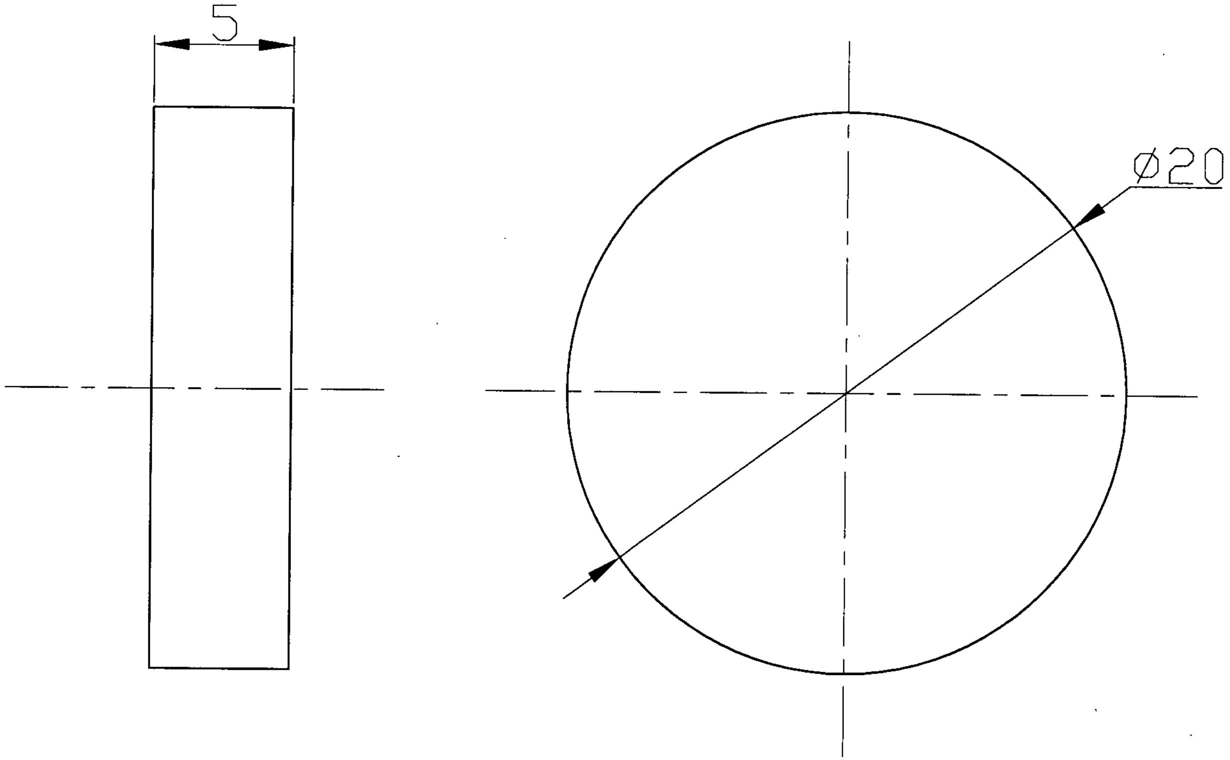

PT. NO.	DESCRIPTION	MATERIAL	NO. OFF
1	ANVIL	MAR-AGING STEEL	2

UNIVERSITY OF CAPE TOWN
Department of Mechanical Engineering

20:5 ANVILS

Dimensions in mm

SCALE 4:1

DATE 20-04-2004

SHEET 1 OF 1

Tolerance unless otherwise stated +-0.1mm

DRAWN BY R. S. HARTLEY

DRAWING NO RH-ANVIL-001

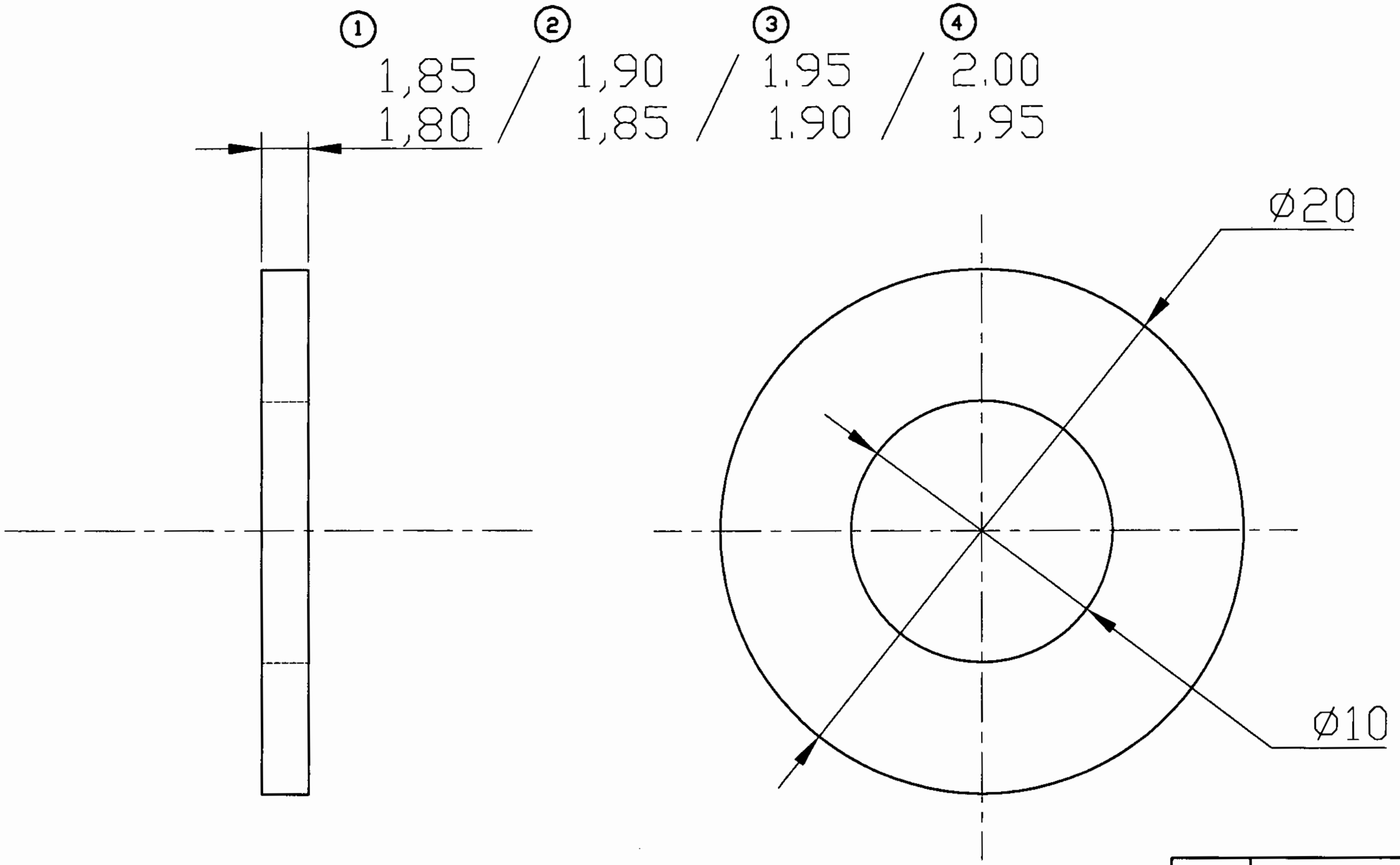

PT. NO.	DESCRIPTION	MATERIAL	NO. OFF
4	1.95mm SPACER	Mar-aging 18Ni (300)	1
3	1.90mm SPACER	Mar-aging 18Ni (300)	1
2	1.85mm SPACER	Mar-aging 18Ni (300)	1
1	1.80mm SPACER	Mar-aging 18Ni (300)	1

	UNIVERSITY OF CAPE TOWN Department of Mechanical Engineering		
	LIMIT COLLAR (MARAGING STEEL)		
Dimensions in mm	SCALE 5:1	DATE 26-02-2004	SHEET 1 OF 1
Tolerance unless otherwise stated +-0.1mm	DRAWN BY R. S. HARTLEY		DRAWING NO RH-COLLAR L-001

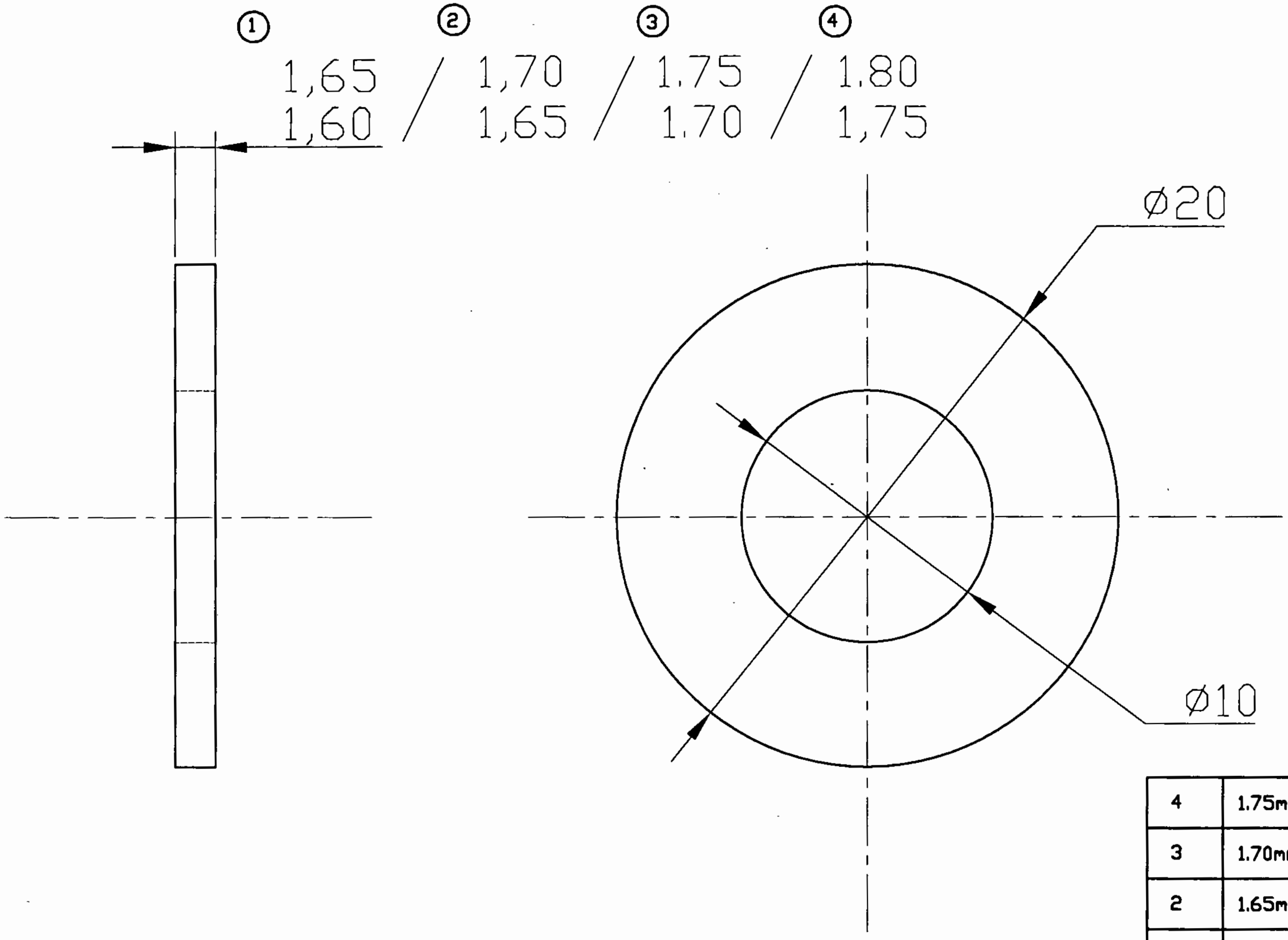

PT. NO.	DESCRIPTION	MATERIAL	NO. OFF
4	1.75mm SPACER	Mar-aging 18Ni (300)	1
3	1.70mm SPACER	Mar-aging 18Ni (300)	1
2	1.65mm SPACER	Mar-aging 18Ni (300)	1
1	1.60mm SPACER	Mar-aging 18Ni (300)	1

UNIVERSITY OF CAPE TOWN
Department of Mechanical Engineering

LIMIT-COLLAR (MARAGING STEEL)

Dimensions in mm
SCALE 5:1
DATE 26-02-2004
SHEET 1 OF 1

Tolerance unless otherwise stated +-0.1mm
DRAWN BY R. S. HARTLEY
DRAWING NO RH-COLLAR S-001